Density Model for Rough-Toothed Dolphin (*Steno bredanensis*) for the U.S. East Coast: Supplementary Report

Model Version 3.1

Duke University Marine Geospatial Ecology Laboratory*

2023-05-27

Citation

When citing our methodology or results generally, please cite Roberts et al. (2016, 2023). The complete references appear at the end of this document. We are preparing a new article for a peer-reviewed journal that will eventually replace those. Until that is published, those are the best general citations.

When citing this model specifically, please use this reference:

Roberts JJ, Yack TM, Cañadas A, Fujioka E, Halpin PN, Barco SG, Boisseau O, Chavez-Rosales S, Cole TVN, Cotter MP, Cummings EW, Davis GE, DiGiovanni Jr. RA, Garrison LP, Gowan TA, Jackson KA, Kenney RD, Khan CB, Lockhart GG, Lomac-MacNair KS, McAlarney RJ, McLellan WA, Mullin KD, Nowacek DP, O'Brien O, Pabst DA, Palka DL, Quintana-Rizzo E, Redfern JV, Rickard ME, White M, Whitt AD, Zoidis AM (2022) Density Model for Rough-Toothed Dolphin (*Steno bredanensis*) for the U.S. East Coast, Version 3.1, 2023-05-27, and Supplementary Report. Marine Geospatial Ecology Laboratory, Duke University, Durham, North Carolina.

Copyright and License

Model Version History

Version	Date	Description
1	2015-01-31	Initial version.
1.1	2015-05-14	Updated calculation of CVs. Switched density rasters to logarithmic breaks. No changes to the model.
1.2	2015-09-26	Updated the documentation. No changes to the model. Model files released as supplementary information to Roberts et al. (2016).
2	2018-04-14	Began update to Roberts et al. (2016) model. Introduced new surveys from AMAPPS, NARWSS, UNCW, VAMSC, and the SEUS NARW teams. Updated modeling methodology. Refitted detection functions and spatial model from scratch using new and reprocessed covariates. Model released as part of a scheduled update to the U.S. Navy Marine Species Density Database (NMSDD).

*For questions or to offer feedback please contact Jason Roberts (jason.roberts@duke.edu) and Tina Yack (tina.yack@duke.edu)

(continued)

Version	Date	Description
3	2022-06-20	This model is a major update over the prior version, with substantial additional data, improved statistical methods, and an increased spatial resolution. It was released as part of the final delivery of the U.S. Navy Marine Species Density Database (NMSDD) for the Atlantic Fleet Testing and Training (AFTT) Phase IV Environmental Impact Statement. Several new collaborators joined and contributed survey data: New York State Department of Environmental Conservation, TetraTech, HDR, and Marine Conservation Research. We incorporated additional surveys from all continuing and new collaborators through the end of 2020. (Because some environmental covariates were only available through 2019, certain models only extend through 2019.) We increased the spatial resolution to 5 km and, at NOAA's request, we extended the model further inshore from New York through Maine. We reformulated and refitted all detection functions and spatial models. We updated all enviromental covariates to newer products, when available, and added several covariates to the set of candidates. For models that incorporated dynamic covariates, we estimated model uncertainty using a new method that accounts for both model parameter error and temporal variability.
3.1	2023-05-27	Completed the supplementary report documenting the details of this model. The model itself was not changed.

1 Survey Data

We built this model from data collected between 1998-2020 (Table 1, Figure 1). We excluded surveys that did not target small cetaceans or were otherwise problematic for modeling them. In keeping with our primary strategy for the 2022 modeling cycle, we excluded data prior to 1998. We restricted the model to aerial survey transects with sea states of Beaufort 4 or less (for a few surveys we used Beaufort 3 or less) and shipboard transects with Beaufort 5 or less (for a few we used Beaufort 4 or less). We also excluded transects with poor weather or visibility for surveys that reported those conditions.

Table 1: Survey effort and observations considered for this model. Effort is tallied as the cumulative length of on-effort transects. Observations are the number of groups and individuals encountered while on effort. Off effort observations and those lacking an estimate of group size or distance to the group were excluded.

			Effort	Observations		
Institution	Program	Period	1000s km	Groups	Individuals	Mean Group Size
Aerial Surveys						
HDR	Navy Norfolk Canyon	2018-2019	10	0	0	
NEFSC	AMAPPS	2010-2019	83	0	0	
NEFSC	NARWSS	2003-2016	380	0	0	
NEFSC	Pre-AMAPPS	1999-2008	45	0	0	
SEFSC	AMAPPS	2010-2020	112	2	26	13.0
SEFSC	MATS	2002-2005	27	0	0	
UNCW	MidA Bottlenose	2002-2002	15	0	0	
UNCW	Navy Cape Hatteras	2011-2017	34	1	4	4.0
UNCW	Navy Jacksonville	2009-2017	92	10	365	36.5
UNCW	Navy Norfolk Canyon	2015-2017	14	0	0	
UNCW	Navy Onslow Bay	2007-2011	49	3	40	13.3
UNCW	SEUS NARW EWS	2005-2008	106	0	0	
VAMSC	MD DNR WEA	2013-2015	15	0	0	
VAMSC	Navy VACAPES	2016-2017	18	0	0	
VAMSC	VA CZM WEA	2012-2015	19	0	0	
		Total	**1,020**	**16**	**435**	**27.2**
Shipboard Surveys						
MCR	SOTW Visual	2012-2019	9	0	0	
NEFSC	AMAPPS	2011-2016	15	6	59	9.8
NEFSC	Pre-AMAPPS	1998-2007	13	0	0	
NJDEP	NJEBS	2008-2009	14	0	0	
SEFSC	AMAPPS	2011-2016	16	2	25	12.5
SEFSC	Pre-AMAPPS	1998-2006	30	2	28	14.0
		Total	**96**	**10**	**112**	**11.2**
		Grand Total	**1,115**	**26**	**547**	**21.0**

Table 2: Institutions that contributed surveys used in this model.

Institution	Full Name
HDR	HDR, Inc.
MCR	Marine Conservation Research
NEFSC	NOAA Northeast Fisheries Science Center
NJDEP	New Jersey Department of Environmental Protection
SEFSC	NOAA Southeast Fisheries Science Center
UNCW	University of North Carolina Wilmington
VAMSC	Virginia Aquarium & Marine Science Center

Table 3: Descriptions and references for survey programs used in this model.

Program	Description	References
AMAPPS	Atlantic Marine Assessment Program for Protected Species	Palka et al. (2017), Palka et al. (2021)
MATS	Mid-Atlantic Tursiops Surveys	
MD DNR WEA	Aerial Surveys of the Maryland Wind Energy Area	Barco et al. (2015)
MidA Bottlenose	Mid-Atlantic Onshore/Offshore Bottlenose Dolphin Surveys	Torres et al. (2005)
NARWSS	North Atlantic Right Whale Sighting Surveys	Cole et al. (2007)
Navy Cape Hatteras	Aerial Surveys of the Navy's Cape Hatteras Study Area	McLellan et al. (2018)
Navy Jacksonville	Aerial Surveys of the Navy's Jacksonville Study Area	Foley et al. (2019)
Navy Norfolk Canyon	Aerial Surveys of the Navy's Norfolk Canyon Study Area	Cotter (2019), McAlarney et al. (2018)
Navy Onslow Bay	Aerial Surveys of the Navy's Onslow Bay Study Area	Read et al. (2014)
Navy VACAPES	Aerial Survey Baseline Monitoring in the Continental Shelf Region of the VACAPES OPAREA	Mallette et al. (2017)
NJEBS	New Jersey Ecological Baseline Study	Geo-Marine, Inc. (2010), Whitt et al. (2015)
Pre-AMAPPS	Pre-AMAPPS Marine Mammal Abundance Surveys	Mullin and Fulling (2003), Garrison et al. (2010), Palka (2006)
SEUS NARW EWS	Southeast U.S. Right Whale Early Warning System Surveys	
SOTW Visual	R/V Song of the Whale Visual Surveys	Ryan et al. (2013)
VA CZM WEA	Virginia CZM Wind Energy Area Surveys	Mallette et al. (2014), Mallette et al. (2015)

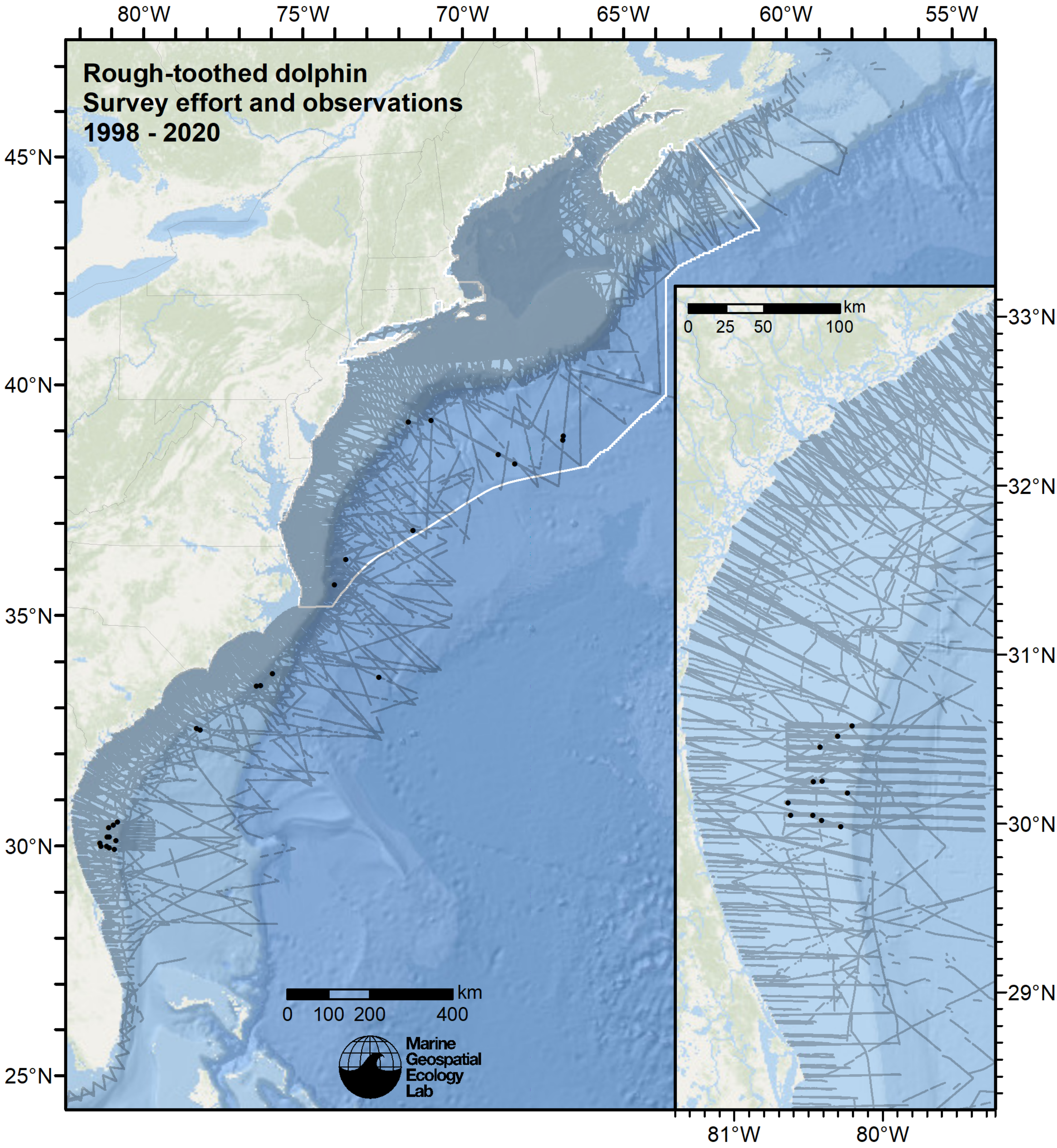

Figure 1: Survey effort and rough-toothed dolphin observations available for density modeling, after detection functions were applied, and excluded segments and truncated observations were removed.

2 Detection Functions

2.1 With a Taxonomic Covariate

We fitted the detection functions in this section to pools of species with similar detectability characteristics and used the taxonomic identification as a covariate (ScientificName) to account for differences between them. We consulted the literature and observer teams to determine appropriate poolings. We usually employed this approach to boost the counts of observations in the detection functions, which increased the chance that other covariates such as Beaufort sea state could be used to account for differences in observing conditions. When defining the taxonomic covariate, we sometimes had too few observations of species to allocate each of them their own level of the covariate and had to group them together, again consulting the literature and observers for advice on species similarity. Also, when species were observed frequently enough to be allocated their own levels but statistical tests indicated no significant difference between the levels, we usually grouped them together into a single level.

2.1.1 Aerial Surveys

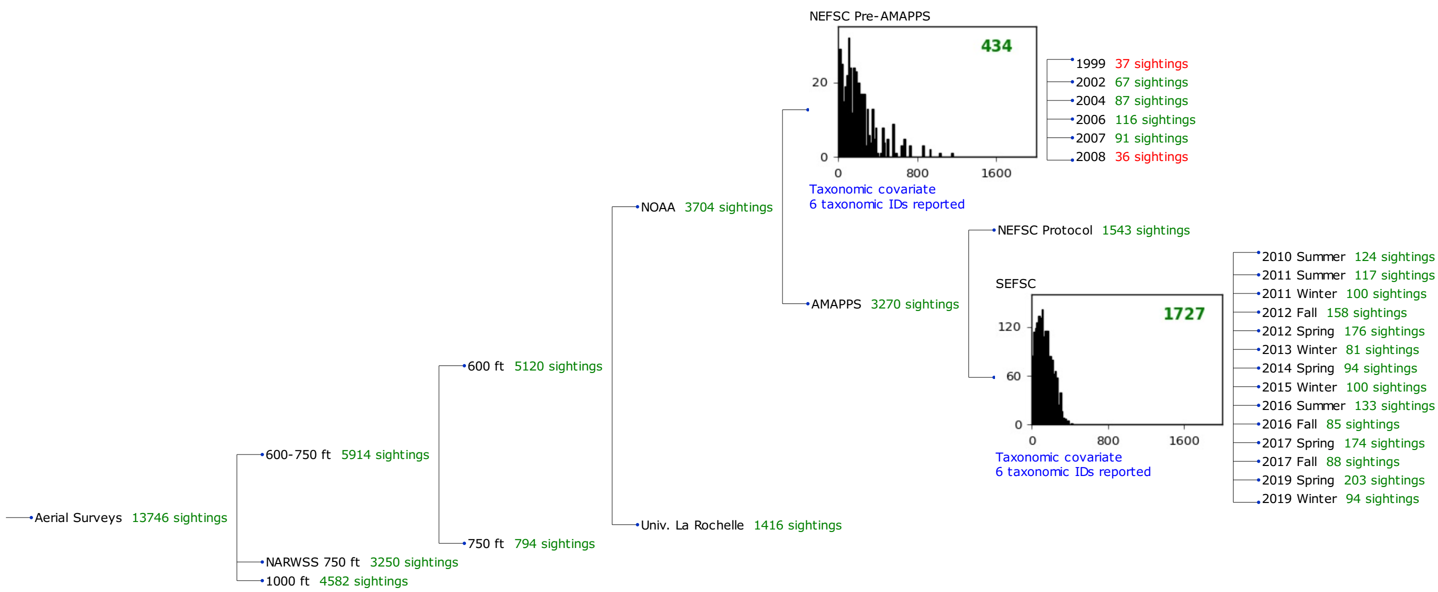

Figure 2: Detection hierarchy for aerial surveys, showing how they were pooled during detectability modeling, for detection functions that pooled multiple taxa and used used a taxonomic covariate to account for differences between them. Each histogram represents a detection function and summarizes the perpendicular distances of observations that were pooled to fit it, prior to truncation. Observation counts, also prior to truncation, are shown in green when they met the recommendation of Buckland et al. (2001) that detection functions utilize at least 60 sightings, and red otherwise. For rare taxa, it was not always possible to meet this recommendation, yielding higher statistical uncertainty. During the spatial modeling stage of the analysis, effective strip widths were computed for each survey using the closest detection function above it in the hierarchy (i.e. moving from right to left in the figure). Surveys that do not have a detection function above them in this figure were either addressed by a detection function presented in a different section of this report, or were omitted from the analysis.

2.1.1.1 NEFSC Pre-AMAPPS

After right-truncating observations greater than 600 m, we fitted the detection function to the 413 observations that remained (Table 4). The selected detection function (Figure 3) used a hazard rate key function with Beaufort (Figure 4) and ScientificName (Figure 5) as covariates.

Table 4: Observations used to fit the NEFSC Pre-AMAPPS detection function.

ScientificName	n
Delphinus, Lagenodelphis, Stenella	239
Lagenorhynchus	128
Tursiops, Steno	46
Total	**413**

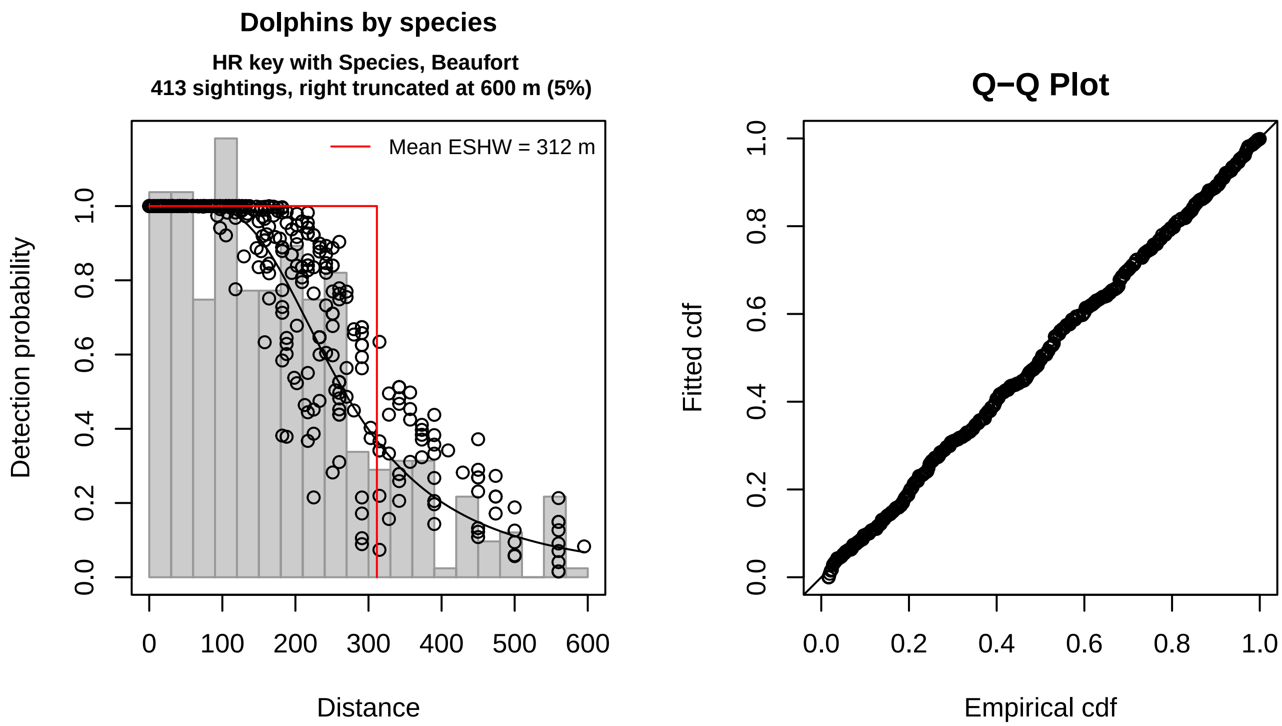

Figure 3: NEFSC Pre-AMAPPS detection function and Q-Q plot showing its goodness of fit.

Statistical output for this detection function:

```
Summary for ds object
Number of observations :  413
Distance range         :  0  -  600
AIC                    :  5043.994

Detection function:
 Hazard-rate key function

Detection function parameters
Scale coefficient(s):
                                estimate         se
(Intercept)                    5.3188665 0.15126469
ScientificNameLagenorhynchus  -0.1872175 0.11165678
ScientificNameTursiops, Steno -0.5457529 0.14785313
Beaufort                       0.1451869 0.05844944

Shape coefficient(s):
            estimate        se
(Intercept) 1.107015 0.1176733

                       Estimate          SE          CV
```

```
Average p             0.4982478  0.02373666 0.04764026
N in covered region 828.9047438 49.28440455 0.05945726

Distance sampling Cramer-von Mises test (unweighted)
Test statistic = 0.023324  p = 0.992716
```

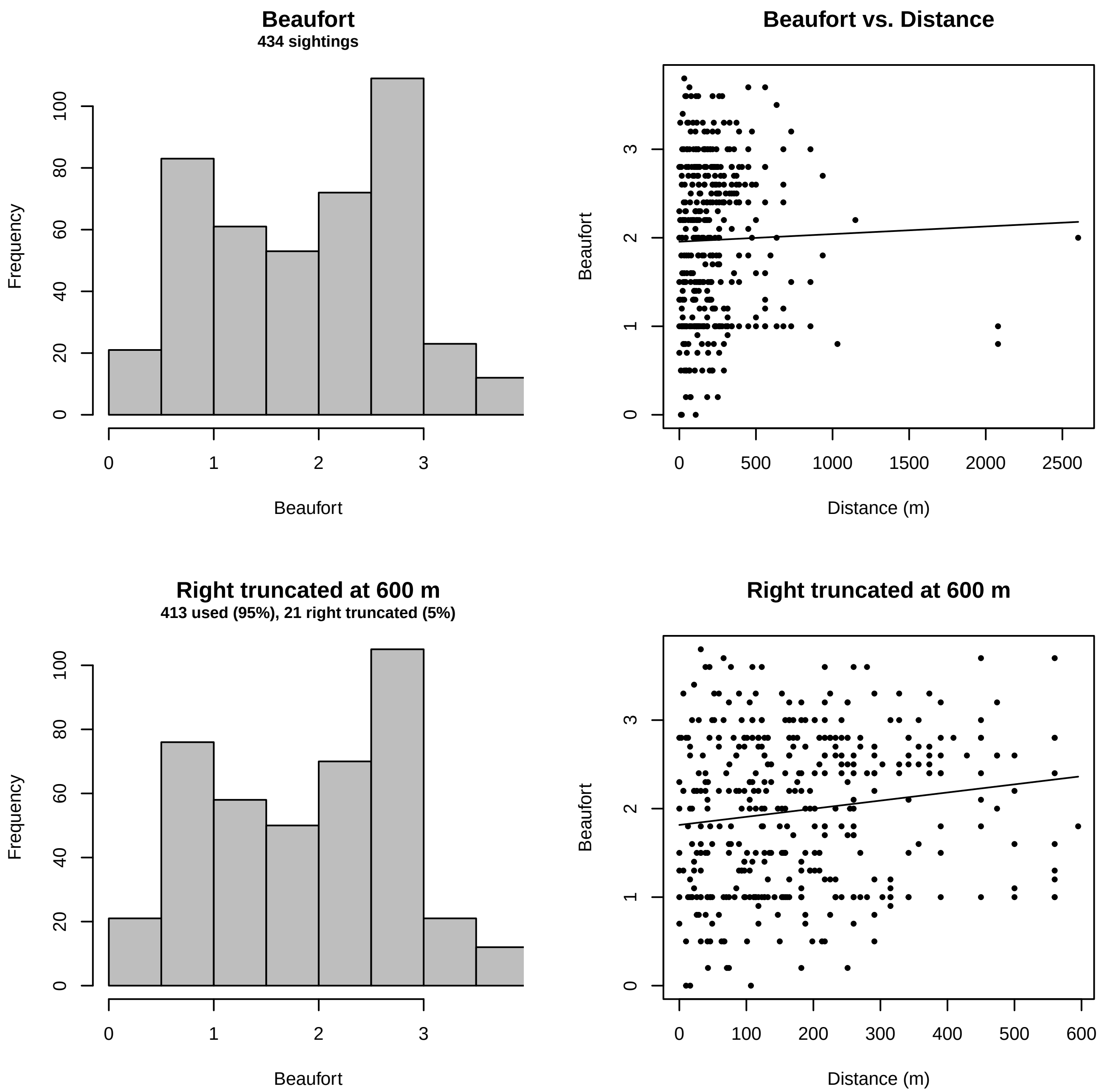

Figure 4: Distribution of the Beaufort covariate before (top row) and after (bottom row) observations were truncated to fit the NEFSC Pre-AMAPPS detection function.

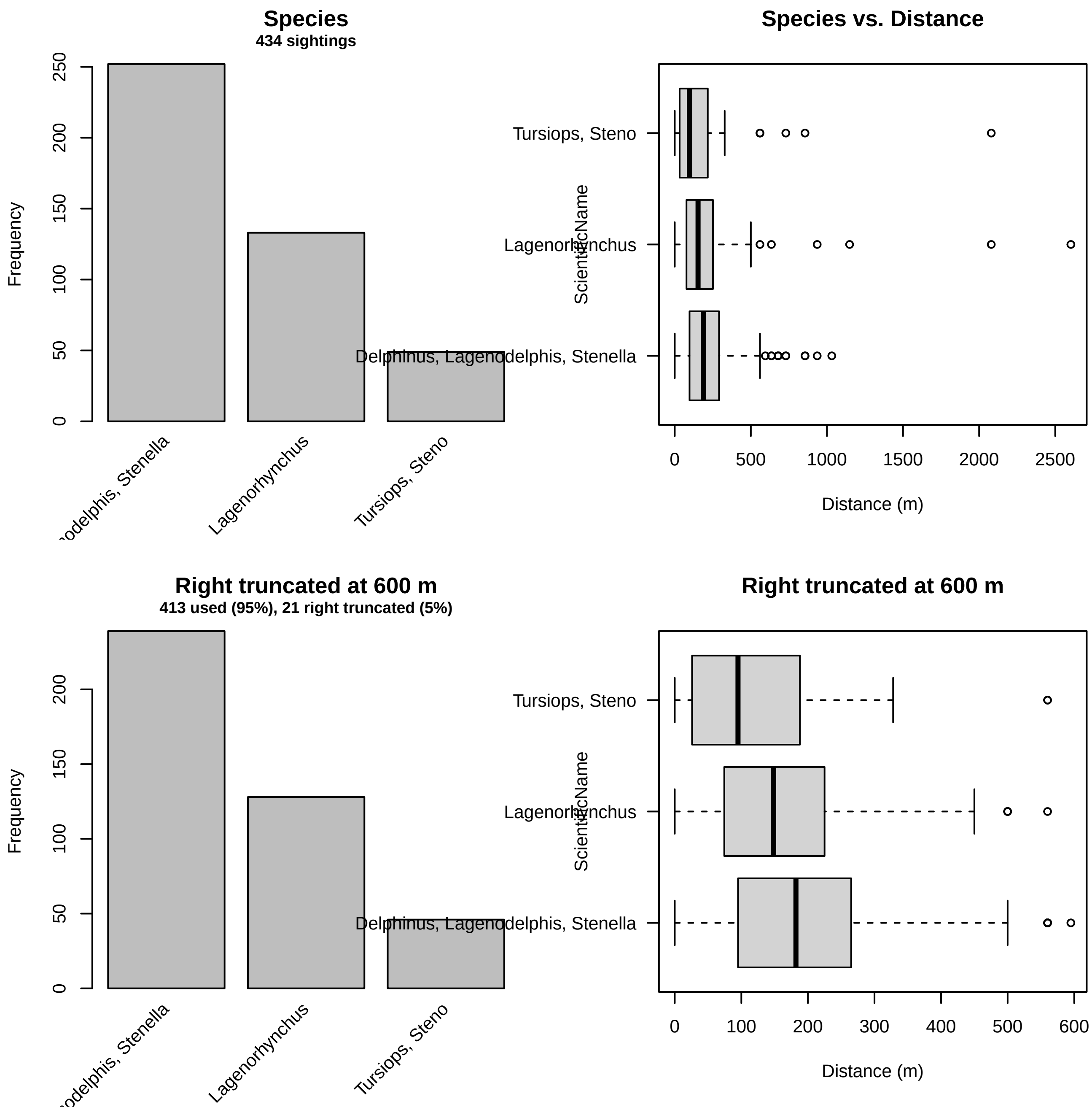

Figure 5: Distribution of the ScientificName covariate before (top row) and after (bottom row) observations were truncated to fit the NEFSC Pre-AMAPPS detection function.

2.1.1.2 SEFSC AMAPPS

After right-truncating observations greater than 325 m and left-truncating observations less than 15 m (Figure 7), we fitted the detection function to the 1628 observations that remained (Table 5). The selected detection function (Figure 6) used a hazard rate key function with Beaufort (Figure 8), ScientificName (Figure 9) and Season (Figure 10) as covariates.

Table 5: Observations used to fit the SEFSC AMAPPS detection function.

ScientificName	n
Delphinus, Tursiops, Lagenorhynchus, Steno	1422
Stenella, Lagenodelphis	206
Total	**1628**

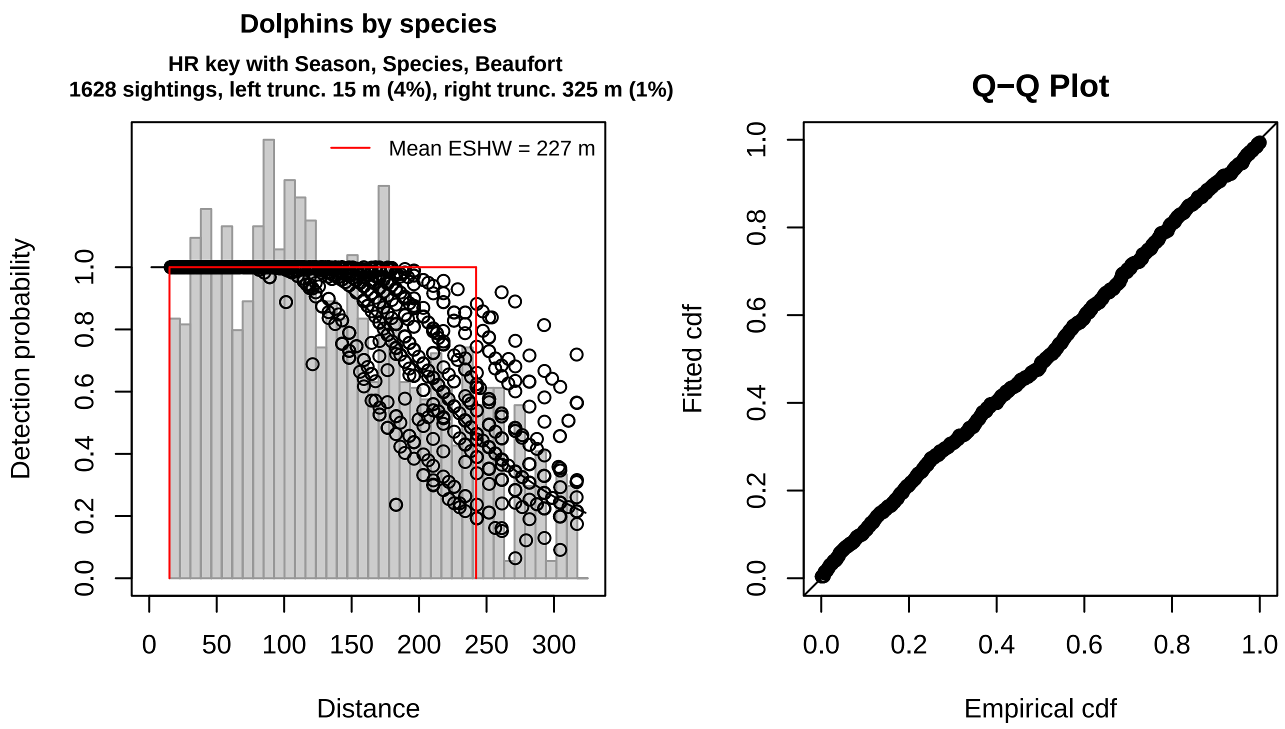

Figure 6: SEFSC AMAPPS detection function and Q-Q plot showing its goodness of fit.

Statistical output for this detection function:

```
Summary for ds object
Number of observations :  1628
Distance range         :  15  -  325
AIC                    :  18351.39

Detection function:
 Hazard-rate key function

Detection function parameters
Scale coefficient(s):
                                        estimate         se
(Intercept)                            5.4780735 0.08251975
SeasonSummer                           0.1269645 0.06172358
SeasonWinter                          -0.2356803 0.06102237
ScientificNameStenella, Lagenodelphis  0.2204074 0.08699872
Beaufort2                             -0.1192230 0.08713320
Beaufort3                             -0.1846083 0.08971655
Beaufort4                             -0.4027356 0.12330363

Shape coefficient(s):
            estimate        se
(Intercept) 1.266688 0.1150367

                       Estimate          SE         CV
Average p              0.720161  0.01522909 0.02114679
N in covered region 2260.605761 56.60731047 0.02504077

Distance sampling Cramer-von Mises test (unweighted)
Test statistic = 0.138923  p = 0.425167
```

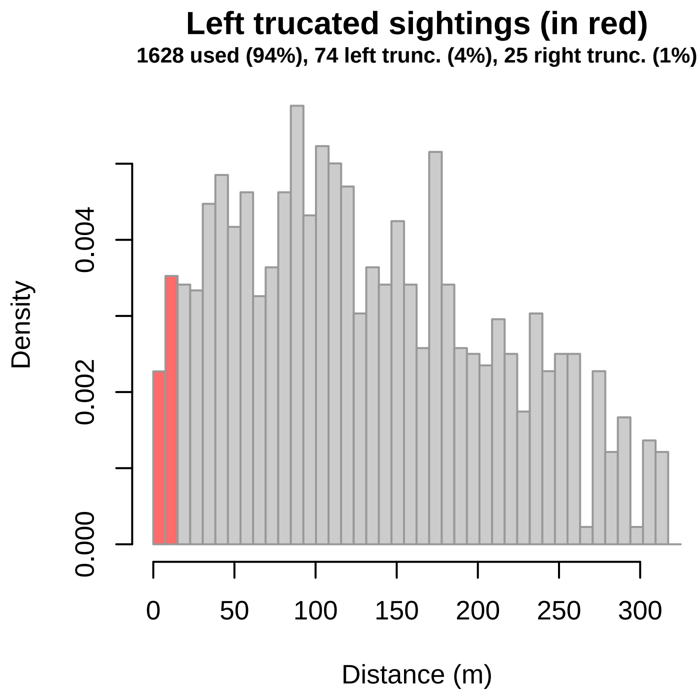

Figure 7: Density histogram of observations used to fit the SEFSC AMAPPS detection function, with the left-most bar showing observations at distances less than 15 m, which were left-truncated and excluded from the analysis [Buckland et al. (2001)]. (This bar may be very short if there were very few left-truncated sightings, or very narrow if the left truncation distance was very small; in either case it may not appear red.)

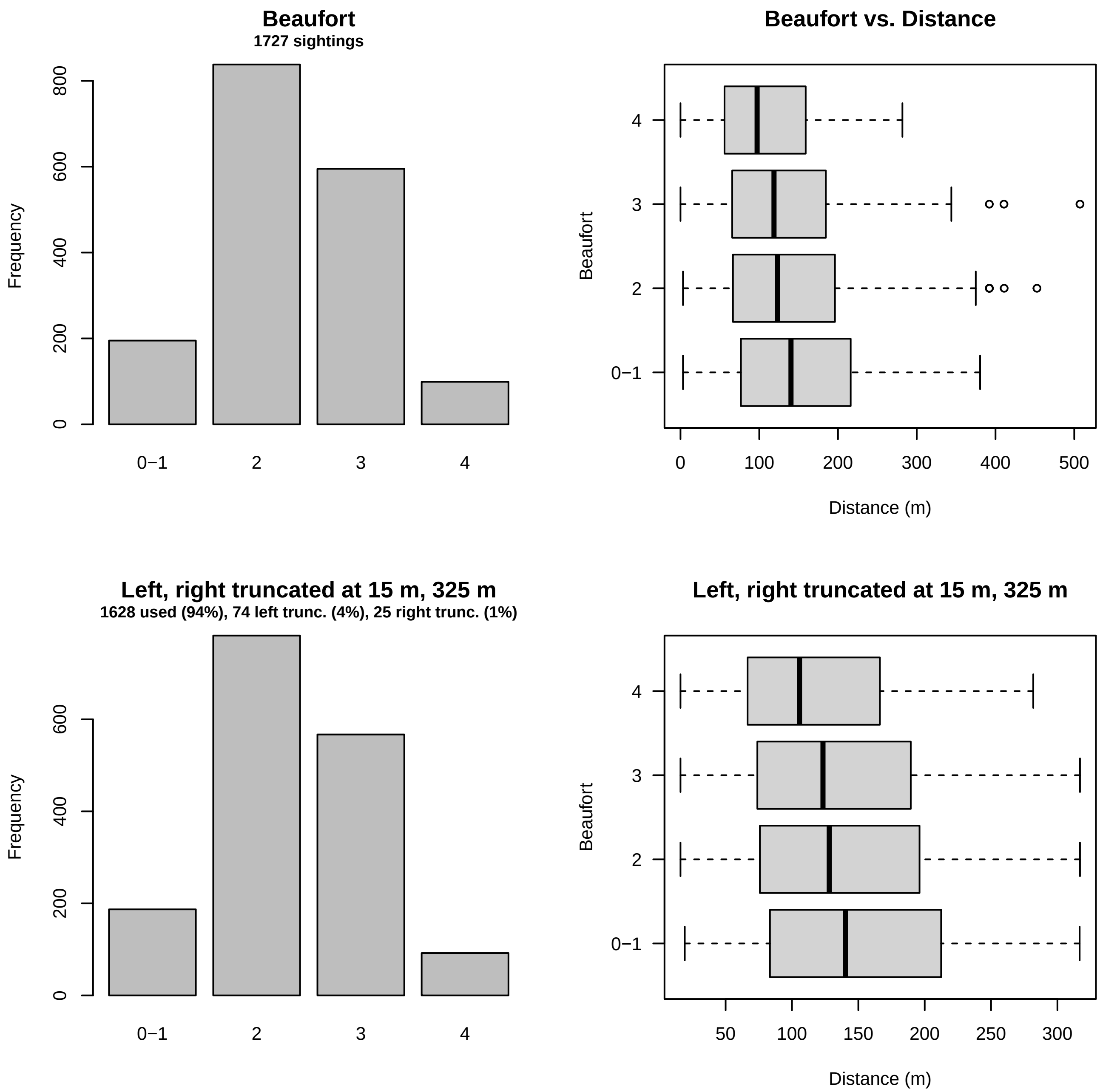

Figure 8: Distribution of the Beaufort covariate before (top row) and after (bottom row) observations were truncated to fit the SEFSC AMAPPS detection function.

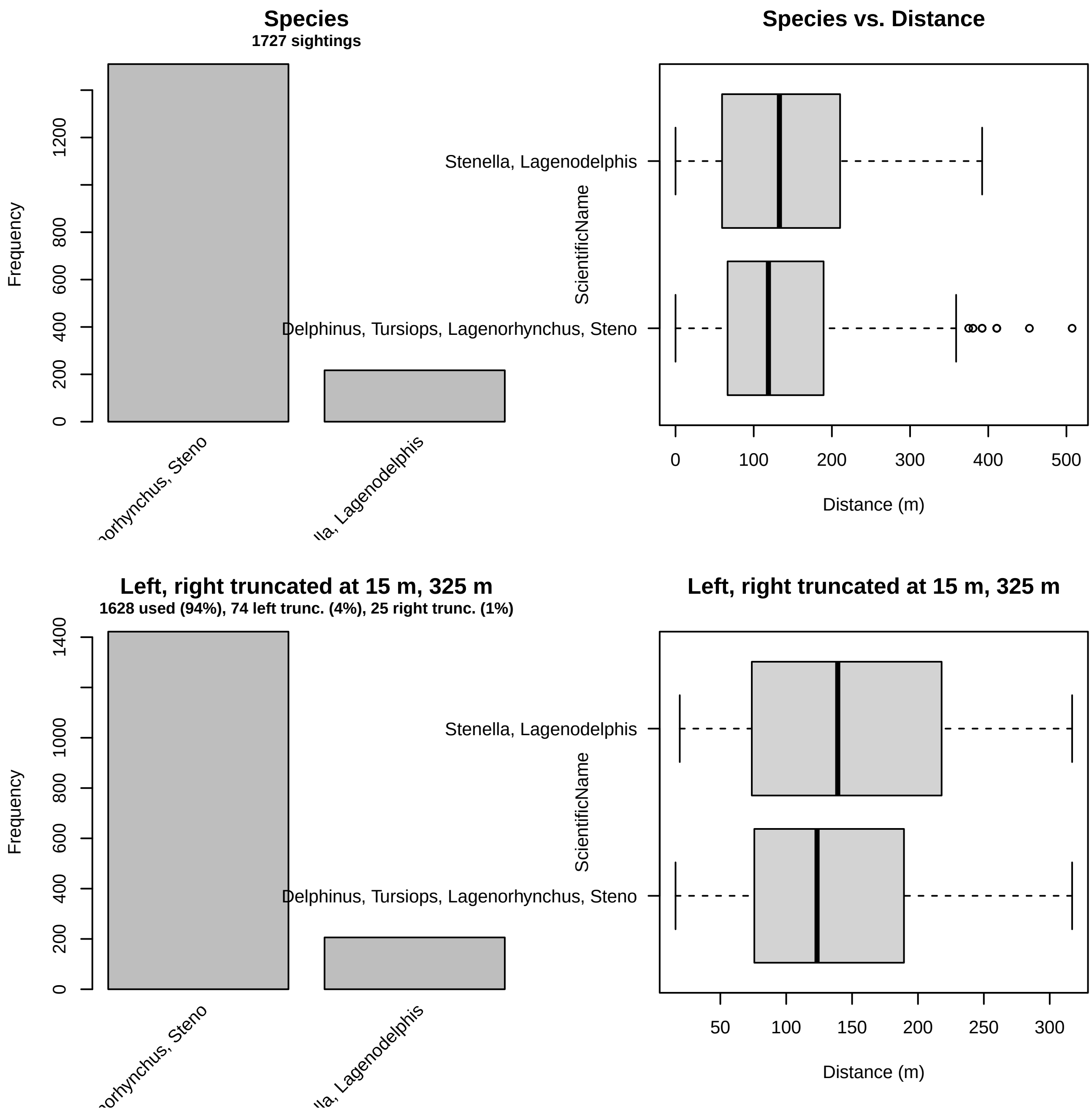

Figure 9: Distribution of the ScientificName covariate before (top row) and after (bottom row) observations were truncated to fit the SEFSC AMAPPS detection function.

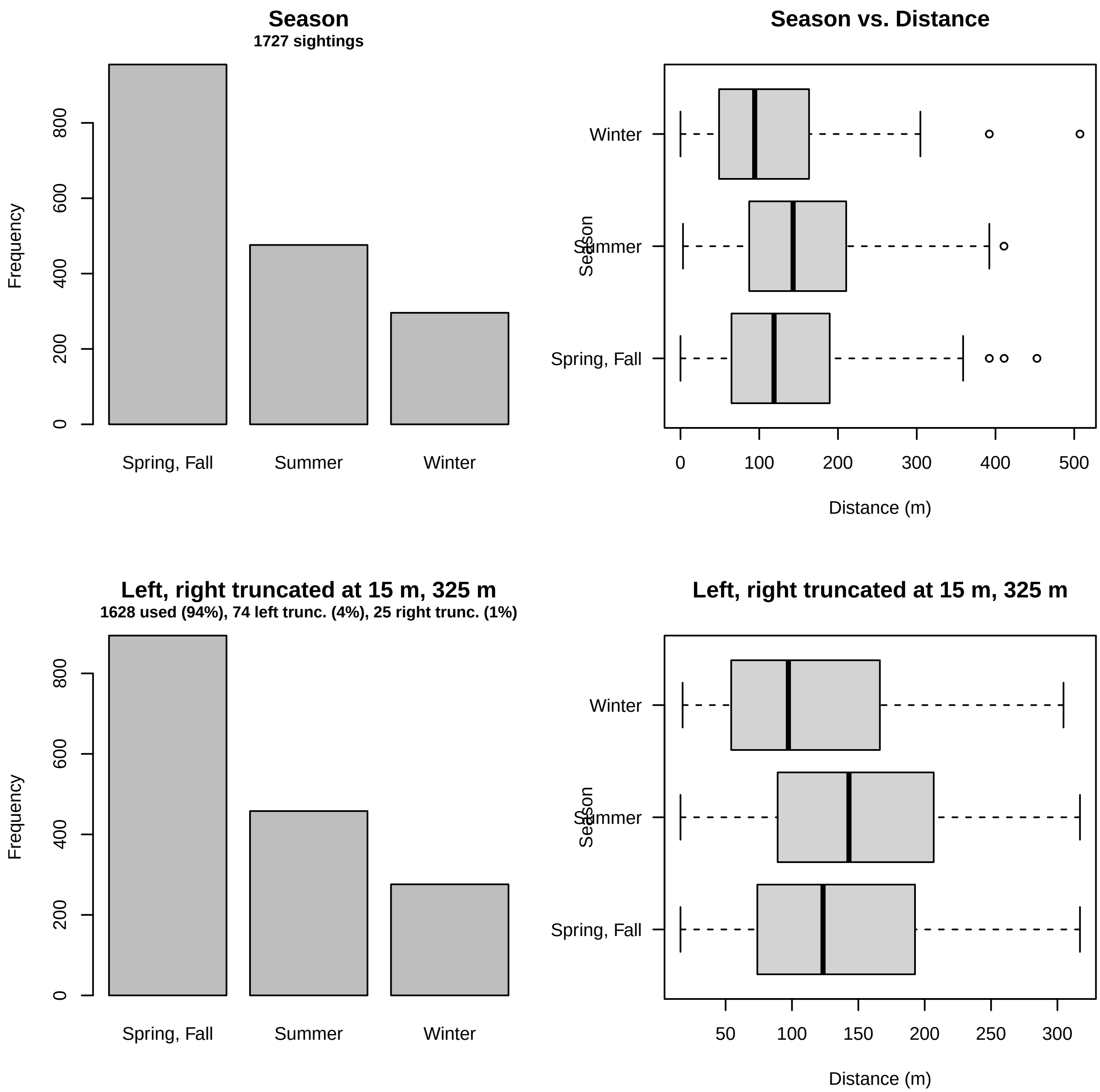

Figure 10: Distribution of the Season covariate before (top row) and after (bottom row) observations were truncated to fit the SEFSC AMAPPS detection function.

2.1.2 Shipboard Surveys

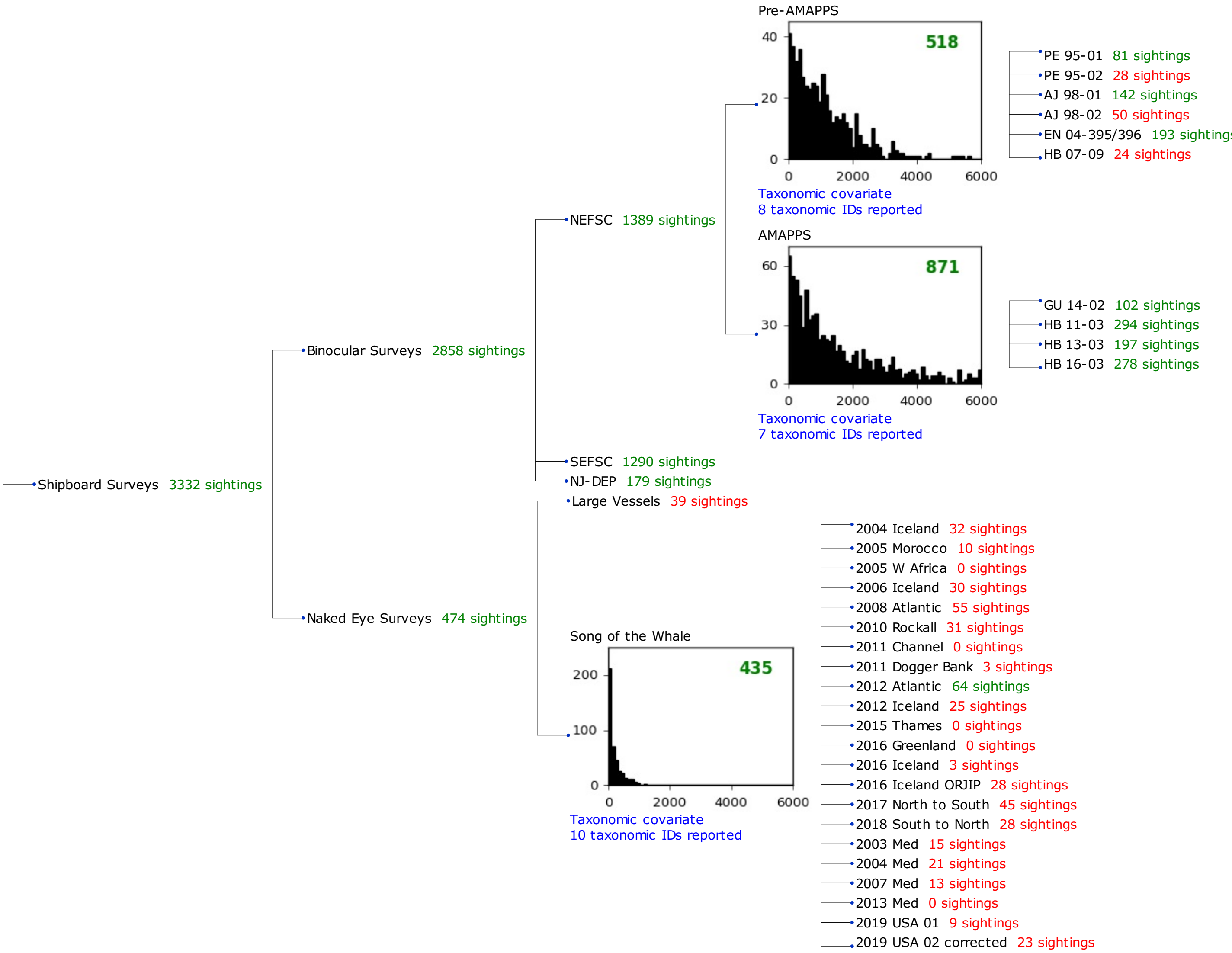

Figure 11: Detection hierarchy for shipboard surveys, showing how they were pooled during detectability modeling, for detection functions that pooled multiple taxa and used used a taxonomic covariate to account for differences between them. Each histogram represents a detection function and summarizes the perpendicular distances of observations that were pooled to fit it, prior to truncation. Observation counts, also prior to truncation, are shown in green when they met the recommendation of Buckland et al. (2001) that detection functions utilize at least 60 sightings, and red otherwise. For rare taxa, it was not always possible to meet this recommendation, yielding higher statistical uncertainty. During the spatial modeling stage of the analysis, effective strip widths were computed for each survey using the closest detection function above it in the hierarchy (i.e. moving from right to left in the figure). Surveys that do not have a detection function above them in this figure were either addressed by a detection function presented in a different section of this report, or were omitted from the analysis.

2.1.2.1 NEFSC Pre-AMAPPS

After right-truncating observations greater than 4000 m, we fitted the detection function to the 508 observations that remained (Table 6). The selected detection function (Figure 12) used a hazard rate key function with Beaufort (Figure 13), ScientificName (Figure 14) and VesselName (Figure 15) as covariates.

Table 6: Observations used to fit the NEFSC Pre-AMAPPS detection function.

ScientificName	n
Delphinus, Lagenorhynchus, Tursiops, Steno	365
Other Stenella, Lagenodelphis	130
Stenella frontalis	13
Total	**508**

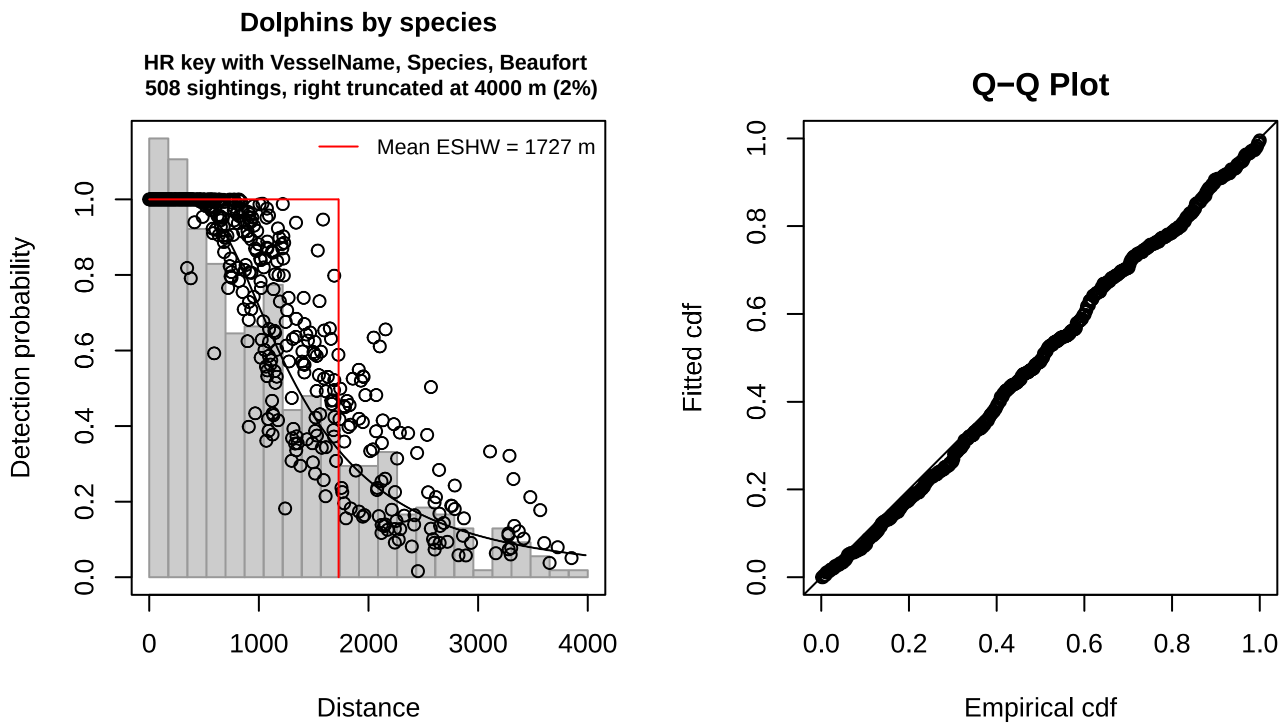

Figure 12: NEFSC Pre-AMAPPS detection function and Q-Q plot showing its goodness of fit.

Statistical output for this detection function:

```
Summary for ds object
Number of observations :  508
Distance range         :  0  -  4000
AIC                    :  8058.614

Detection function:
 Hazard-rate key function

Detection function parameters
Scale coefficient(s):
                                               estimate        se
(Intercept)                                   7.3979634 0.1986065
VesselNameEndeavor, Bigelow                   0.2529041 0.1095209
ScientificNameOther Stenella, Lagenodelphis   0.3555978 0.1258179
ScientificNameStenella frontalis             -0.8556981 0.3078540
Beaufort                                     -0.1897812 0.0694737

Shape coefficient(s):
             estimate        se
(Intercept) 0.8752144 0.1006522
```

```
                          Estimate          SE         CV
Average p                0.4071518  0.02118698 0.05203705
N in covered region 1247.6919609 78.15195776 0.06263722

Distance sampling Cramer-von Mises test (unweighted)
Test statistic = 0.120847  p = 0.492001
```

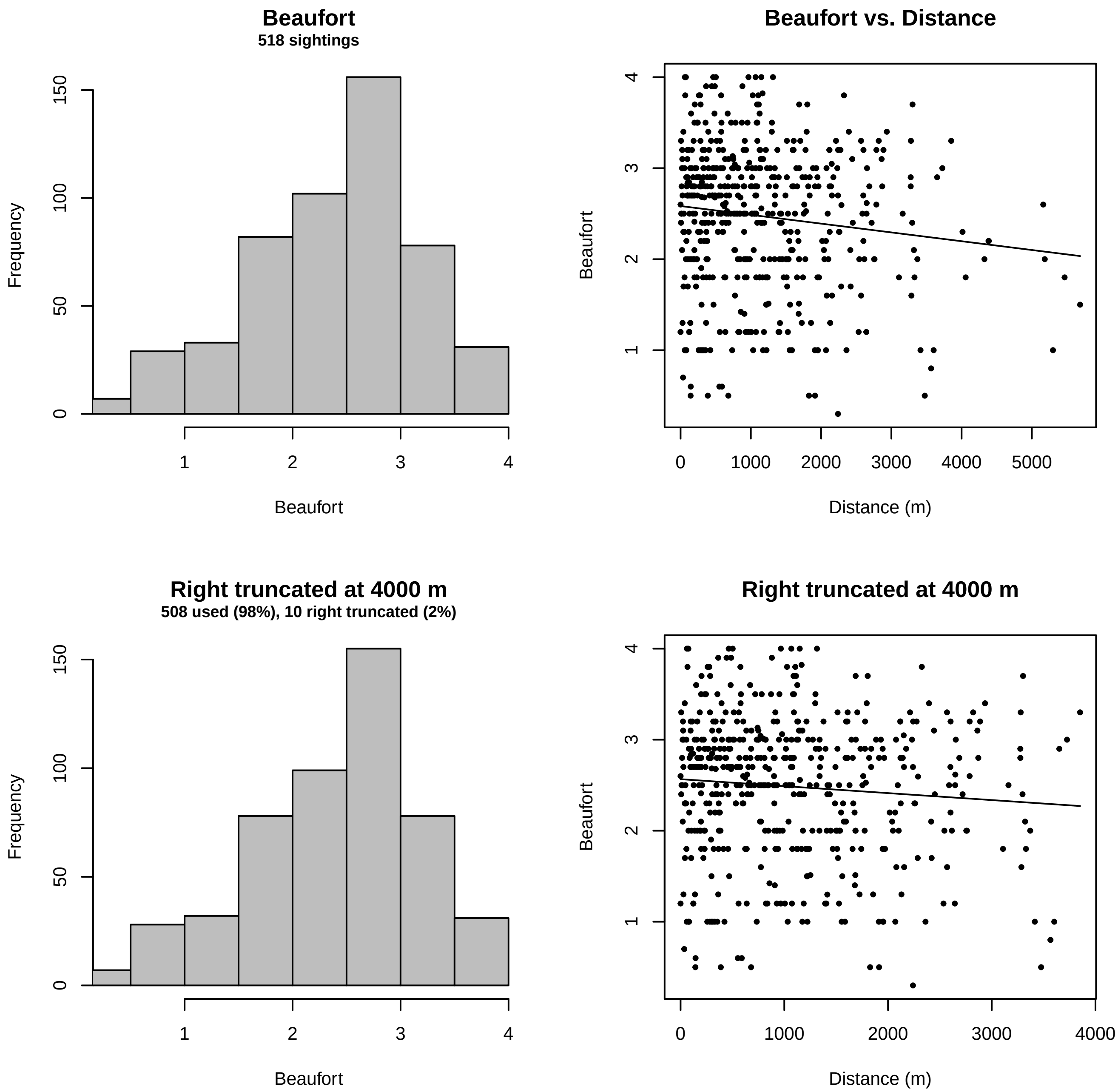

Figure 13: Distribution of the Beaufort covariate before (top row) and after (bottom row) observations were truncated to fit the NEFSC Pre-AMAPPS detection function.

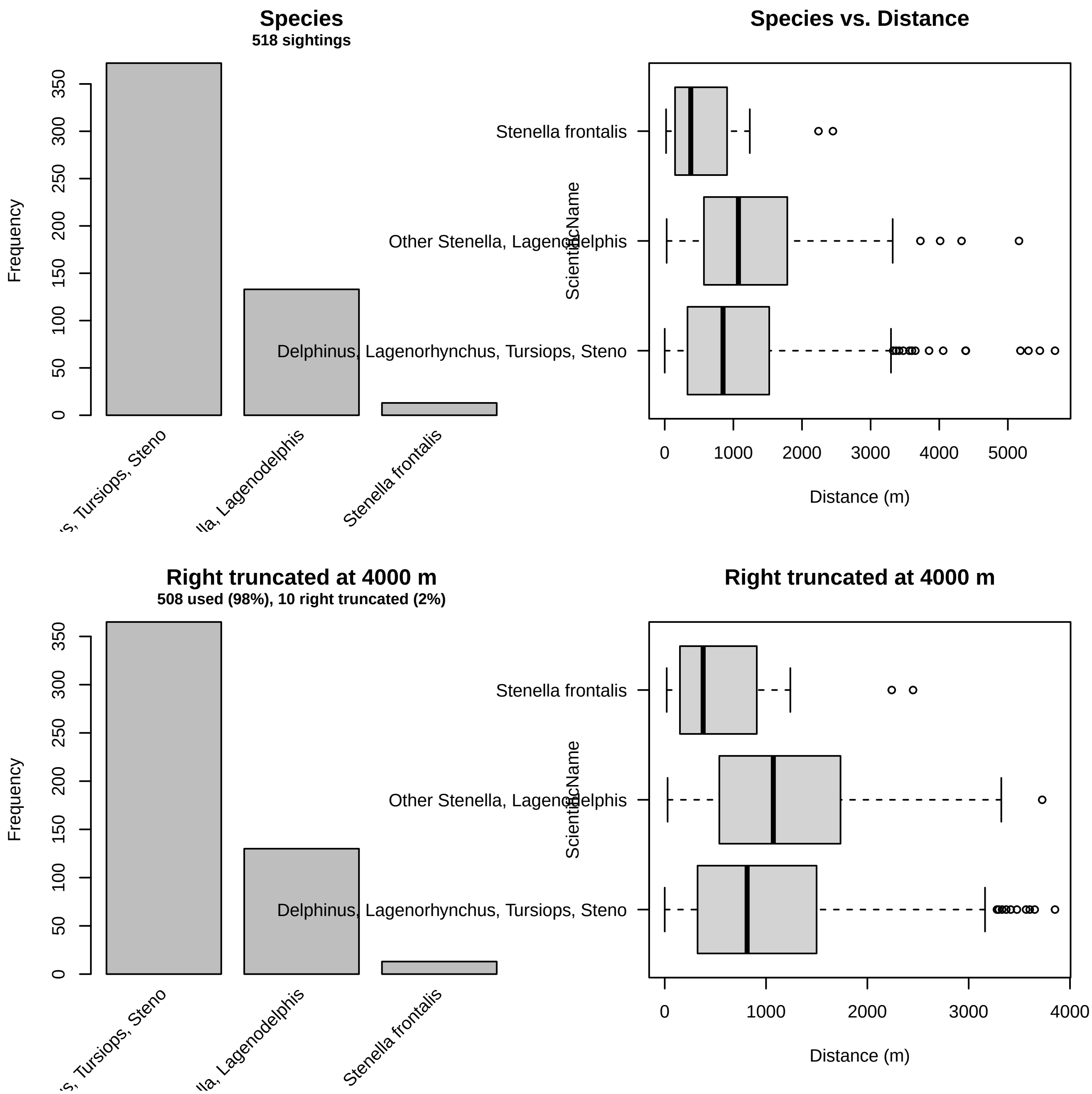

Figure 14: Distribution of the ScientificName covariate before (top row) and after (bottom row) observations were truncated to fit the NEFSC Pre-AMAPPS detection function.

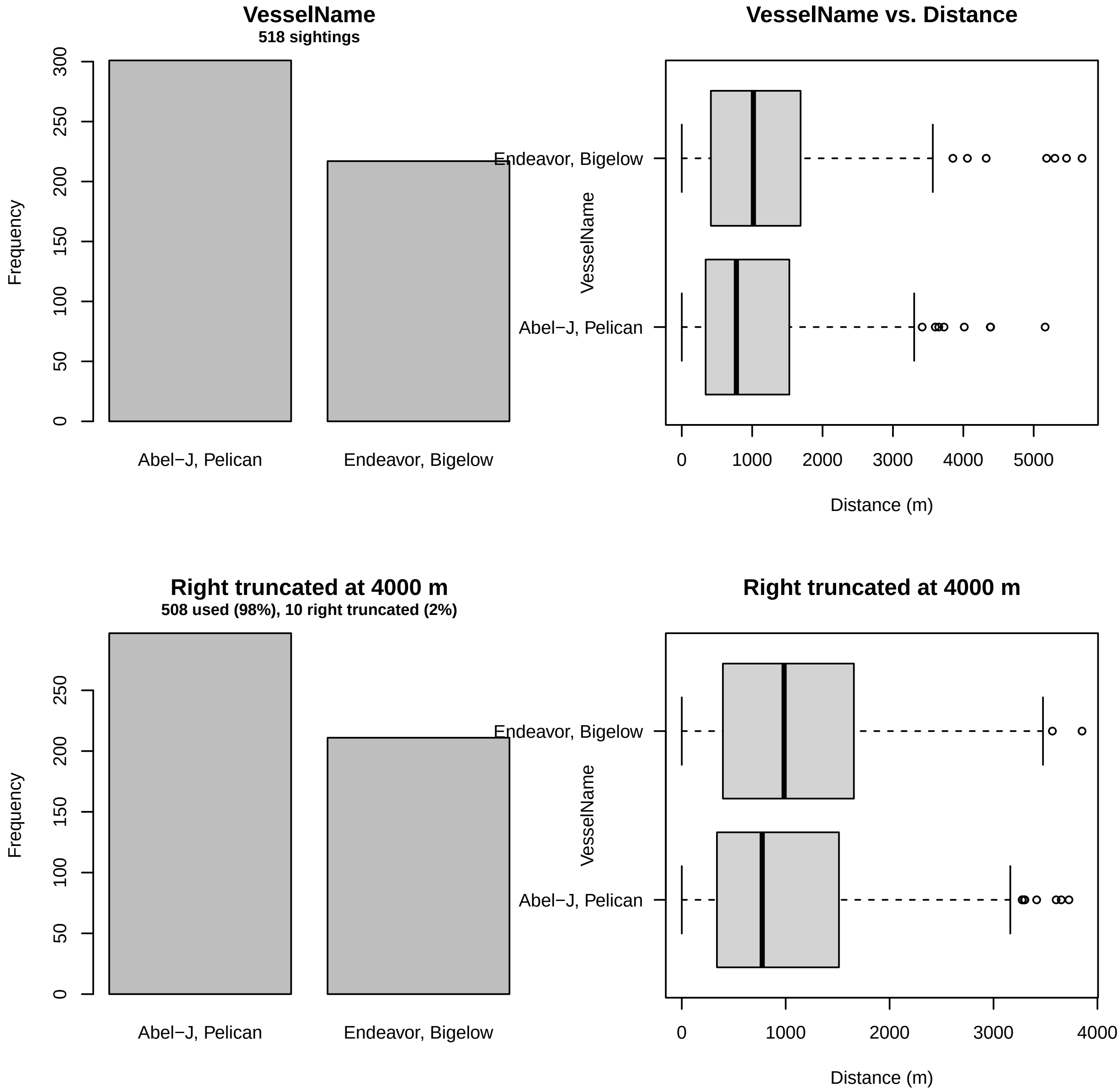

Figure 15: Distribution of the VesselName covariate before (top row) and after (bottom row) observations were truncated to fit the NEFSC Pre-AMAPPS detection function.

2.1.2.2 NEFSC AMAPPS

After right-truncating observations greater than 6000 m, we fitted the detection function to the 857 observations that remained (Table 7). The selected detection function (Figure 16) used a hazard rate key function with Beaufort (Figure 17) and ScientificName (Figure 18) as covariates.

Table 7: Observations used to fit the NEFSC AMAPPS detection function.

ScientificName	n
Delphinus, Lagenorhynchus	358
Other Stenella, Lagenodelphis	175
Stenella frontalis	53
Tursiops, Steno	271
Total	**857**

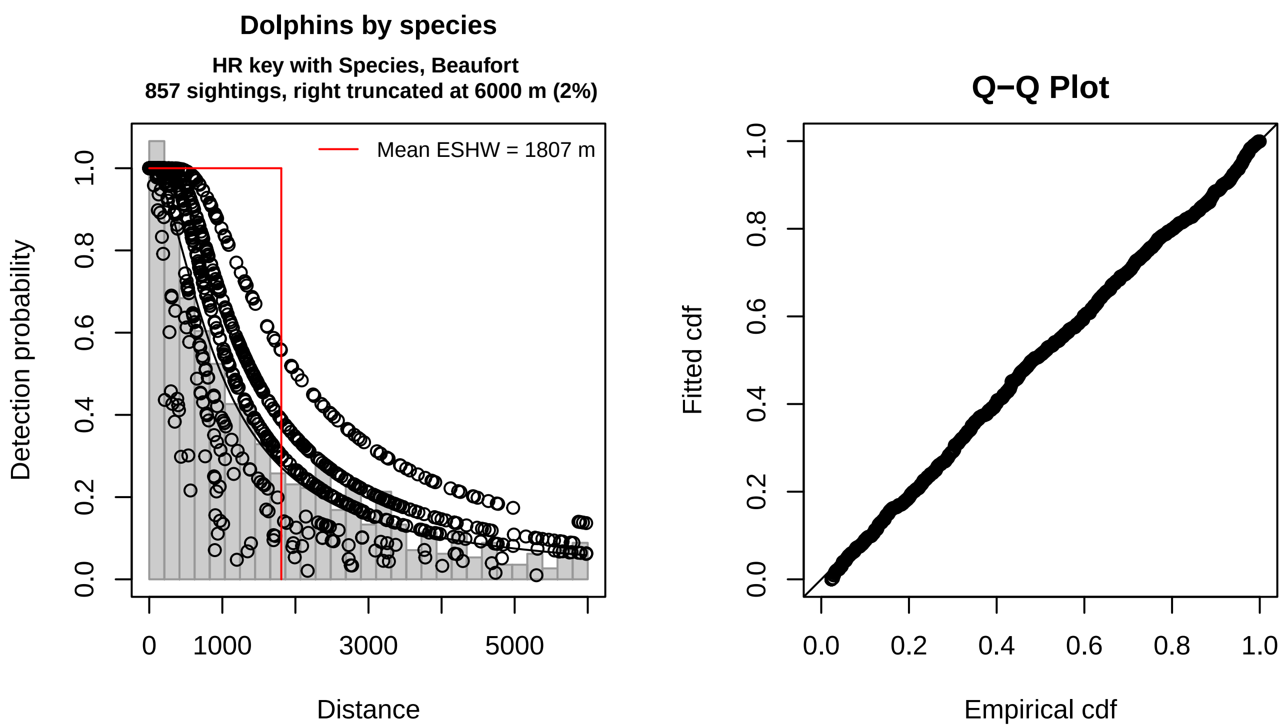

Figure 16: NEFSC AMAPPS detection function and Q-Q plot showing its goodness of fit.

Statistical output for this detection function:

```
Summary for ds object
Number of observations :  857
Distance range         :  0  -  6000
AIC                    :  14222.66

Detection function:
 Hazard-rate key function

Detection function parameters
Scale coefficient(s):
                                              estimate        se
(Intercept)                                  7.0022801 0.1342692
ScientificNameOther Stenella, Lagenodelphis  0.3515378 0.1854896
ScientificNameStenella frontalis            -0.5910499 0.3033455
ScientificNameTursiops, Steno               -0.2176361 0.1602756
Beaufort3-4                                 -0.5842019 0.1839783
Beaufort4-5                                 -1.4374209 0.2667762

Shape coefficient(s):
            estimate        se
```

```
(Intercept) 0.356339 0.0663051

                        Estimate           SE         CV
Average p              0.2624967   0.01868208 0.07117073
N in covered region 3264.8026106 252.27662296 0.07727163

Distance sampling Cramer-von Mises test (unweighted)
Test statistic = 0.089267  p = 0.640081
```

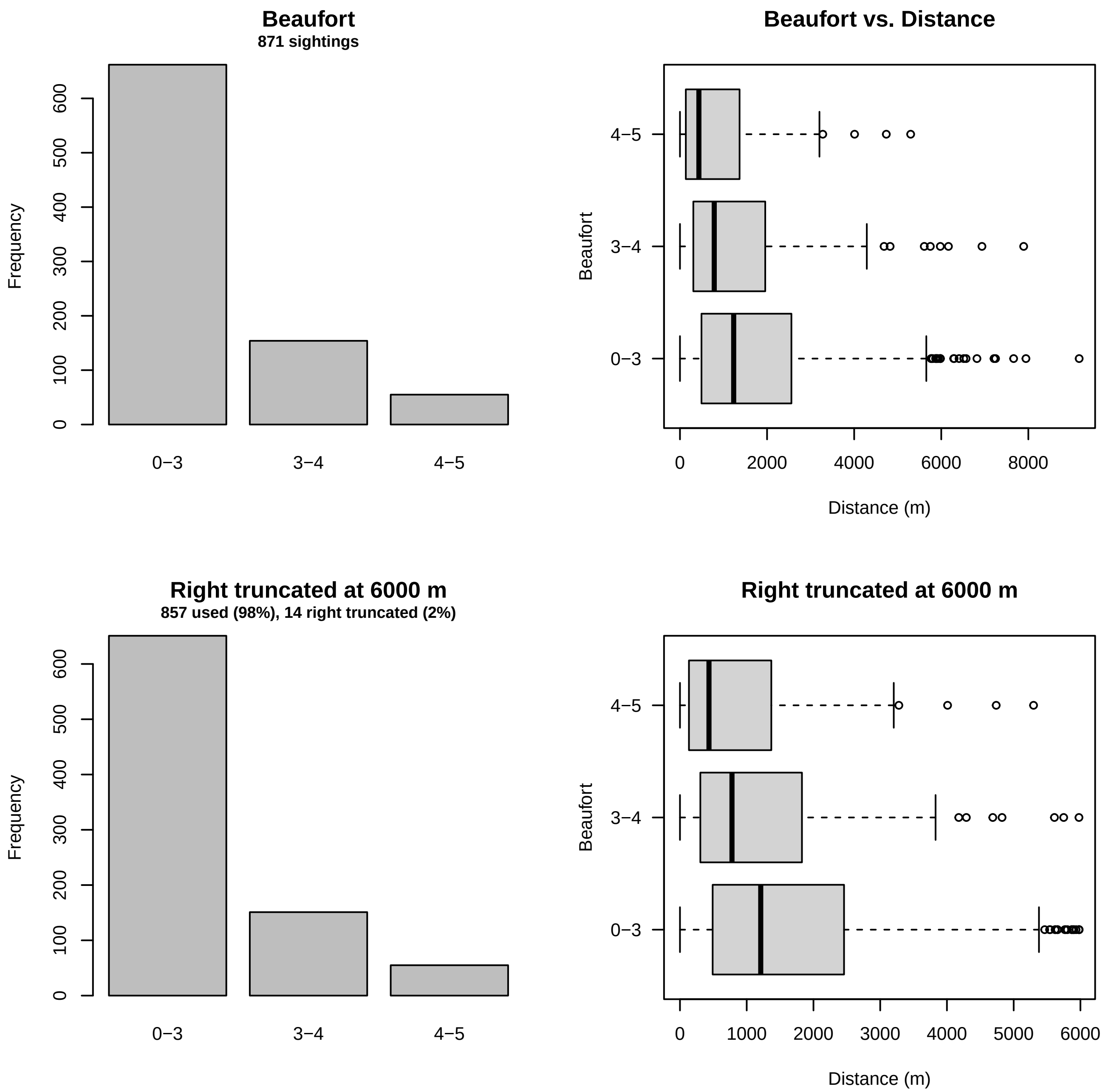

Figure 17: Distribution of the Beaufort covariate before (top row) and after (bottom row) observations were truncated to fit the NEFSC AMAPPS detection function.

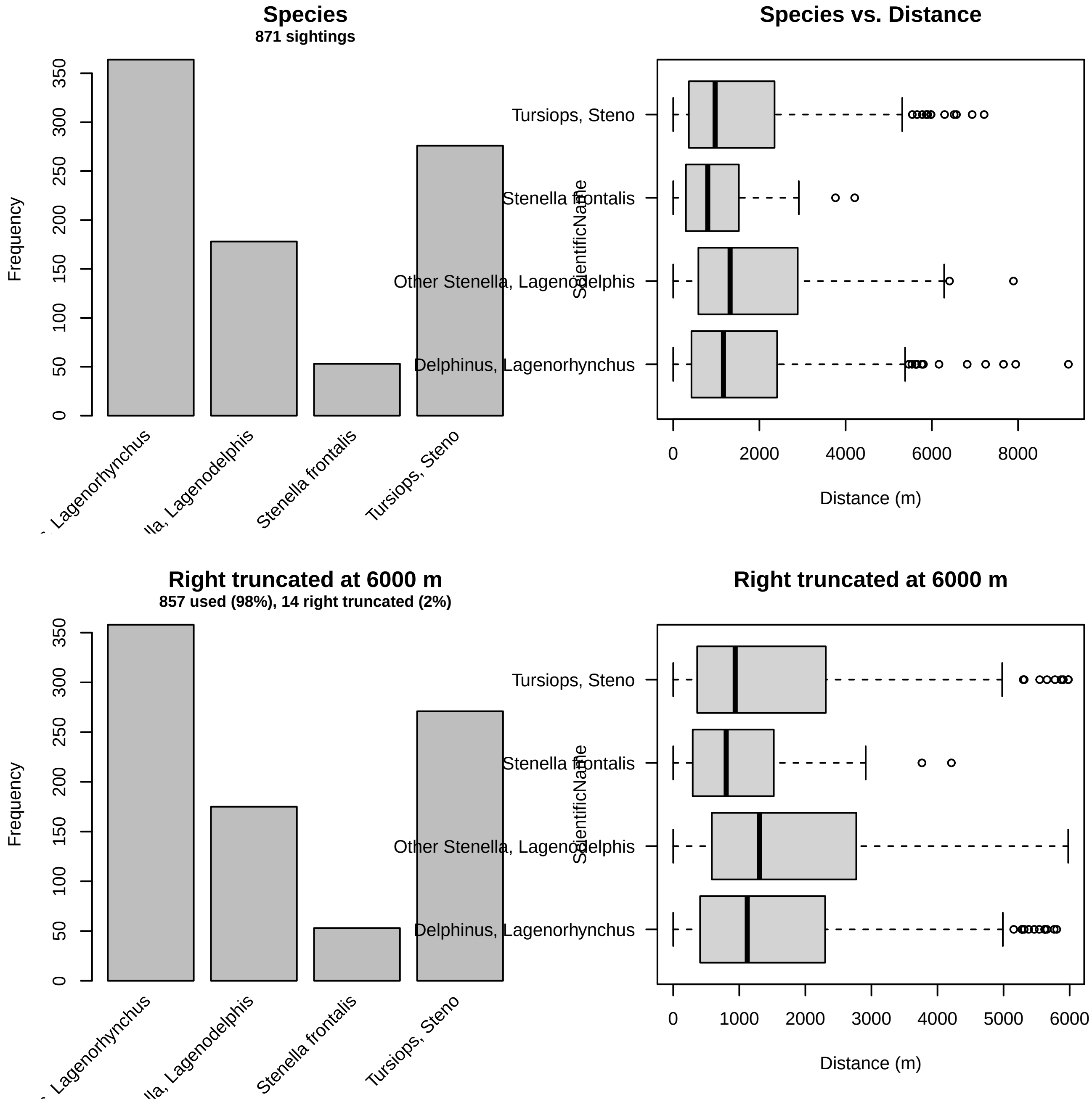

Figure 18: Distribution of the ScientificName covariate before (top row) and after (bottom row) observations were truncated to fit the NEFSC AMAPPS detection function.

2.1.2.3 Song of the Whale

After right-truncating observations greater than 700 m and left-truncating observations less than 1 m (Figure 20), we fitted the detection function to the 360 observations that remained (Table 8). The selected detection function (Figure 19) used a hazard rate key function with Beaufort (Figure 21), ScientificName (Figure 22) and Visibility (Figure 23) as covariates.

Table 8: Observations used to fit the Song of the Whale detection function.

ScientificName	n
All others	211
Delphinus	149
Total	**360**

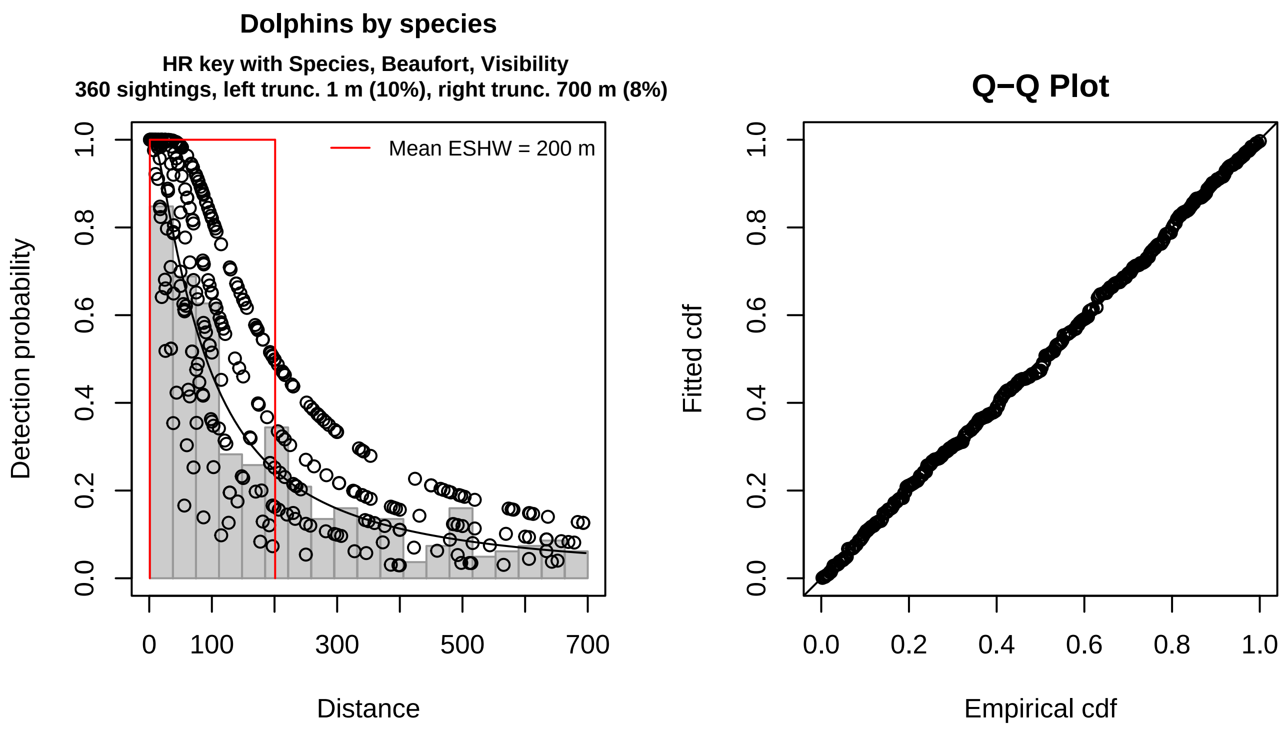

Figure 19: Song of the Whale detection function and Q-Q plot showing its goodness of fit.

Statistical output for this detection function:

```
Summary for ds object
Number of observations :  360
Distance range         :  1  -  700
AIC                    :  4434.06

Detection function:
 Hazard-rate key function

Detection function parameters
Scale coefficient(s):
                              estimate        se
(Intercept)                  5.0168382 0.2118228
ScientificNameDelphinus     -0.3746003 0.2526245
Beaufort3                   -0.6586604 0.2922112
Beaufort3.5-4               -1.3223280 0.3841776
VisibilityModerate (2-5nmi) -0.9687696 0.4363084

Shape coefficient(s):
             estimate         se
(Intercept) 0.2728327 0.09542948

                       Estimate           SE        CV
Average p              0.232512   0.02944422 0.1266352
N in covered region 1548.306965 209.54903632 0.1353408

Distance sampling Cramer-von Mises test (unweighted)
Test statistic = 0.019198  p = 0.997687
```

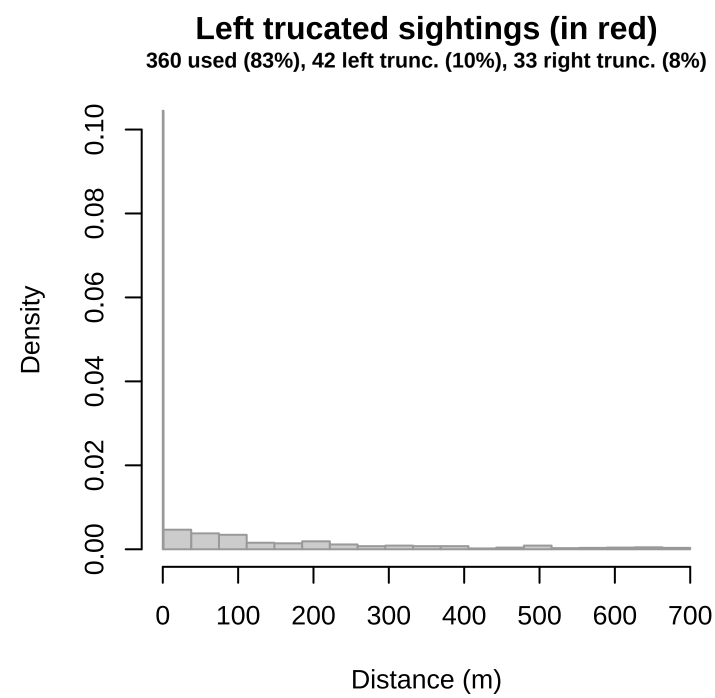

Figure 20: Density histogram of observations used to fit the Song of the Whale detection function, with the left-most bar showing observations at distances less than 1 m, which were left-truncated and not used to fit the detection function. (This bar may be very short if there were very few left-truncated sightings, or very narrow if the left truncation distance was very small; in either case it may not appear red.) These were excluded because they formed a problematic "spike" in detections close to the trackline, suggesting that animals approached the vessel (e.g. to bow-ride) prior to being detected. To address this, we fitted the detection function to the observations beyond the spike and assumed that within it, detection probability was 1, effectively treating it like a strip transect. We then added the left-truncated observations back into the analysis as if they occurred in this strip. This treatment may have resulted in an underestimation of detection probability.

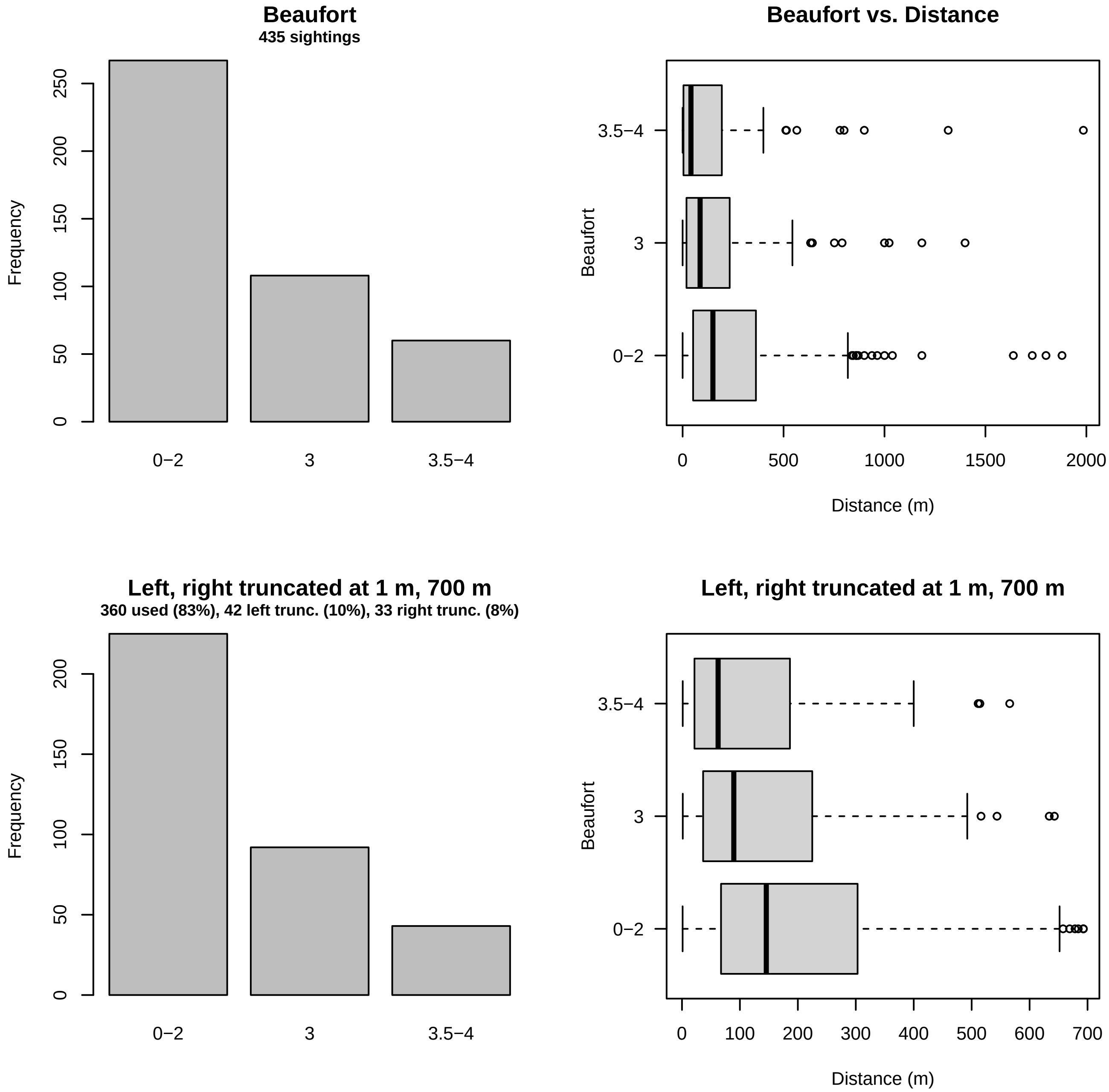

Figure 21: Distribution of the Beaufort covariate before (top row) and after (bottom row) observations were truncated to fit the Song of the Whale detection function.

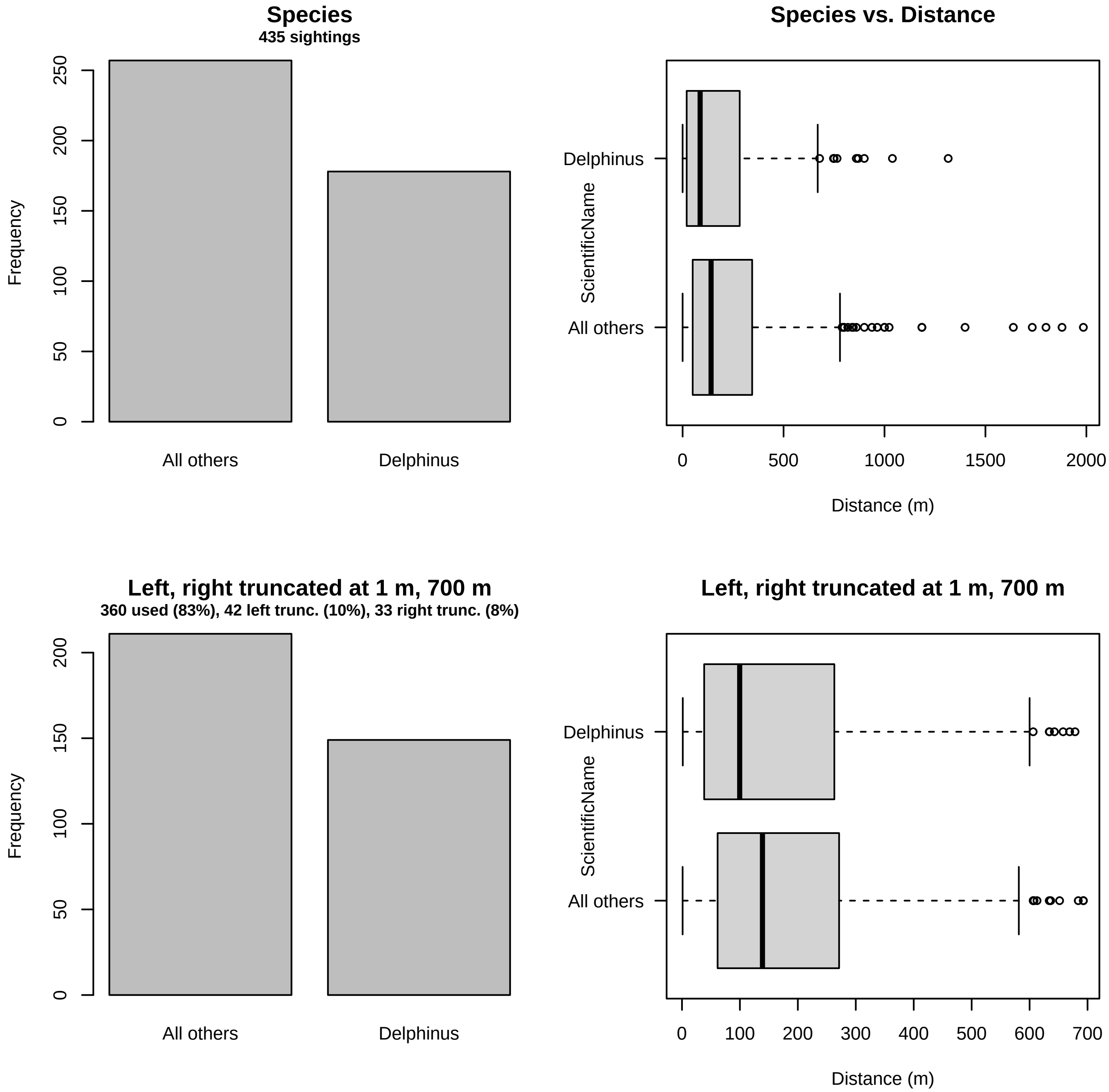

Figure 22: Distribution of the ScientificName covariate before (top row) and after (bottom row) observations were truncated to fit the Song of the Whale detection function.

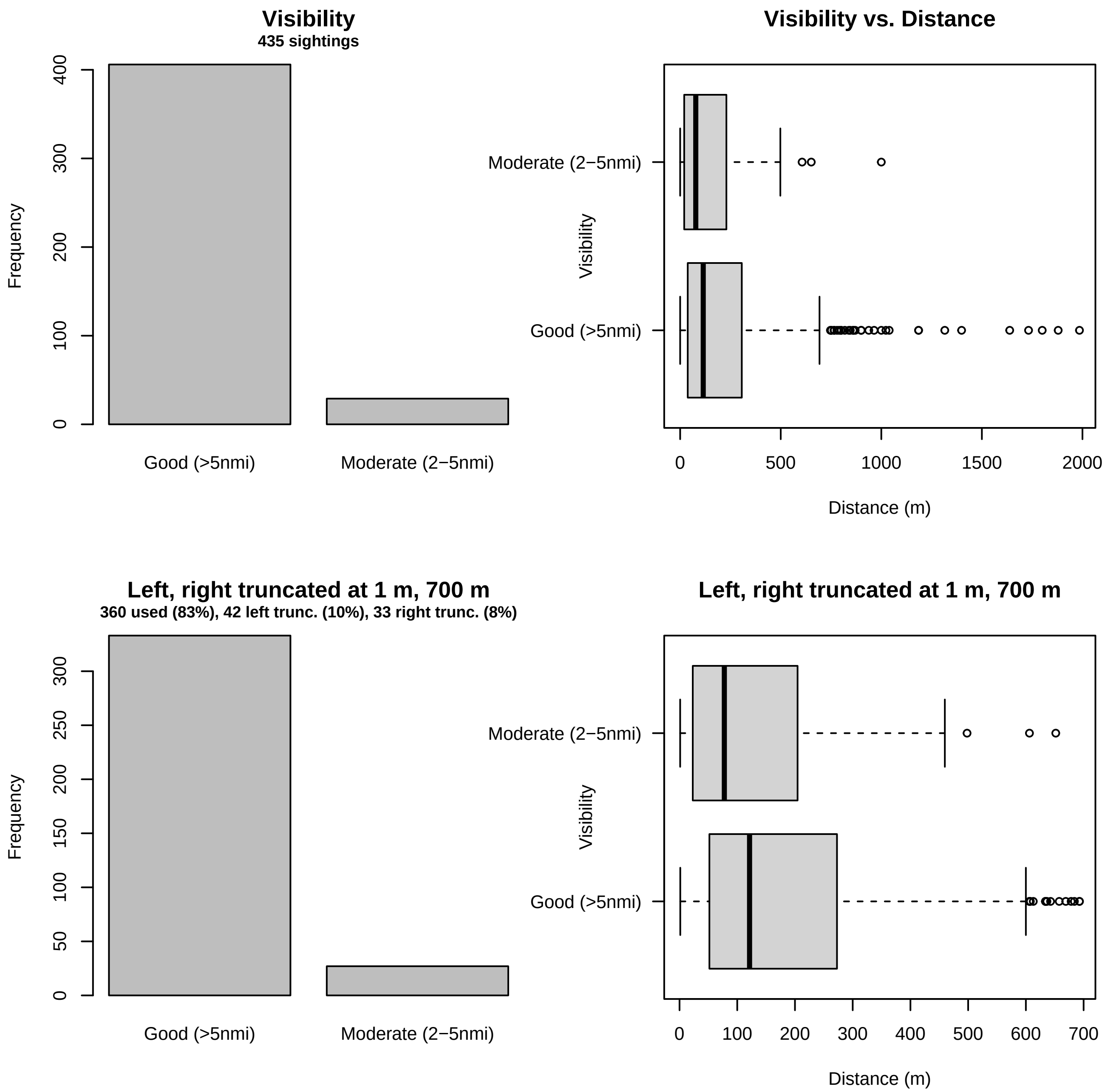

Figure 23: Distribution of the Visibility covariate before (top row) and after (bottom row) observations were truncated to fit the Song of the Whale detection function.

2.2 Without a Taxonomic Covariate

We fitted the detection functions in this section to pools of species with similar detectability characteristics but could not use a taxonomic identification as a covariate to account for differences between them. We usually took this approach after trying the taxonomic covariate and finding it had insufficient statistical power to be retained. We also resorted to it when the focal taxon being modeled had too few observations to be allocated its own taxonomic covariate level and was too poorly known for us to confidently determine which other taxa we could group it with.

2.2.1 Aerial Surveys

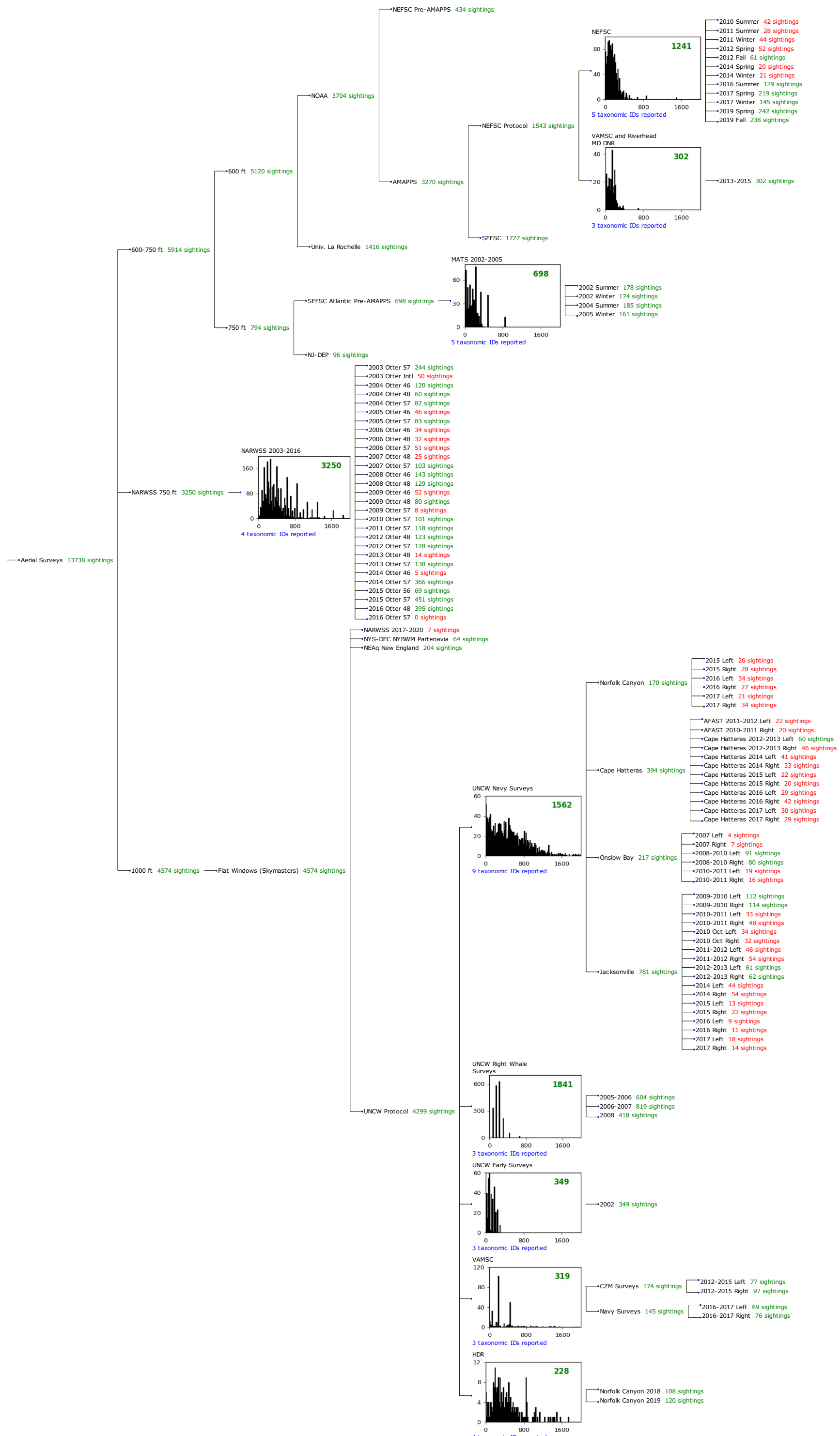

Figure 24: Detection hierarchy for aerial surveys, showing how they were pooled during detectability modeling, for detection functions that pooled multiple taxa but could not use a taxonomic covariate to account for differences between them. Each histogram represents a detection function and summarizes the perpendicular distances of observations that were pooled to fit it, prior to truncation. Observation counts, also prior to truncation, are shown in green when they met the recommendation of Buckland et al. (2001) that detection functions utilize at least 60 sightings, and red otherwise. For rare taxa, it was not always possible to meet this recommendation, yielding higher statistical uncertainty. During the spatial modeling stage of the analysis, effective strip widths were computed for each survey using the closest detection function above it in the hierarchy (i.e. moving from right to left in the figure). Surveys that do not have a detection function above them in this figure were either addressed by a detection function presented in a different section of this report, or were omitted from the analysis.

2.2.1.1 NEFSC AMAPPS

After right-truncating observations greater than 600 m, we fitted the detection function to the 1218 observations that remained (Table 9). The selected detection function (Figure 25) used a hazard rate key function with Season (Figure 26) as a covariate.

Table 9: Observations used to fit the NEFSC AMAPPS detection function.

ScientificName	n
Delphinus delphis	817
Lagenorhynchus acutus	280
Lagenorhynchus albirostris	3
Stenella coeruleoalba	13
Tursiops truncatus	105
Total	**1218**

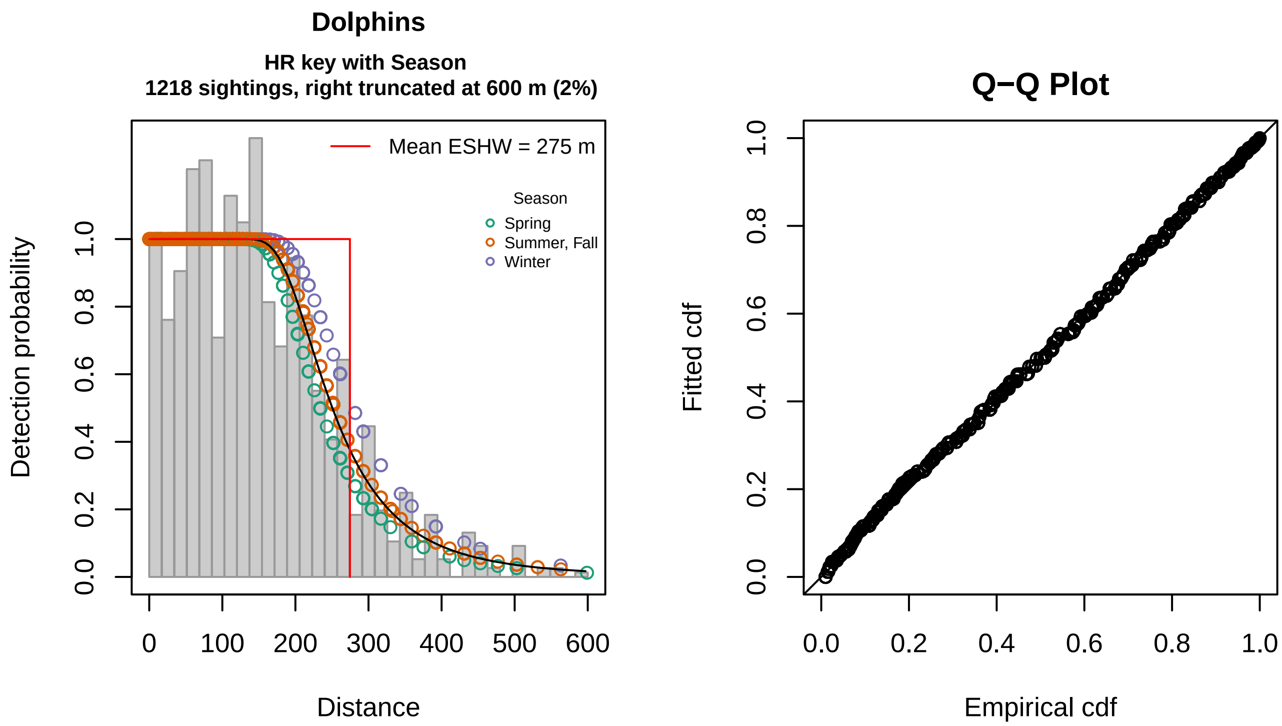

Figure 25: NEFSC AMAPPS detection function and Q-Q plot showing its goodness of fit.

Statistical output for this detection function:

```
Summary for ds object
Number of observations :  1218
Distance range         :  0  -  600
AIC                    :  14460.69

Detection function:
 Hazard-rate key function

Detection function parameters
Scale coefficient(s):
                    estimate         se
(Intercept)       5.36944749 0.04422696
SeasonSummer, Fall 0.08083579 0.04638562
SeasonWinter      0.17600218 0.07702020
```

```
Shape coefficient(s):
            estimate       se
(Intercept) 1.452854 0.065484

                       Estimate          SE         CV
Average p              0.456561  0.00970389 0.02125431
N in covered region 2667.770370 79.97999993 0.02998009

Distance sampling Cramer-von Mises test (unweighted)
Test statistic = 0.126854  p = 0.468488
```

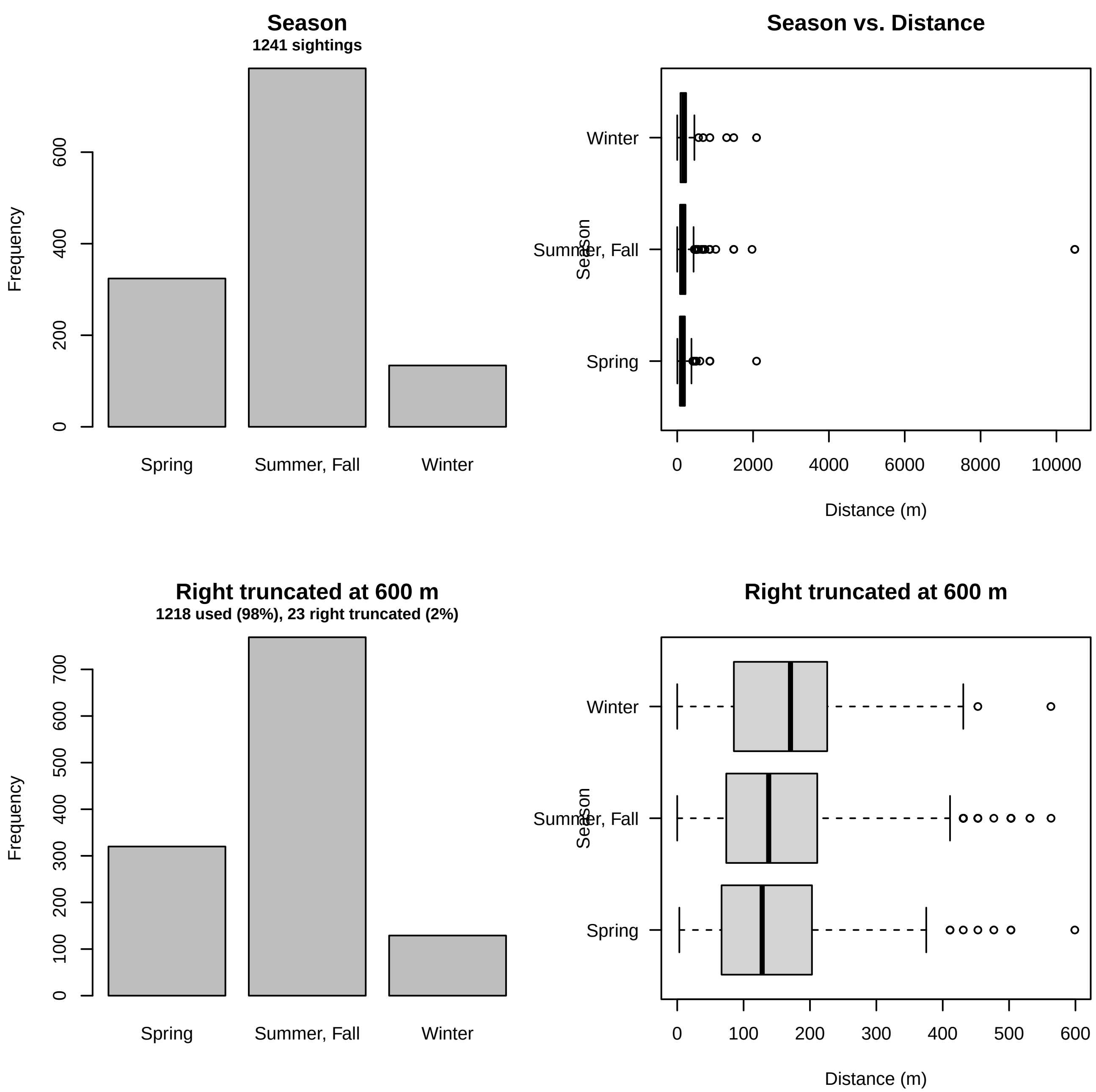

Figure 26: Distribution of the Season covariate before (top row) and after (bottom row) observations were truncated to fit the NEFSC AMAPPS detection function.

2.2.1.2 VAMSC and Riverhead MD DNR

After right-truncating observations greater than 400 m, we fitted the detection function to the 301 observations that remained (Table 10). The selected detection function (Figure 27) used a hazard rate key function with no covariates.

Table 10: Observations used to fit the VAMSC and Riverhead MD DNR detection function.

ScientificName	n
Delphinus delphis	22
Stenella frontalis	1
Tursiops truncatus	278
Total	**301**

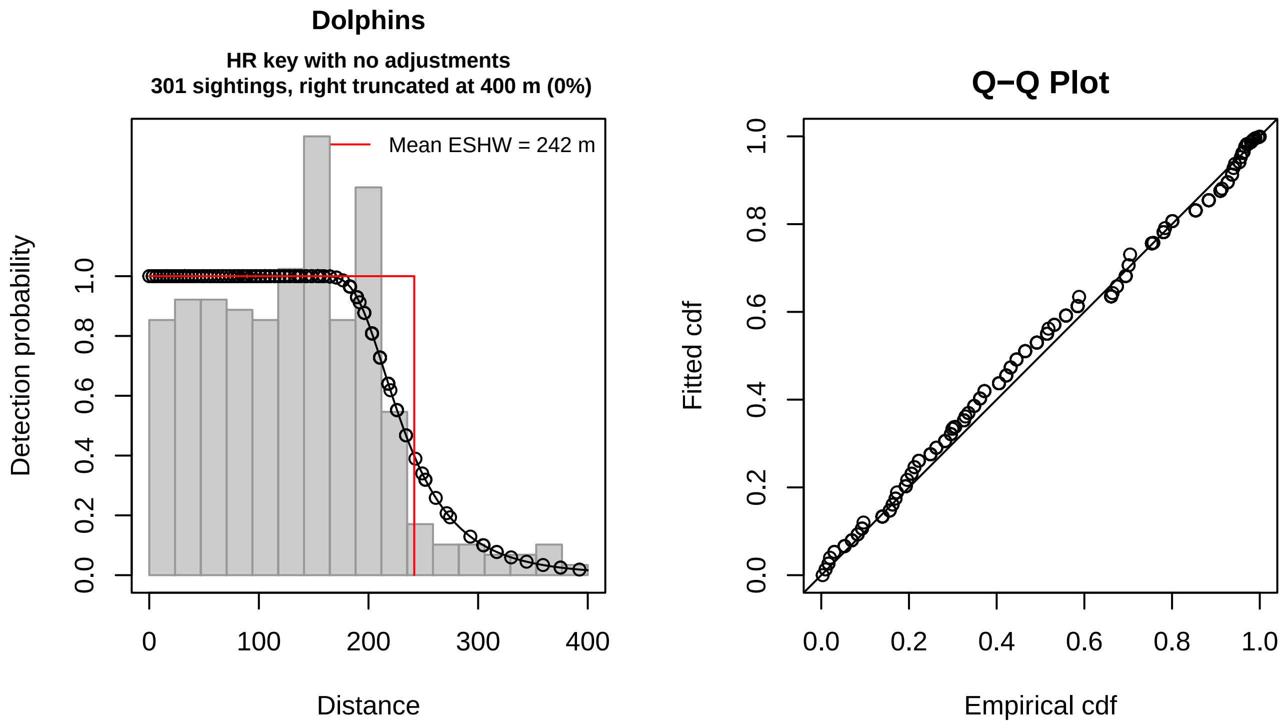

Figure 27: VAMSC and Riverhead MD DNR detection function and Q-Q plot showing its goodness of fit.

Statistical output for this detection function:

```
Summary for ds object
Number of observations :  301
Distance range         :  0  -  400
AIC                    :  3426.124

Detection function:
 Hazard-rate key function

Detection function parameters
Scale coefficient(s):
            estimate         se
(Intercept) 5.388208 0.04209556

Shape coefficient(s):
            estimate        se
(Intercept)  1.91525 0.1331166
```

```
                         Estimate          SE         CV
Average p              0.6042969  0.0203517 0.03367831
N in covered region 498.0995265 24.6489147 0.04948592

Distance sampling Cramer-von Mises test (unweighted)
Test statistic = 0.302011  p = 0.133421
```

2.2.1.3 MATS 2002-2005

After right-truncating observations greater than 629 m, we fitted the detection function to the 684 observations that remained (Table 11). The selected detection function (Figure 28) used a hazard rate key function with Beaufort (Figure 29) as a covariate.

Table 11: Observations used to fit the MATS 2002-2005 detection function.

ScientificName	n
Delphinus delphis	2
Stenella attenuata	2
Stenella frontalis	104
Tursiops truncatus	576
Total	**684**

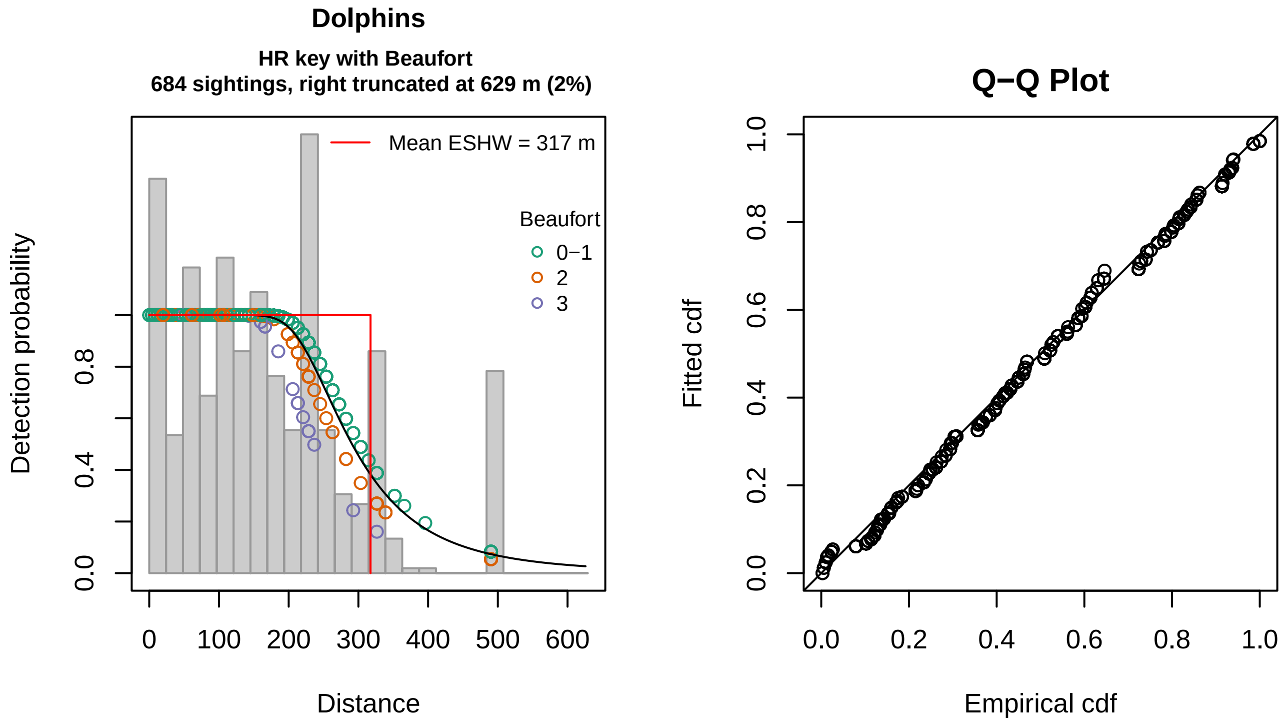

Figure 28: MATS 2002-2005 detection function and Q-Q plot showing its goodness of fit.

Statistical output for this detection function:

```
Summary for ds object
Number of observations :  684
Distance range         :  0  -  629
AIC                    :  8306.088

Detection function:
```

```
 Hazard-rate key function

Detection function parameters
Scale coefficient(s):
              estimate         se
(Intercept)  5.6213531 0.04325709
Beaufort2   -0.1046854 0.06814971
Beaufort3   -0.2421057 0.13060115

Shape coefficient(s):
            estimate         se
(Intercept) 1.449025 0.08965229

                        Estimate         SE         CV
Average p              0.5026836  0.0147185 0.02927984
N in covered region 1360.6968013 54.2106880 0.03984039

Distance sampling Cramer-von Mises test (unweighted)
Test statistic = 0.194502  p = 0.278380
```

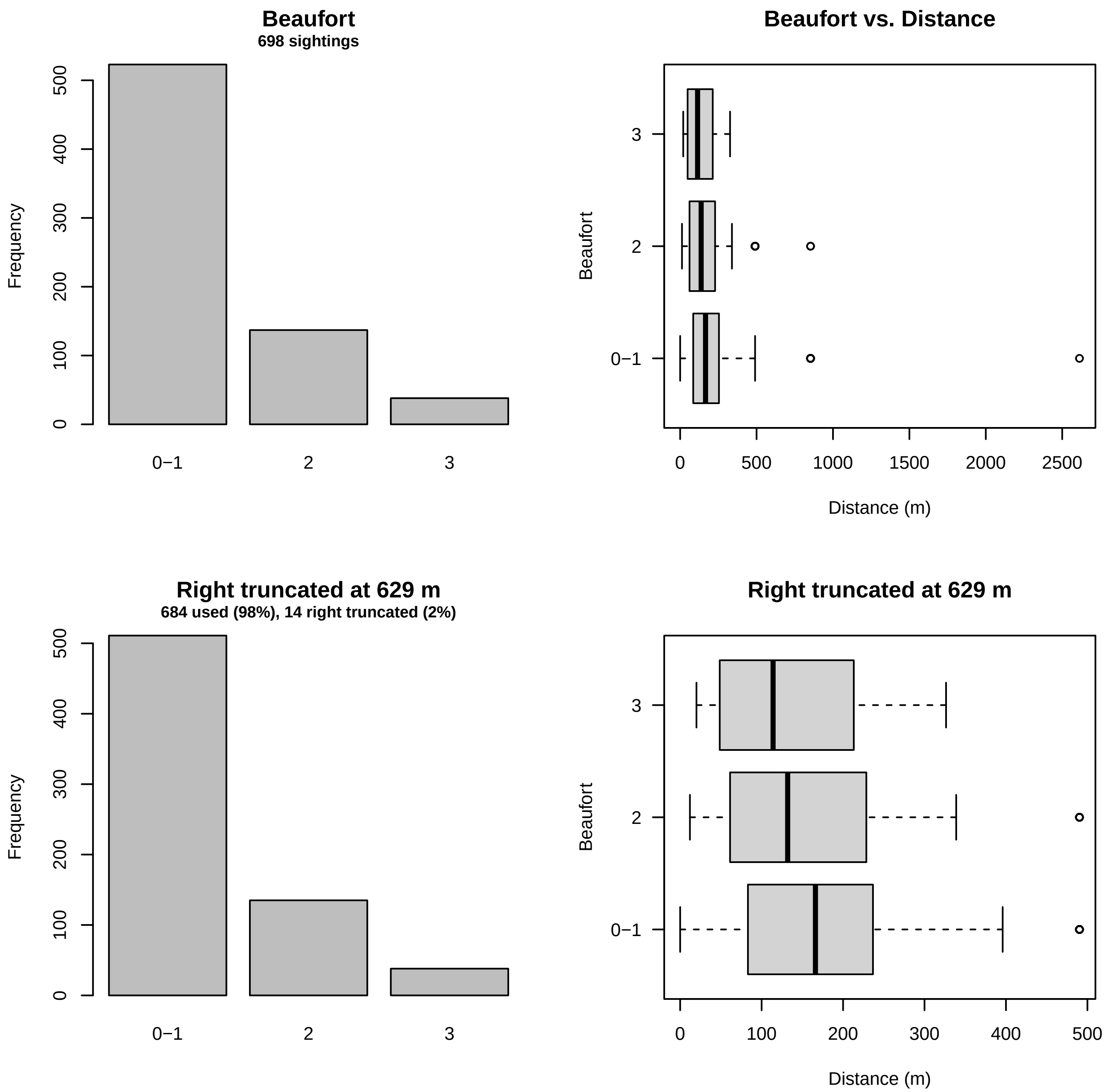

Figure 29: Distribution of the Beaufort covariate before (top row) and after (bottom row) observations were truncated to fit the MATS 2002-2005 detection function.

2.2.1.4 NARWSS 2003-2016

After right-truncating observations greater than 1367 m and left-truncating observations less than 61 m (Figure 31), we fitted the detection function to the 3073 observations that remained (Table 12). The selected detection function (Figure 30) used a hazard rate key function with Beaufort (Figure 32) and Season (Figure 33) as covariates.

Table 12: Observations used to fit the NARWSS 2003-2016 detection function.

ScientificName	n
Delphinus delphis	607
Lagenorhynchus acutus	2404
Lagenorhynchus albirostris	6
Tursiops truncatus	56
Total	**3073**

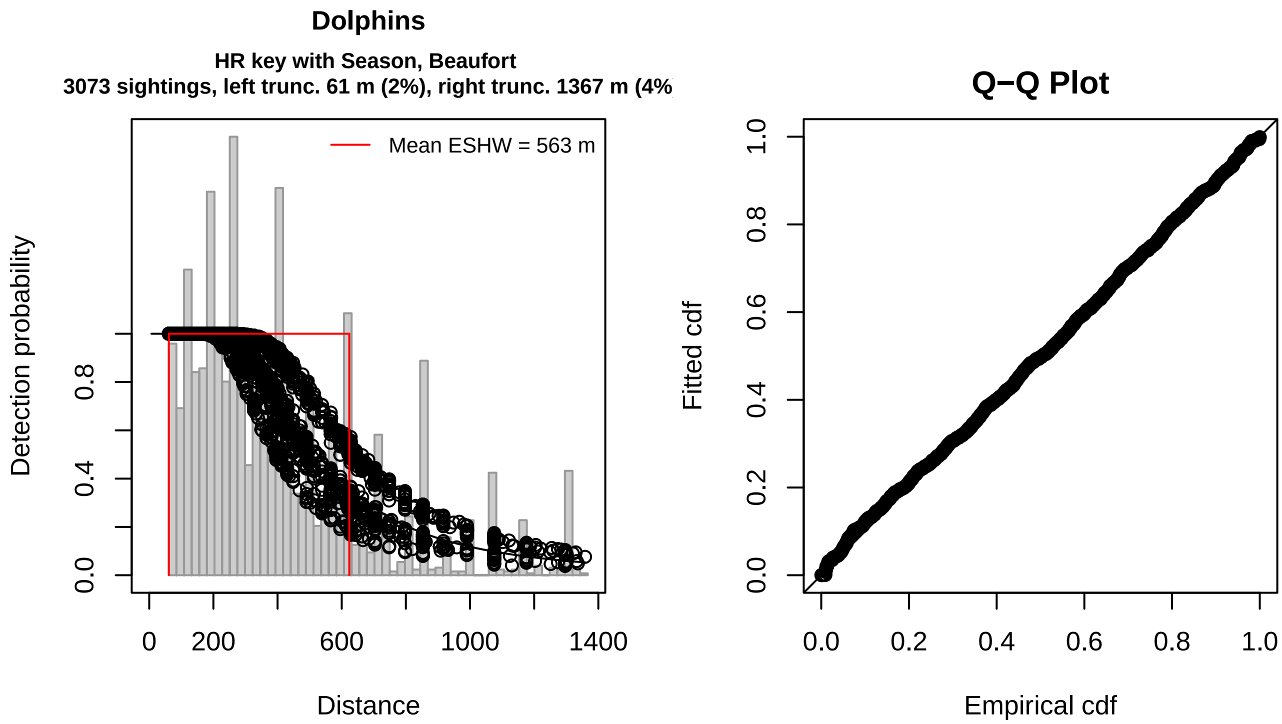

Figure 30: NARWSS 2003-2016 detection function and Q-Q plot showing its goodness of fit.

Statistical output for this detection function:

```
Summary for ds object
Number of observations :  3073
Distance range         :  61  -  1367
AIC                    :  41850.8

Detection function:
 Hazard-rate key function

Detection function parameters
Scale coefficient(s):
                estimate         se
(Intercept)   6.10469263 0.07579397
SeasonSpring  0.06689438 0.05622050
SeasonSummer  0.29278056 0.05383279
SeasonWinter -0.15259970 0.06804643
Beaufort     -0.03572691 0.02383833

Shape coefficient(s):
            estimate        se
(Intercept) 1.009361 0.0398862
```

```
                        Estimate           SE         CV
Average p              0.4196247 8.827249e-03 0.02103606
N in covered region 7323.2113220 1.845410e+02 0.02519946

Distance sampling Cramer-von Mises test (unweighted)
Test statistic = 0.246036  p = 0.193531
```

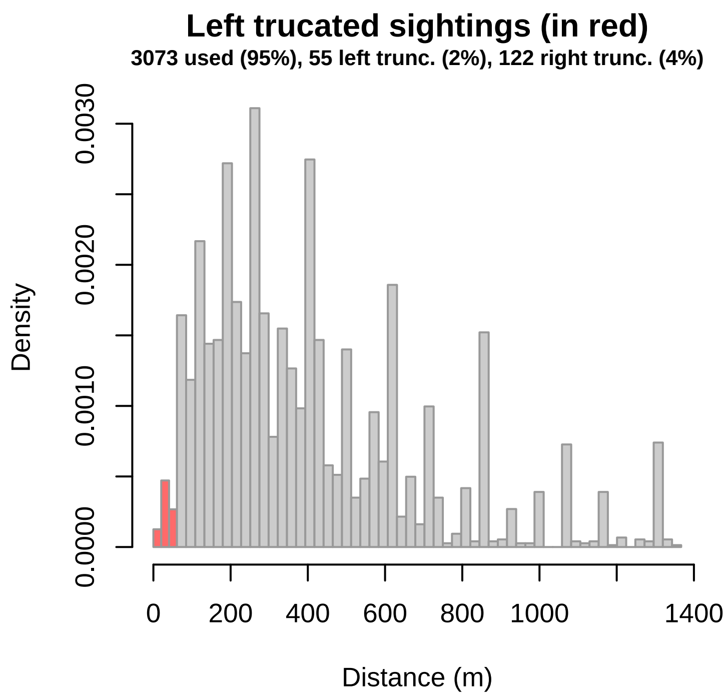

Figure 31: Density histogram of observations used to fit the NARWSS 2003-2016 detection function, with the left-most bar showing observations at distances less than 61 m, which were left-truncated and excluded from the analysis [Buckland et al. (2001)]. (This bar may be very short if there were very few left-truncated sightings, or very narrow if the left truncation distance was very small; in either case it may not appear red.)

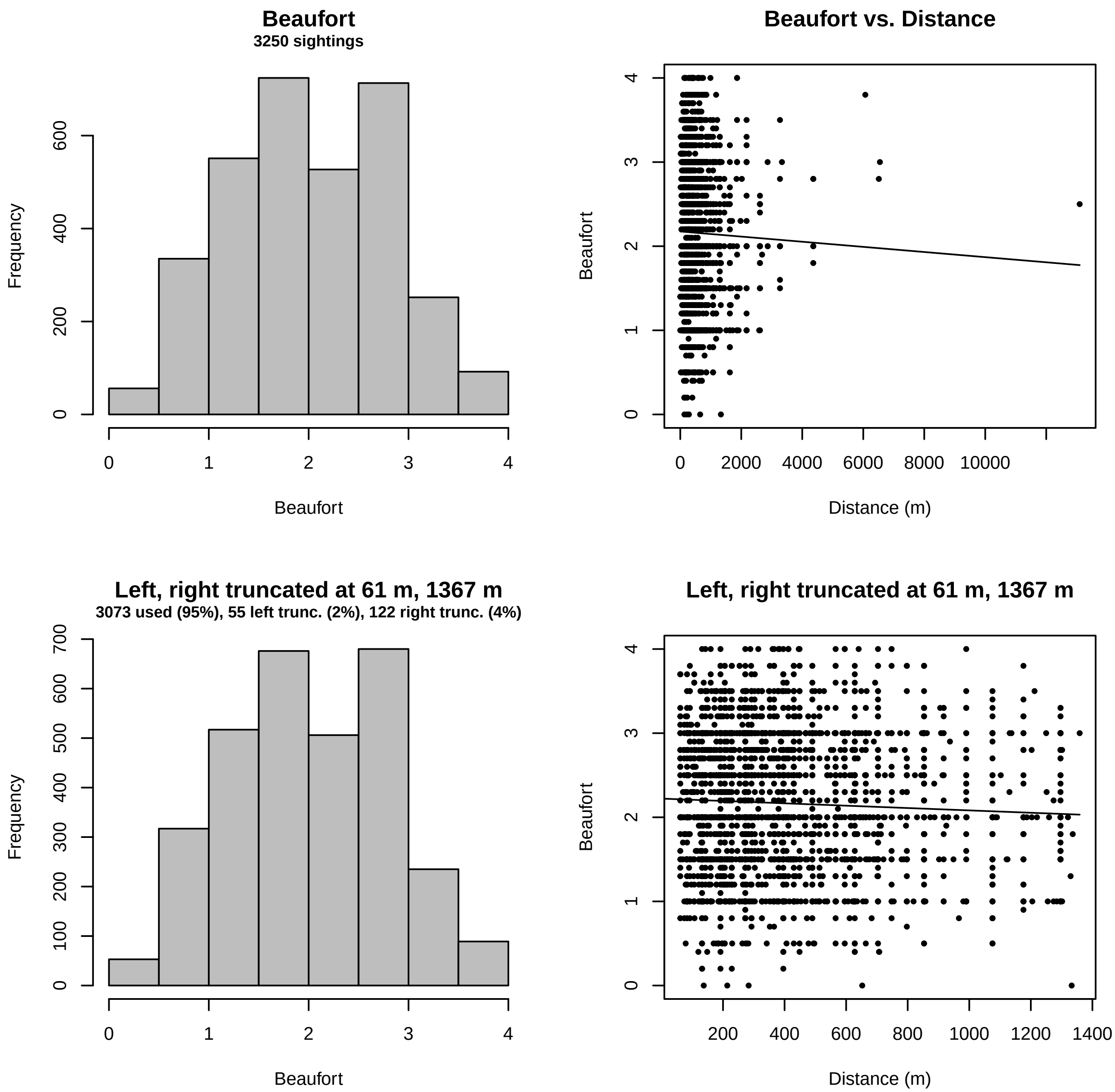

Figure 32: Distribution of the Beaufort covariate before (top row) and after (bottom row) observations were truncated to fit the NARWSS 2003-2016 detection function.

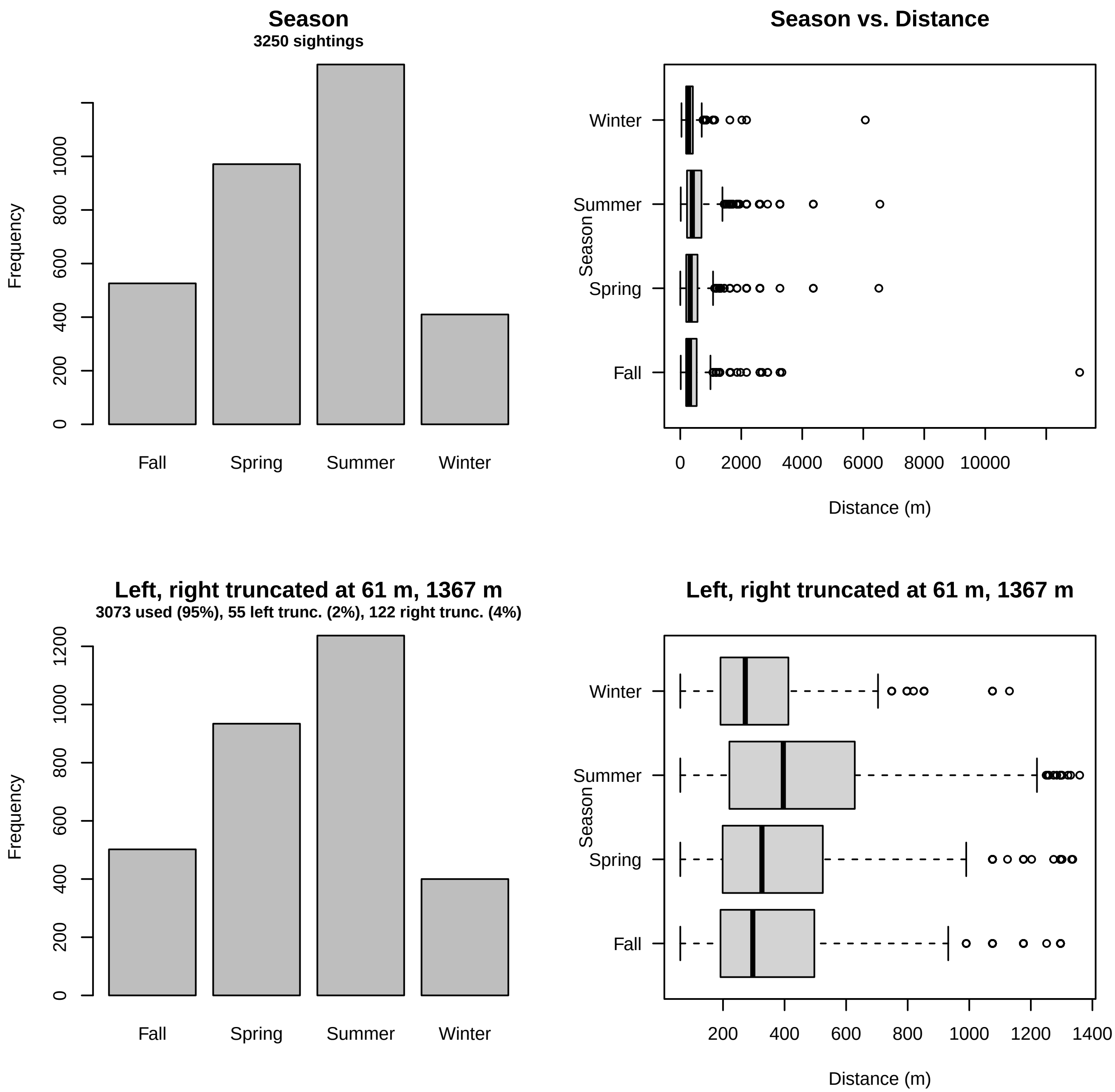

Figure 33: Distribution of the Season covariate before (top row) and after (bottom row) observations were truncated to fit the NARWSS 2003-2016 detection function.

2.2.1.5 UNCW Navy Surveys

After right-truncating observations greater than 1600 m, we fitted the detection function to the 1523 observations that remained (Table 13). The selected detection function (Figure 34) used a half normal key function with Glare (Figure 35) and Visibility (Figure 36) as covariates.

Table 13: Observations used to fit the UNCW Navy Surveys detection function.

ScientificName	n
Delphinus delphis	77
Lagenodelphis hosei	1
Stenella attenuata	2
Stenella clymene	11
Stenella coeruleoalba	19
Stenella frontalis	480
Stenella longirostris	1
Steno bredanensis	14
Tursiops truncatus	918
Total	**1523**

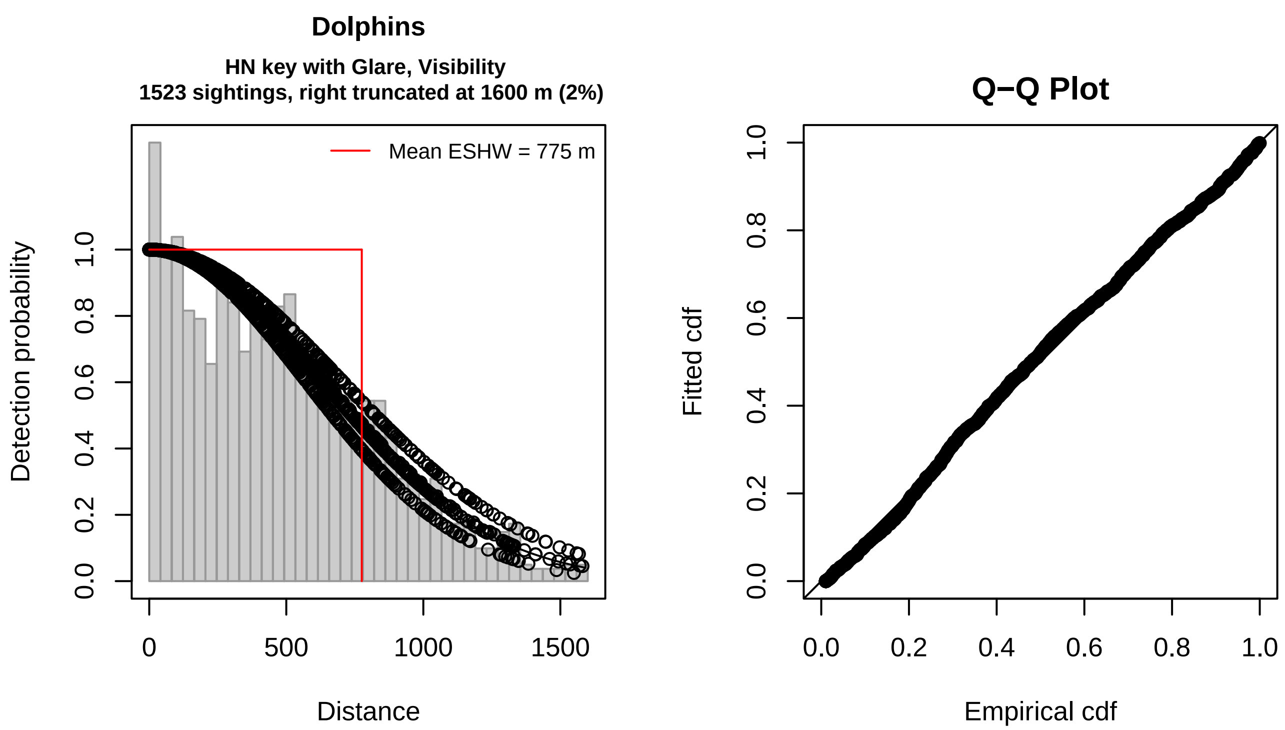

Figure 34: UNCW Navy Surveys detection function and Q-Q plot showing its goodness of fit.

Statistical output for this detection function:

```
Summary for ds object
Number of observations :  1523
Distance range         :  0  -  1600
AIC                    :  21665.78

Detection function:
 Half-normal key function

Detection function parameters
Scale coefficient(s):
                          estimate         se
(Intercept)             6.55223233 0.04798577
GlareNone, 0-25%, Unk. -0.10934970 0.05247015
VisibilityHalf         -0.09759271 0.04601702
```

```
                          Estimate          SE         CV
Average p                0.4827398  0.01003395 0.02078542
N in covered region 3154.9084328 87.71221948 0.02780183

Distance sampling Cramer-von Mises test (unweighted)
Test statistic = 0.331909  p = 0.110182
```

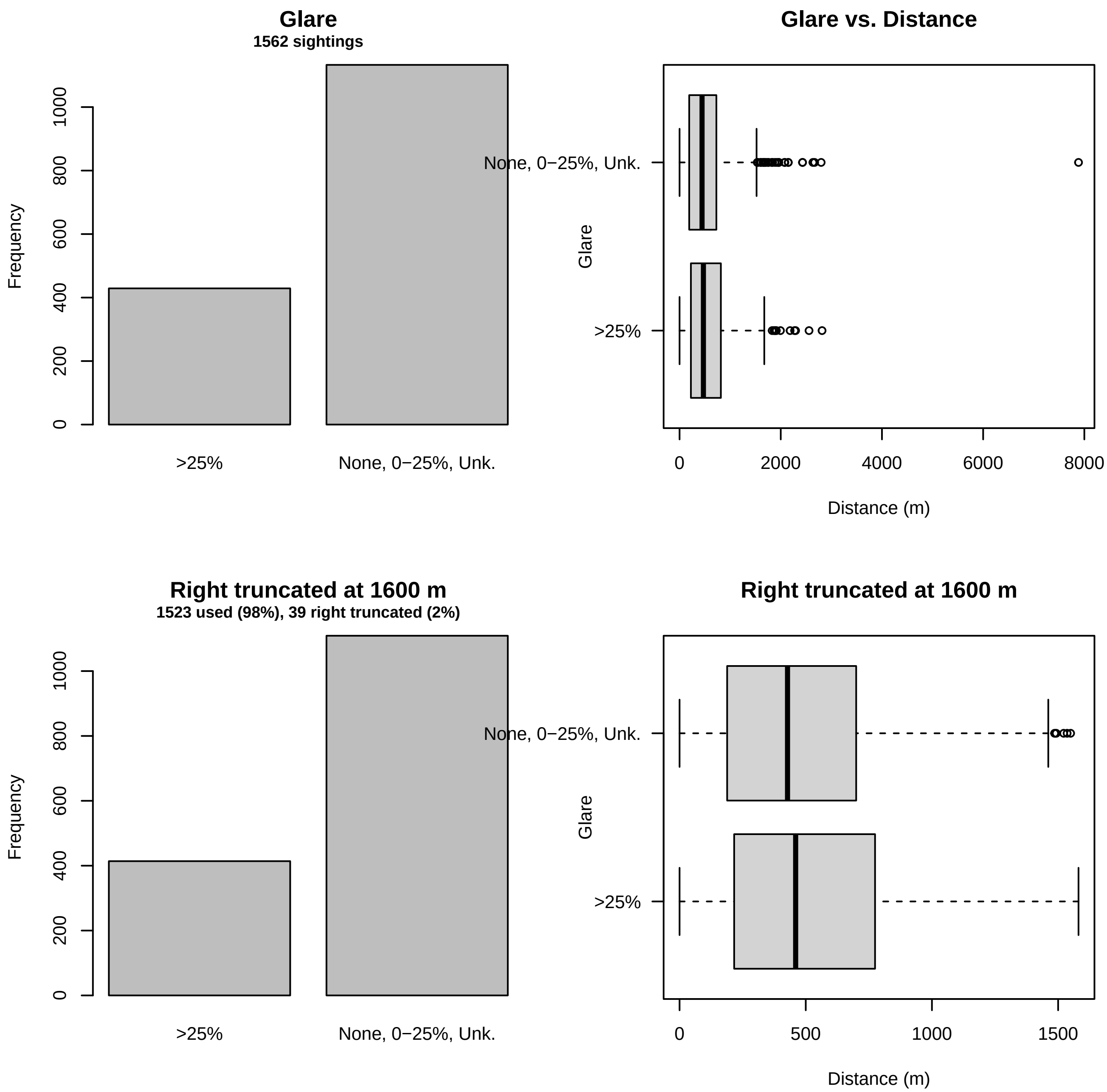

Figure 35: Distribution of the Glare covariate before (top row) and after (bottom row) observations were truncated to fit the UNCW Navy Surveys detection function.

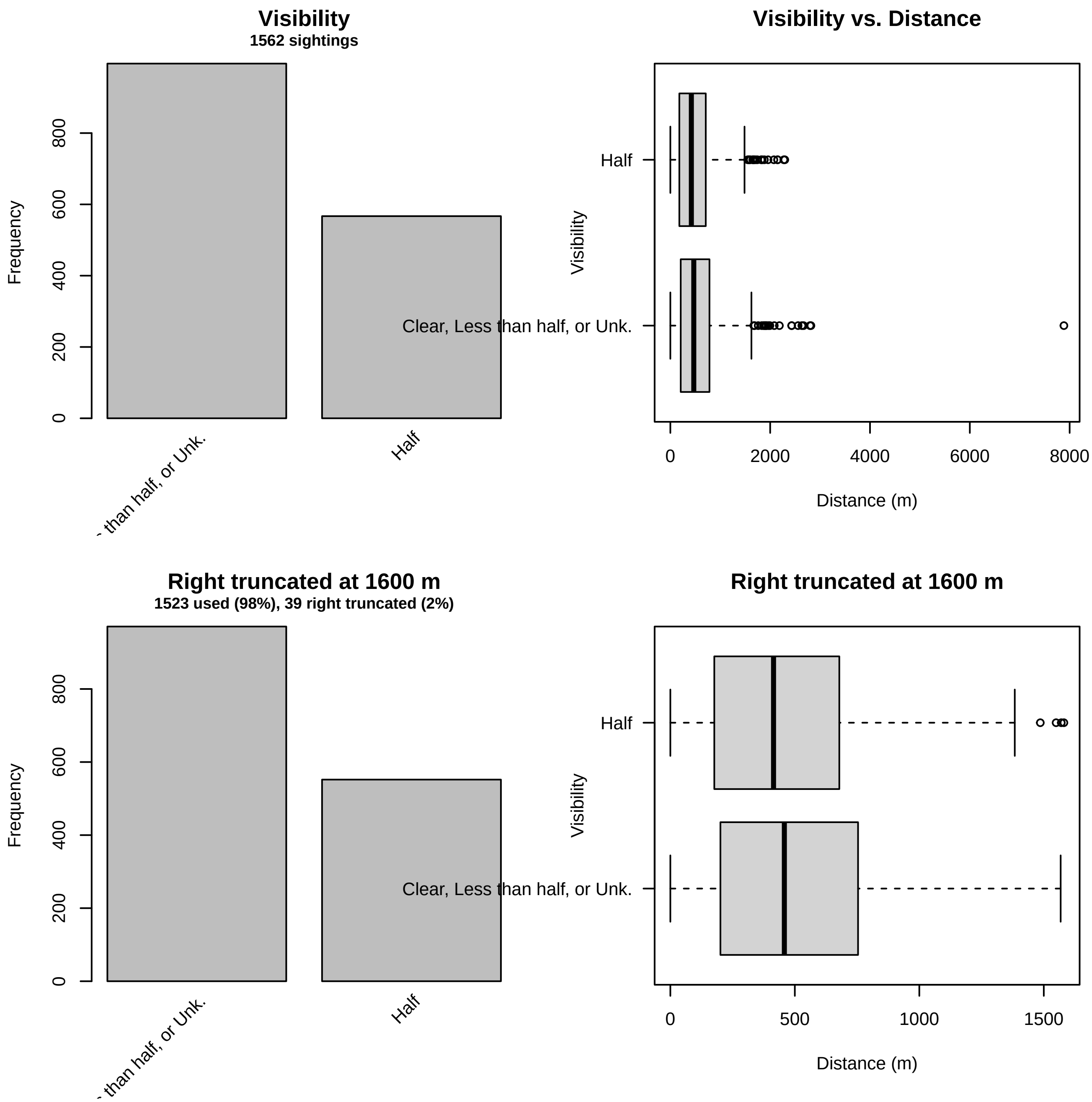

Figure 36: Distribution of the Visibility covariate before (top row) and after (bottom row) observations were truncated to fit the UNCW Navy Surveys detection function.

2.2.1.6 UNCW Right Whale Surveys

After right-truncating observations greater than 528 m and left-truncating observations less than 54 m (Figure 38), we fitted the detection function to the 1821 observations that remained (Table 14). The selected detection function (Figure 37) used a hazard rate key function with no covariates.

Table 14: Observations used to fit the UNCW Right Whale Surveys detection function.

ScientificName	n
Delphinus delphis	26
Stenella frontalis	4
Tursiops truncatus	1791
Total	**1821**

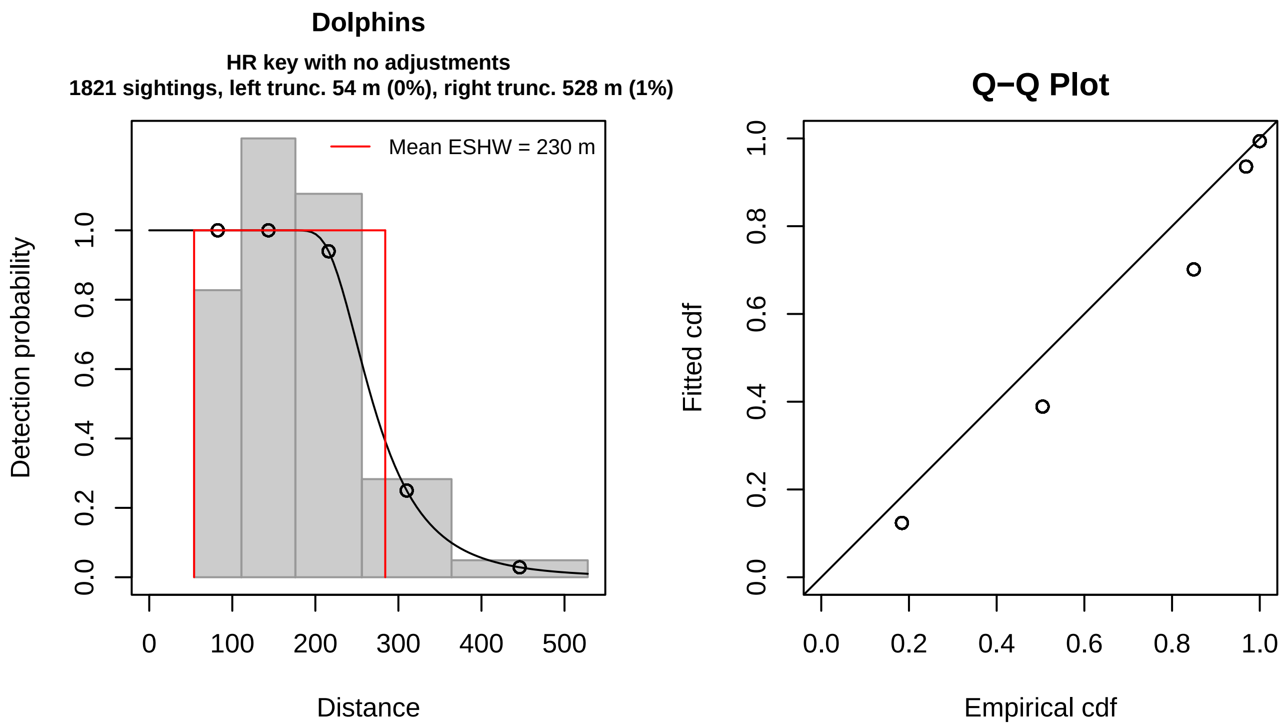

Figure 37: UNCW Right Whale Surveys detection function and Q-Q plot showing its goodness of fit.

Statistical output for this detection function:

```
Summary for ds object
Number of observations :  1821
Distance range         :  54  -  528
AIC                    :  5176.116

Detection function:
 Hazard-rate key function

Detection function parameters
Scale coefficient(s):
            estimate         se
(Intercept) 5.538954 0.02098751

Shape coefficient(s):
            estimate         se
(Intercept) 1.841299 0.06464608

                        Estimate          SE         CV
Average p              0.4855453  0.009233858 0.01901750
N in covered region 3750.4226341 95.188173832 0.02538065
```

```
Distance sampling Cramer-von Mises test (unweighted)
Test statistic = 14.468539  p = 0.010416
```

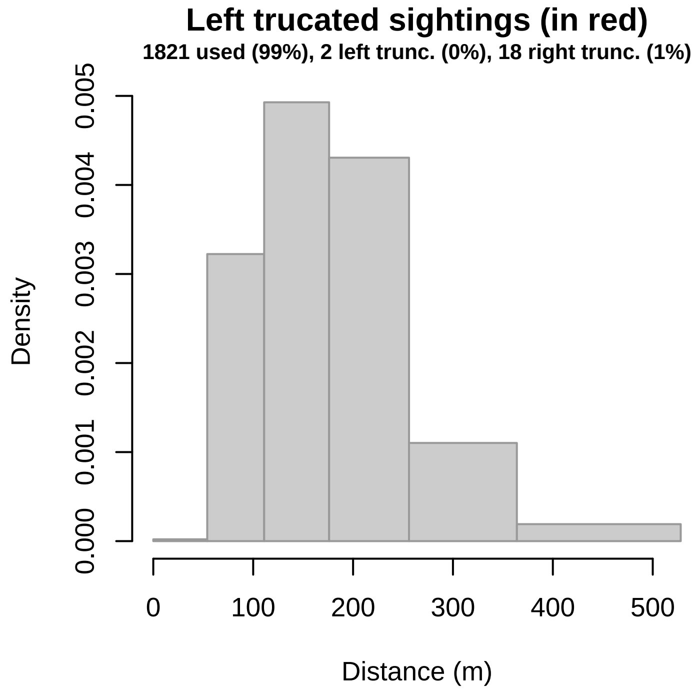

Figure 38: Density histogram of observations used to fit the UNCW Right Whale Surveys detection function, with the left-most bar showing observations at distances less than 54 m, which were left-truncated and excluded from the analysis [Buckland et al. (2001)]. (This bar may be very short if there were very few left-truncated sightings, or very narrow if the left truncation distance was very small; in either case it may not appear red.)

2.2.1.7 UNCW Early Surveys

After right-truncating observations greater than 333 m and left-truncating observations less than 14 m (Figure 40), we fitted the detection function to the 349 observations that remained (Table 15). The selected detection function (Figure 39) used a half normal key function with Beaufort (Figure 41) as a covariate.

Table 15: Observations used to fit the UNCW Early Surveys detection function.

ScientificName	n
Delphinus delphis	5
Stenella frontalis	1
Tursiops truncatus	343
Total	**349**

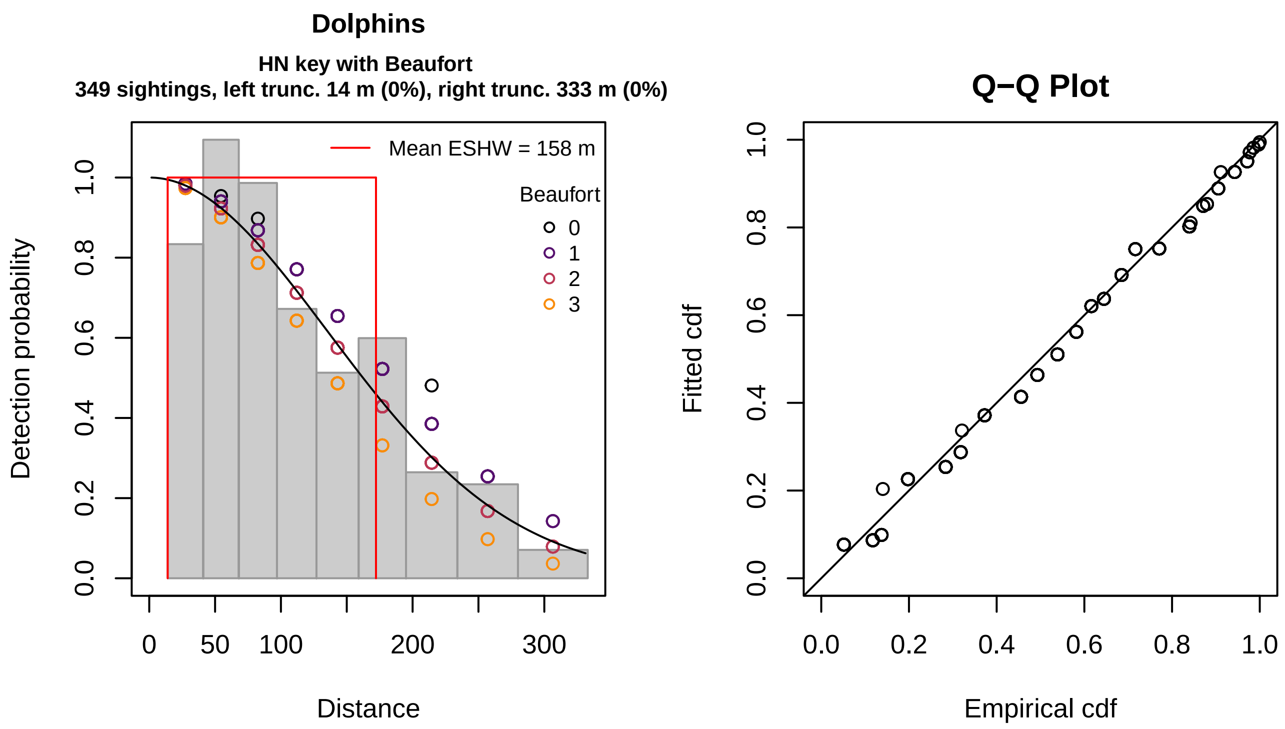

Figure 39: UNCW Early Surveys detection function and Q-Q plot showing its goodness of fit.

Statistical output for this detection function:

```
Summary for ds object
Number of observations :  349
Distance range         :  14  -  333
AIC                    :  1464.597

Detection function:
 Half-normal key function

Detection function parameters
Scale coefficient(s):
              estimate         se
(Intercept)  5.1778911 0.14575211
Beaufort    -0.1325498 0.07066838

                        Estimate          SE         CV
Average p              0.4915207  0.02352103 0.04785360
N in covered region 710.0413079 43.53534195 0.06131382

Distance sampling Cramer-von Mises test (unweighted)
Test statistic = 0.278162  p = 0.155953
```

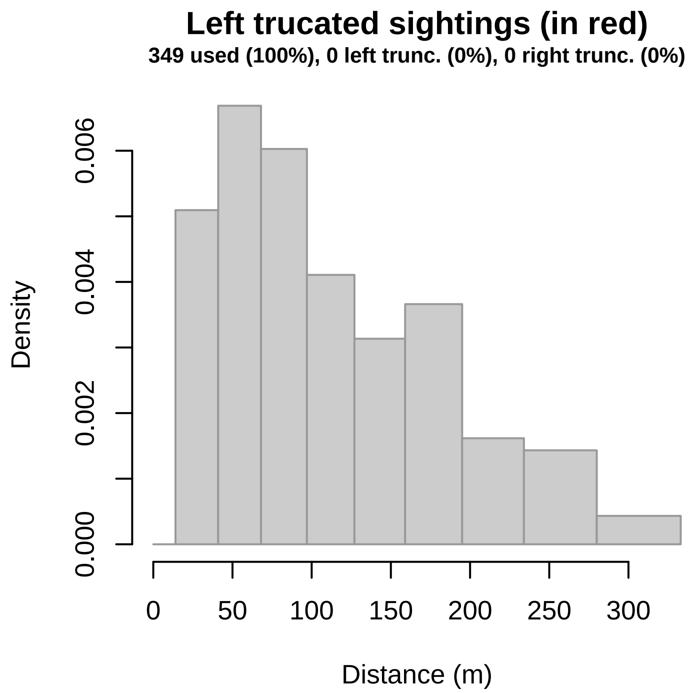

Figure 40: Density histogram of observations used to fit the UNCW Early Surveys detection function, with the left-most bar showing observations at distances less than 14 m, which were left-truncated and excluded from the analysis [Buckland et al. (2001)]. (This bar may be very short if there were very few left-truncated sightings, or very narrow if the left truncation distance was very small; in either case it may not appear red.)

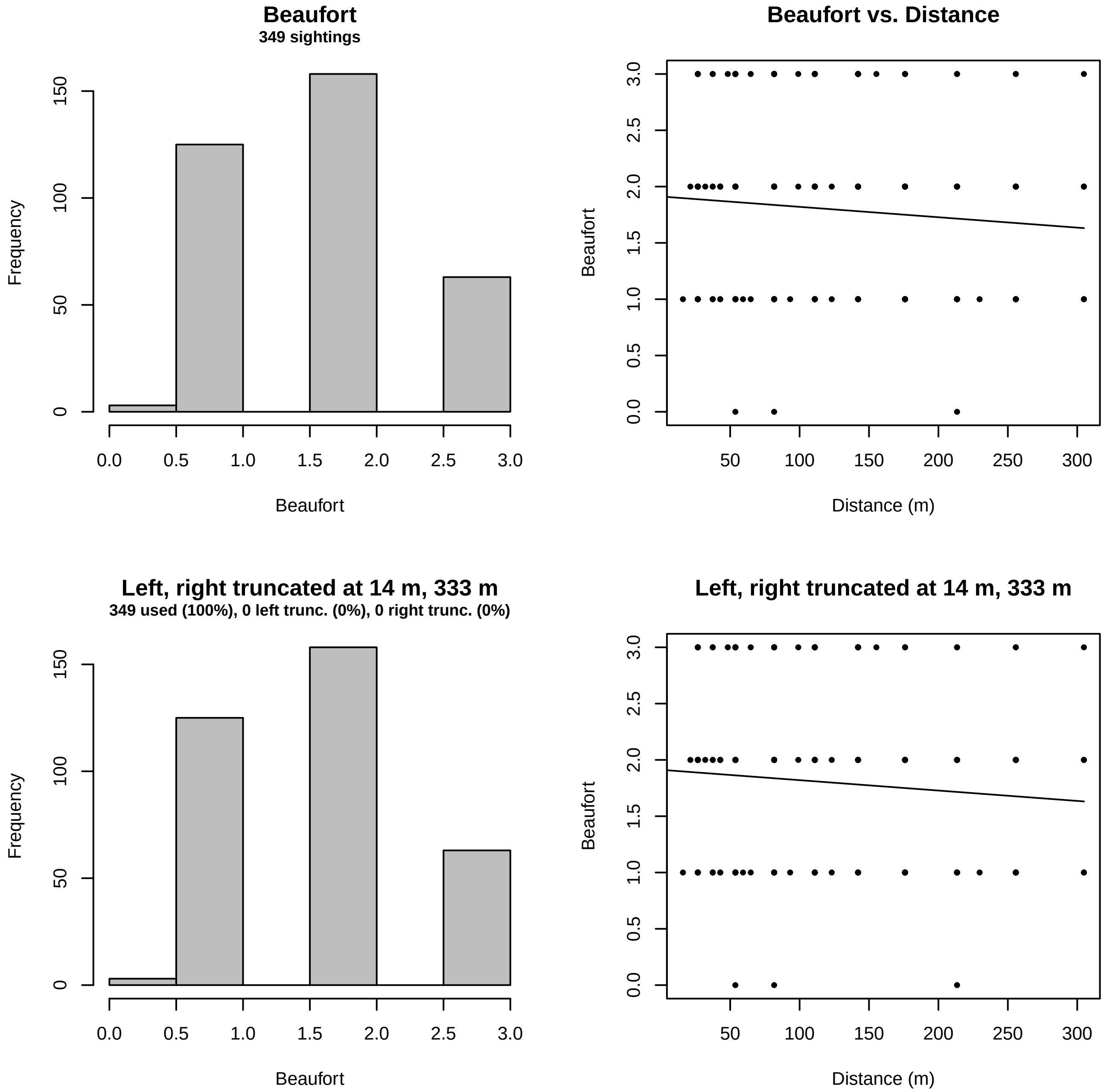

Figure 41: Distribution of the Beaufort covariate before (top row) and after (bottom row) observations were truncated to fit the UNCW Early Surveys detection function.

2.2.1.8 VAMSC

After right-truncating observations greater than 1000 m, we fitted the detection function to the 303 observations that remained (Table 16). The selected detection function (Figure 42) used a hazard rate key function with no covariates.

Table 16: Observations used to fit the VAMSC detection function.

ScientificName	n
Delphinus delphis	30
Stenella frontalis	4
Tursiops truncatus	269
Total	**303**

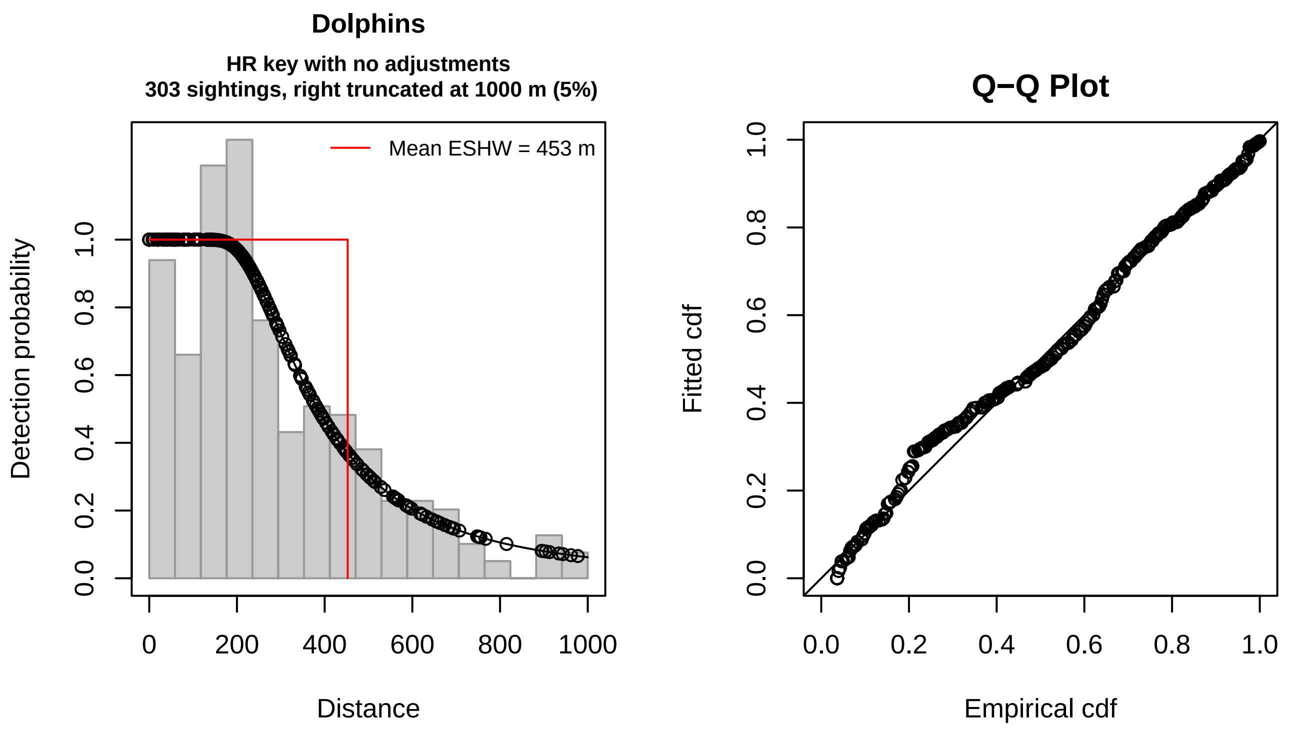

Figure 42: VAMSC detection function and Q-Q plot showing its goodness of fit.

Statistical output for this detection function:

```
Summary for ds object
Number of observations :  303
Distance range         :  0  -  1000
AIC                    :  3992.632

Detection function:
 Hazard-rate key function

Detection function parameters
Scale coefficient(s):
            estimate        se
(Intercept) 5.803823 0.1019737

Shape coefficient(s):
             estimate        se
(Intercept) 0.9119562 0.1438459

                       Estimate          SE         CV
Average p             0.4525805  0.02853931 0.06305908
N in covered region 669.4942067 50.91287837 0.07604678

Distance sampling Cramer-von Mises test (unweighted)
Test statistic = 0.212402  p = 0.244680
```

2.2.1.9 HDR

After right-truncating observations greater than 1500 m and left-truncating observations less than 111 m (Figure 44), we fitted the detection function to the 203 observations that remained (Table 17). The selected detection function (Figure 43) used a hazard rate key function with Season (Figure 45) and Swell (Figure 46) as covariates.

Table 17: Observations used to fit the HDR detection function.

ScientificName	n
Delphinus delphis	47
Stenella coeruleoalba	14
Stenella frontalis	19
Tursiops truncatus	123
Total	**203**

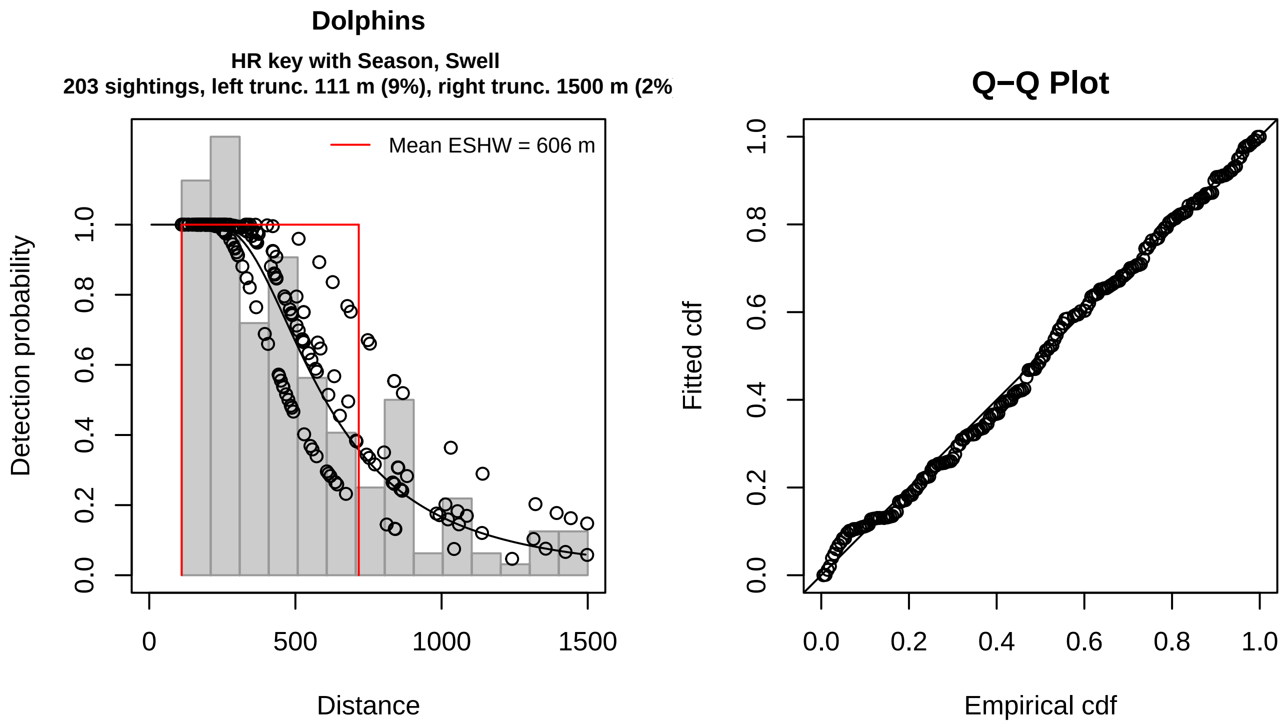

Figure 43: HDR detection function and Q-Q plot showing its goodness of fit.

Statistical output for this detection function:

```
Summary for ds object
Number of observations :  203
Distance range         :  111  -  1500
AIC                    :  2802.845

Detection function:
 Hazard-rate key function

Detection function parameters
Scale coefficient(s):
                       estimate        se
(Intercept)           6.3015171 0.1328018
SeasonWinter, Spring -0.2671651 0.1458664
Swell3-4              0.3527933 0.1530784

Shape coefficient(s):
            estimate        se
(Intercept) 1.026101 0.1620057

                      Estimate          SE          CV
```

```
Average p             0.419883  0.03654238 0.08702991
N in covered region 483.467993 49.56848062 0.10252691

Distance sampling Cramer-von Mises test (unweighted)
Test statistic = 0.059652  p = 0.816171
```

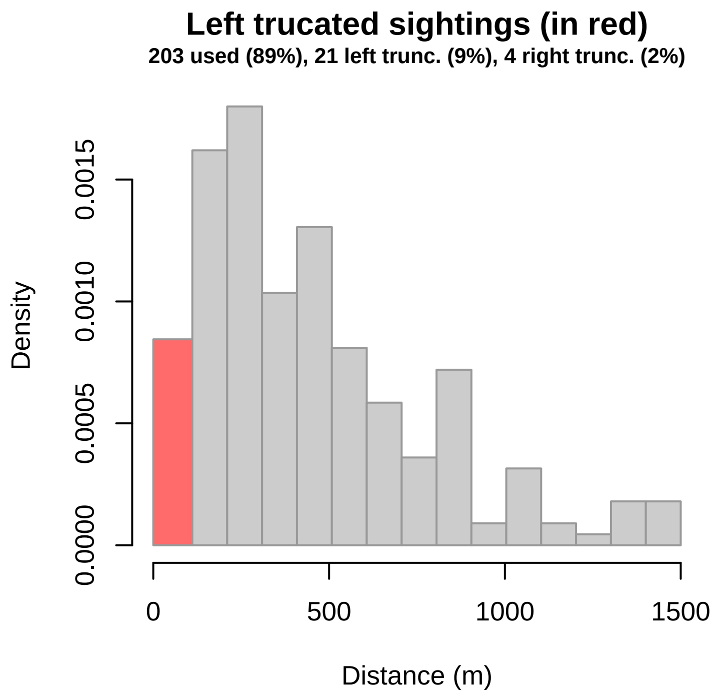

Figure 44: Density histogram of observations used to fit the HDR detection function, with the left-most bar showing observations at distances less than 111 m, which were left-truncated and excluded from the analysis [Buckland et al. (2001)]. (This bar may be very short if there were very few left-truncated sightings, or very narrow if the left truncation distance was very small; in either case it may not appear red.)

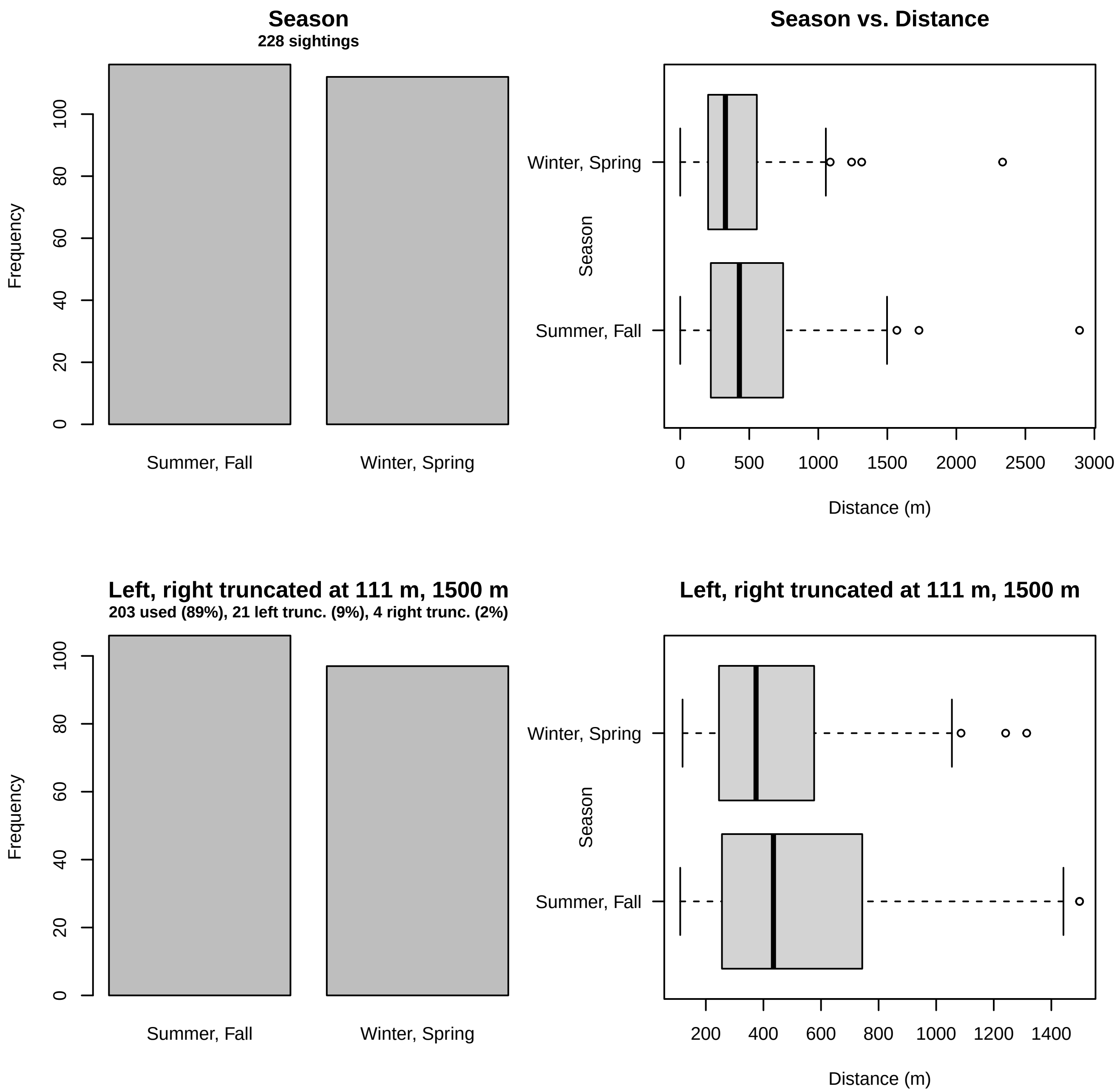

Figure 45: Distribution of the Season covariate before (top row) and after (bottom row) observations were truncated to fit the HDR detection function.

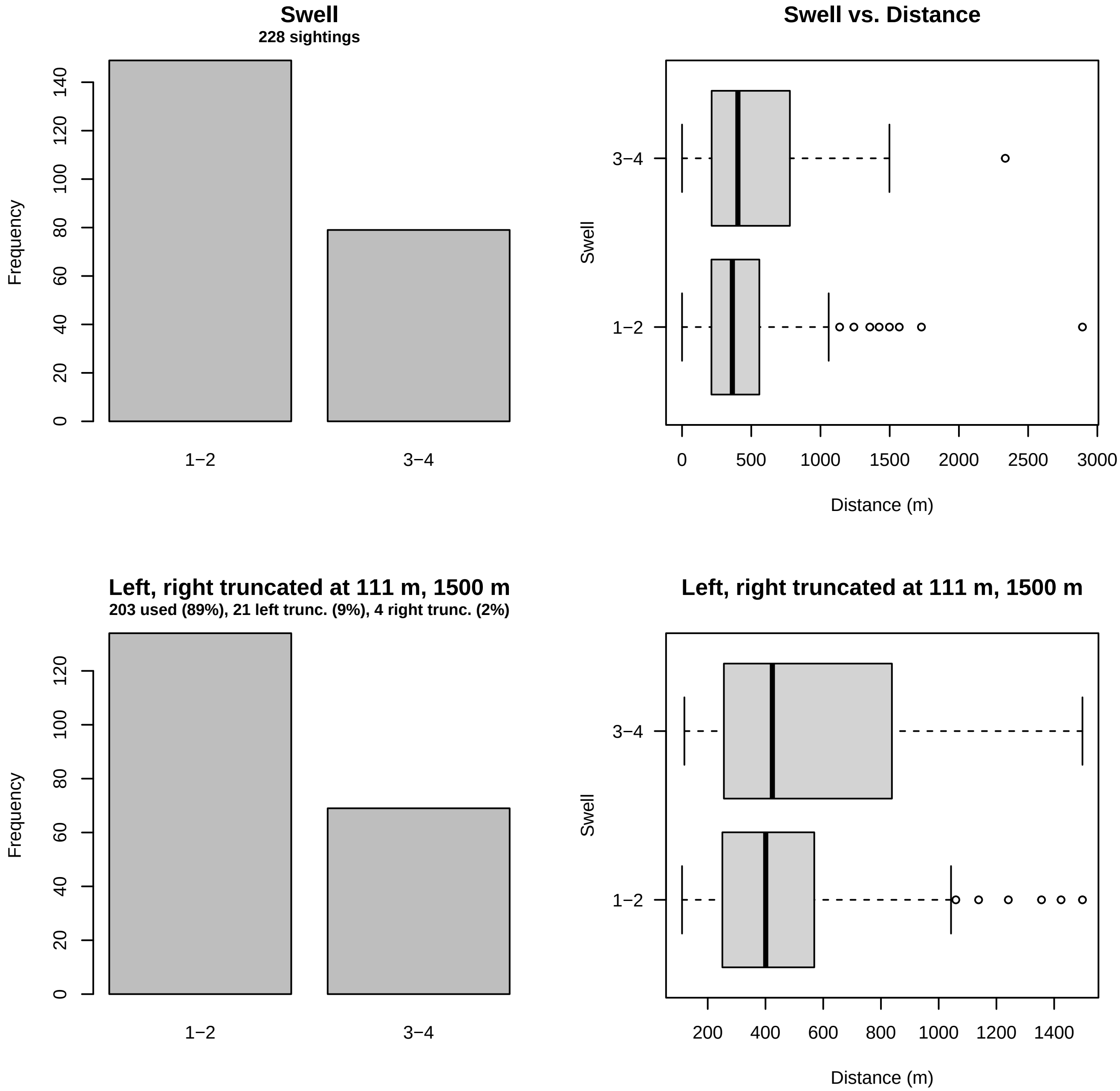

Figure 46: Distribution of the Swell covariate before (top row) and after (bottom row) observations were truncated to fit the HDR detection function.

2.2.2 Shipboard Surveys

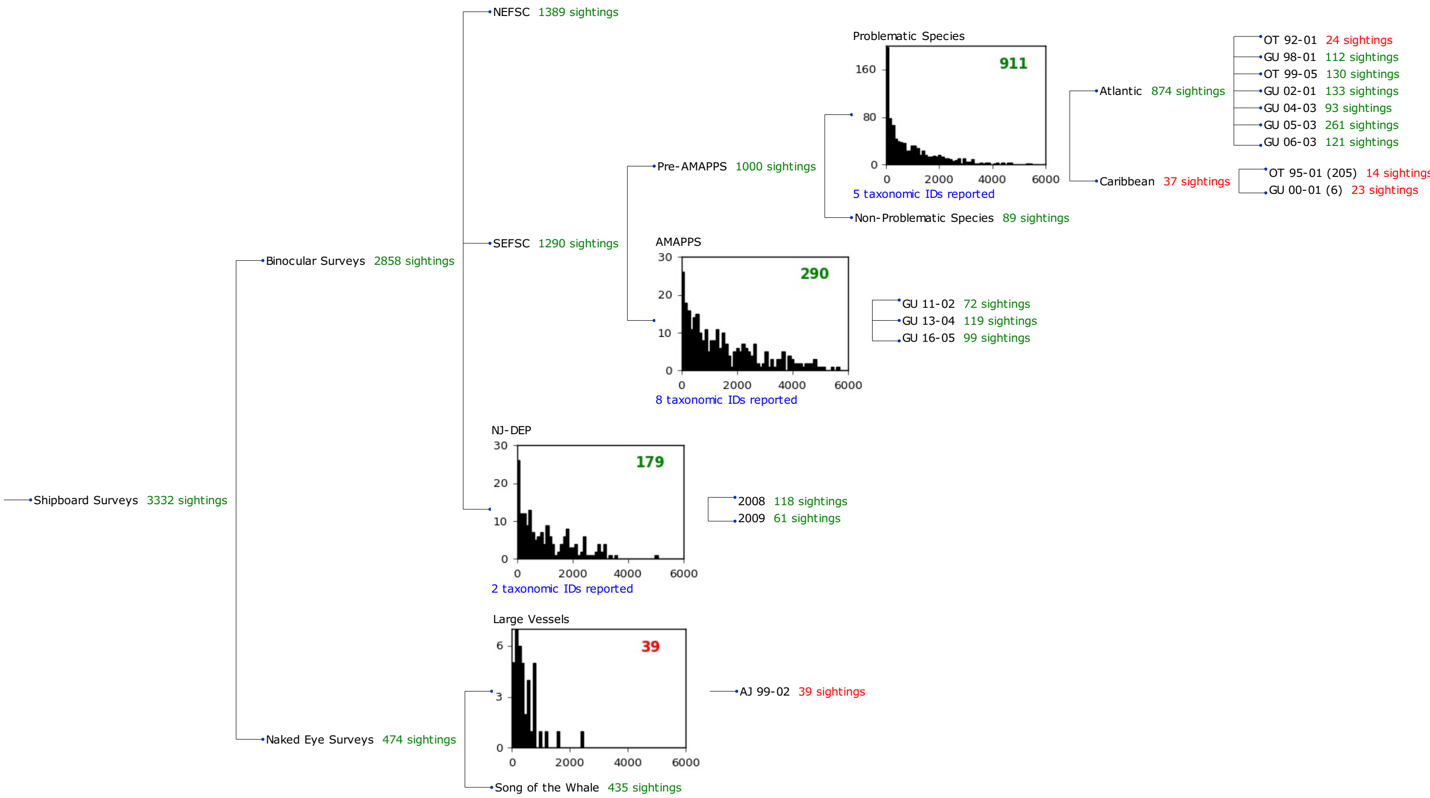

Figure 47: Detection hierarchy for shipboard surveys, showing how they were pooled during detectability modeling, for detection functions that pooled multiple taxa but could not use a taxonomic covariate to account for differences between them. Each histogram represents a detection function and summarizes the perpendicular distances of observations that were pooled to fit it, prior to truncation. Observation counts, also prior to truncation, are shown in green when they met the recommendation of Buckland et al. (2001) that detection functions utilize at least 60 sightings, and red otherwise. For rare taxa, it was not always possible to meet this recommendation, yielding higher statistical uncertainty. During the spatial modeling stage of the analysis, effective strip widths were computed for each survey using the closest detection function above it in the hierarchy (i.e. moving from right to left in the figure). Surveys that do not have a detection function above them in this figure were either addressed by a detection function presented in a different section of this report, or were omitted from the analysis.

2.2.2.1 SEFSC Pre-AMAPPS Problematic Species

After right-truncating observations greater than 4000 m and left-truncating observations less than 200 m (Figure 49), we fitted the detection function to the 616 observations that remained (Table 18). The selected detection function (Figure 48) used a hazard rate key function with Beaufort (Figure 50) and VesselName (Figure 51) as covariates.

Table 18: Observations used to fit the SEFSC Pre-AMAPPS Problematic Species detection function.

ScientificName	n
Delphinus delphis	34
Stenella attenuata	14
Stenella frontalis	262
Steno bredanensis	4
Tursiops truncatus	302
Total	**616**

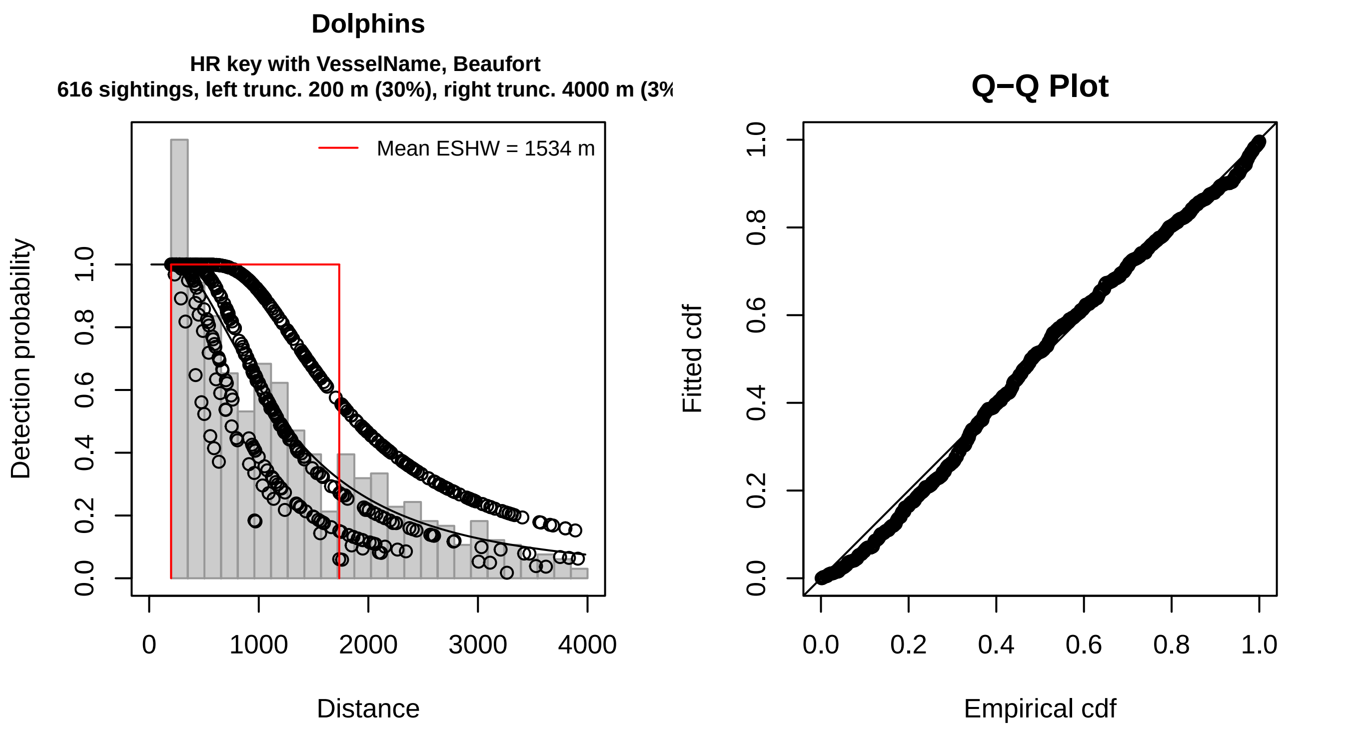

Figure 48: SEFSC Pre-AMAPPS Problematic Species detection function and Q-Q plot showing its goodness of fit.

Statistical output for this detection function:

```
Summary for ds object
Number of observations :  616
Distance range         :  200  -  4000
AIC                    :  9753.004

Detection function:
 Hazard-rate key function

Detection function parameters
Scale coefficient(s):
                      estimate         se
(Intercept)          7.3628462 0.09422017
VesselNameOregon II -0.4793018 0.17480366
Beaufort3           -0.4668391 0.14302976
Beaufort4-5         -0.8137669 0.16103824

Shape coefficient(s):
            estimate         se
(Intercept) 0.689867 0.09372714

                        Estimate           SE         CV
Average p              0.3555714   0.02671315 0.07512737
N in covered region 1732.4228173 142.52885613 0.08227140

Distance sampling Cramer-von Mises test (unweighted)
Test statistic = 0.313292  p = 0.124062
```

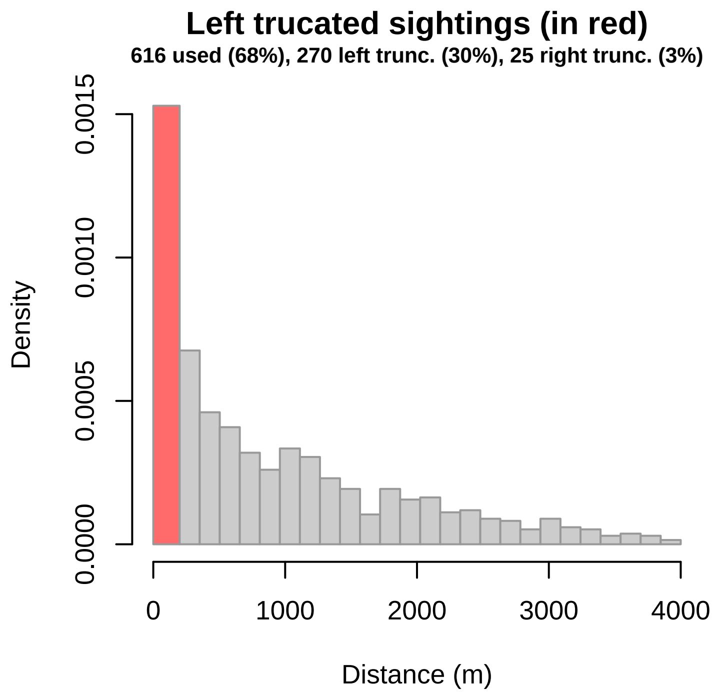

Figure 49: Density histogram of observations used to fit the SEFSC Pre-AMAPPS Problematic Species detection function, with the left-most bar showing observations at distances less than 200 m, which were left-truncated and not used to fit the detection function. (This bar may be very short if there were very few left-truncated sightings, or very narrow if the left truncation distance was very small; in either case it may not appear red.) These were excluded because they formed a problematic "spike" in detections close to the trackline, suggesting that animals approached the vessel (e.g. to bow-ride) prior to being detected. To address this, we fitted the detection function to the observations beyond the spike and assumed that within it, detection probability was 1, effectively treating it like a strip transect. We then added the left-truncated observations back into the analysis as if they occurred in this strip. This treatment may have resulted in an underestimation of detection probability.

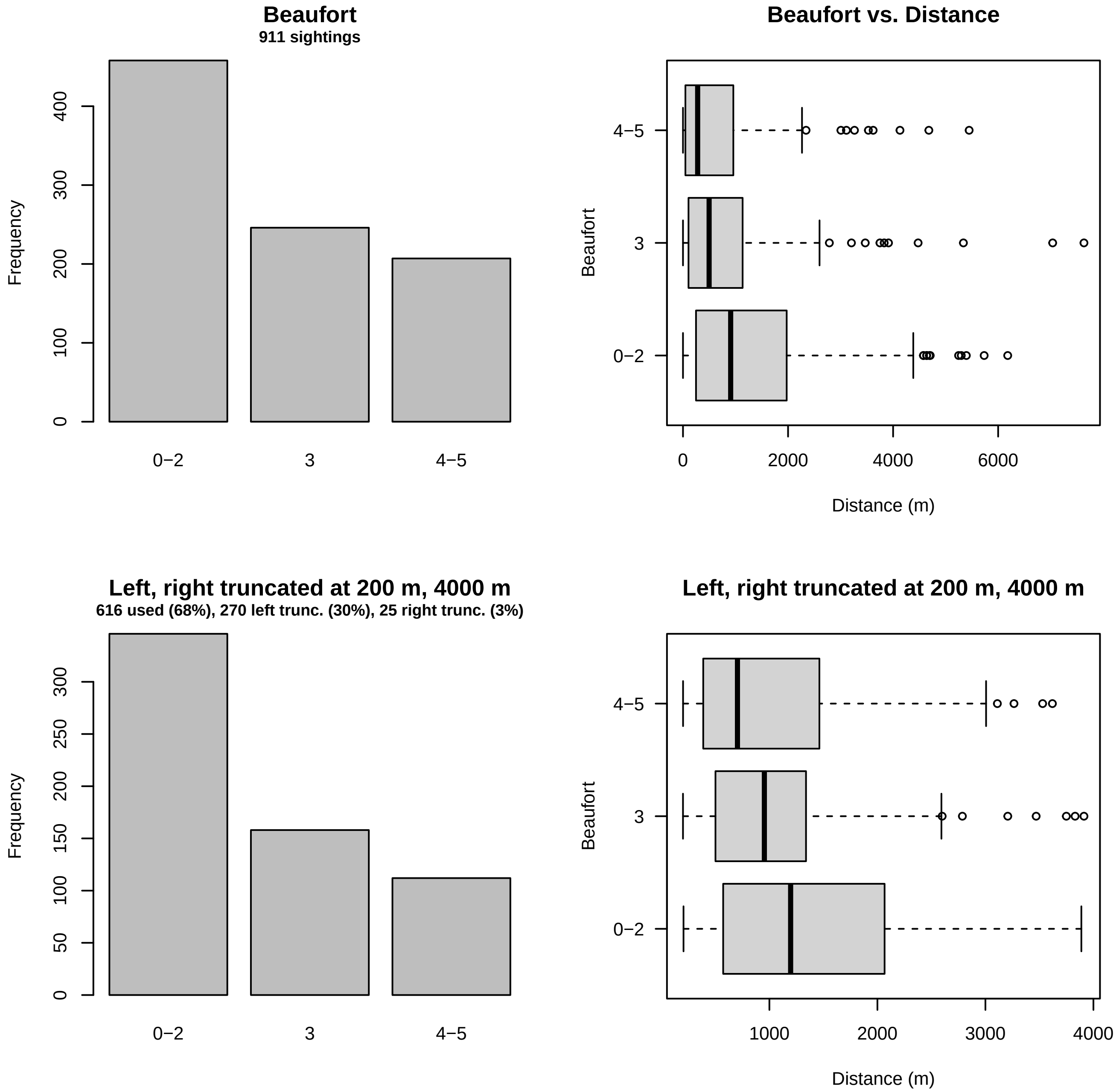

Figure 50: Distribution of the Beaufort covariate before (top row) and after (bottom row) observations were truncated to fit the SEFSC Pre-AMAPPS Problematic Species detection function.

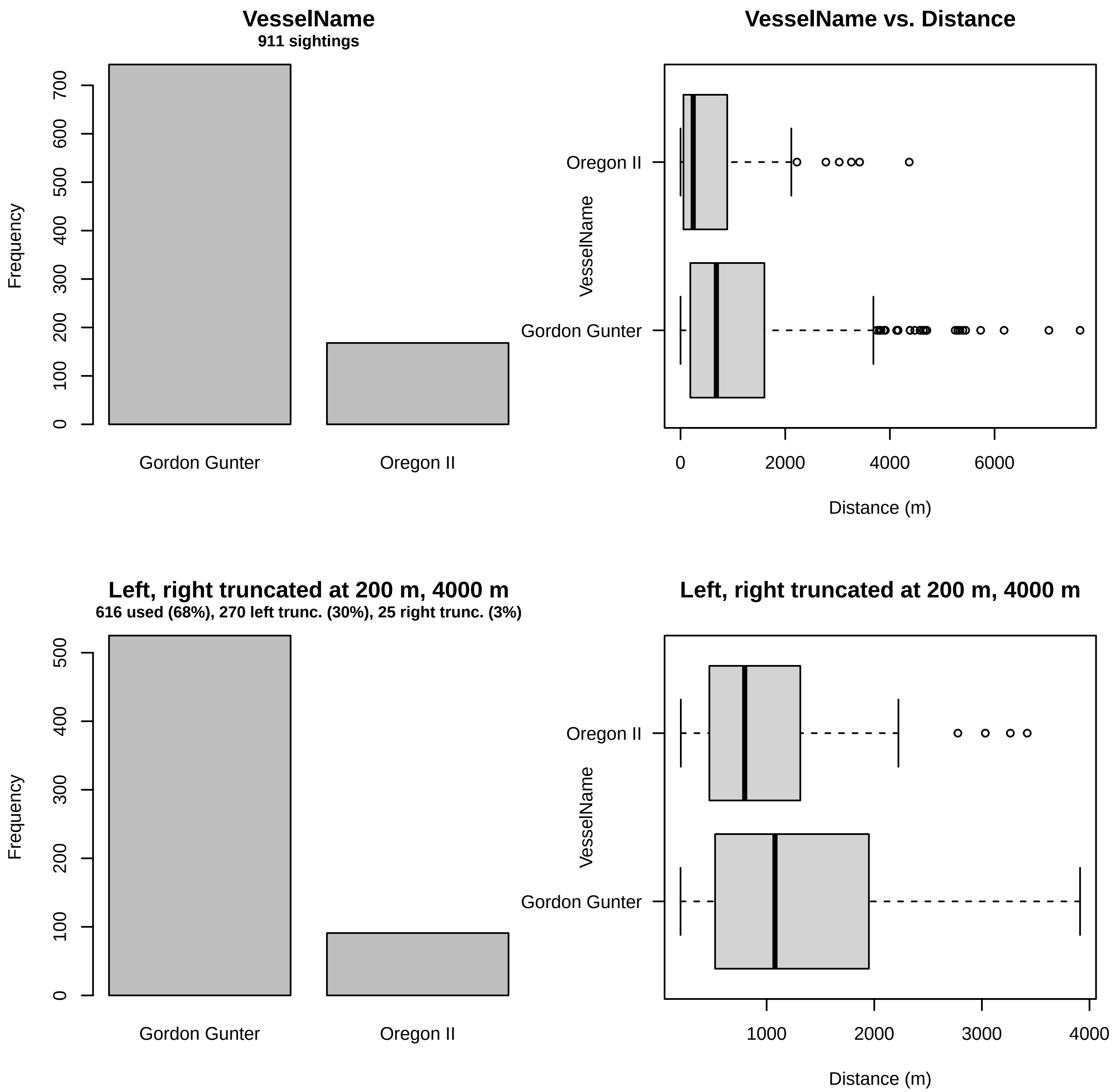

Figure 51: Distribution of the VesselName covariate before (top row) and after (bottom row) observations were truncated to fit the SEFSC Pre-AMAPPS Problematic Species detection function.

2.2.2.2 SEFSC AMAPPS

After right-truncating observations greater than 5000 m, we fitted the detection function to the 284 observations that remained (Table 19). The selected detection function (Figure 52) used a hazard rate key function with Beaufort (Figure 53) as a covariate.

Table 19: Observations used to fit the SEFSC AMAPPS detection function.

ScientificName	n
Delphinus delphis	2
Stenella attenuata	10
Stenella clymene	3
Stenella coeruleoalba	11
Stenella frontalis	84
Stenella longirostris	1
Steno bredanensis	2
Tursiops truncatus	171
Total	**284**

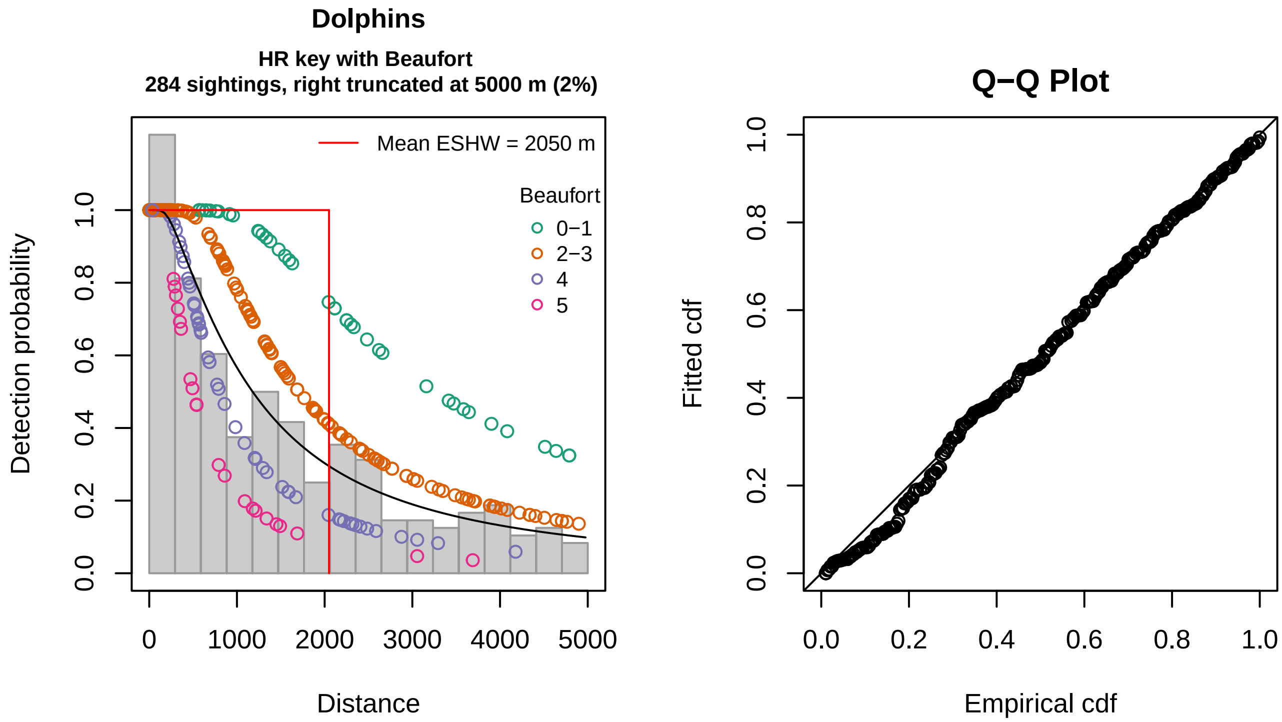

Figure 52: SEFSC AMAPPS detection function and Q-Q plot showing its goodness of fit.

Statistical output for this detection function:

```
Summary for ds object
Number of observations :  284
Distance range         :  0  -  5000
AIC                    :  4678.464

Detection function:
 Hazard-rate key function

Detection function parameters
Scale coefficient(s):
              estimate        se
(Intercept)  7.8386611 0.3487749
Beaufort2-3 -0.6450433 0.3816484
Beaufort4   -1.3990617 0.4441169
Beaufort5   -1.8689041 0.5186901
```

```
Shape coefficient(s):
             estimate        se
(Intercept) 0.3878689 0.1380351

                        Estimate           SE        CV
Average p              0.3478259   0.03965009 0.1139941
N in covered region 816.5004271 101.68622285 0.1245391

Distance sampling Cramer-von Mises test (unweighted)
Test statistic = 0.107898  p = 0.547527
```

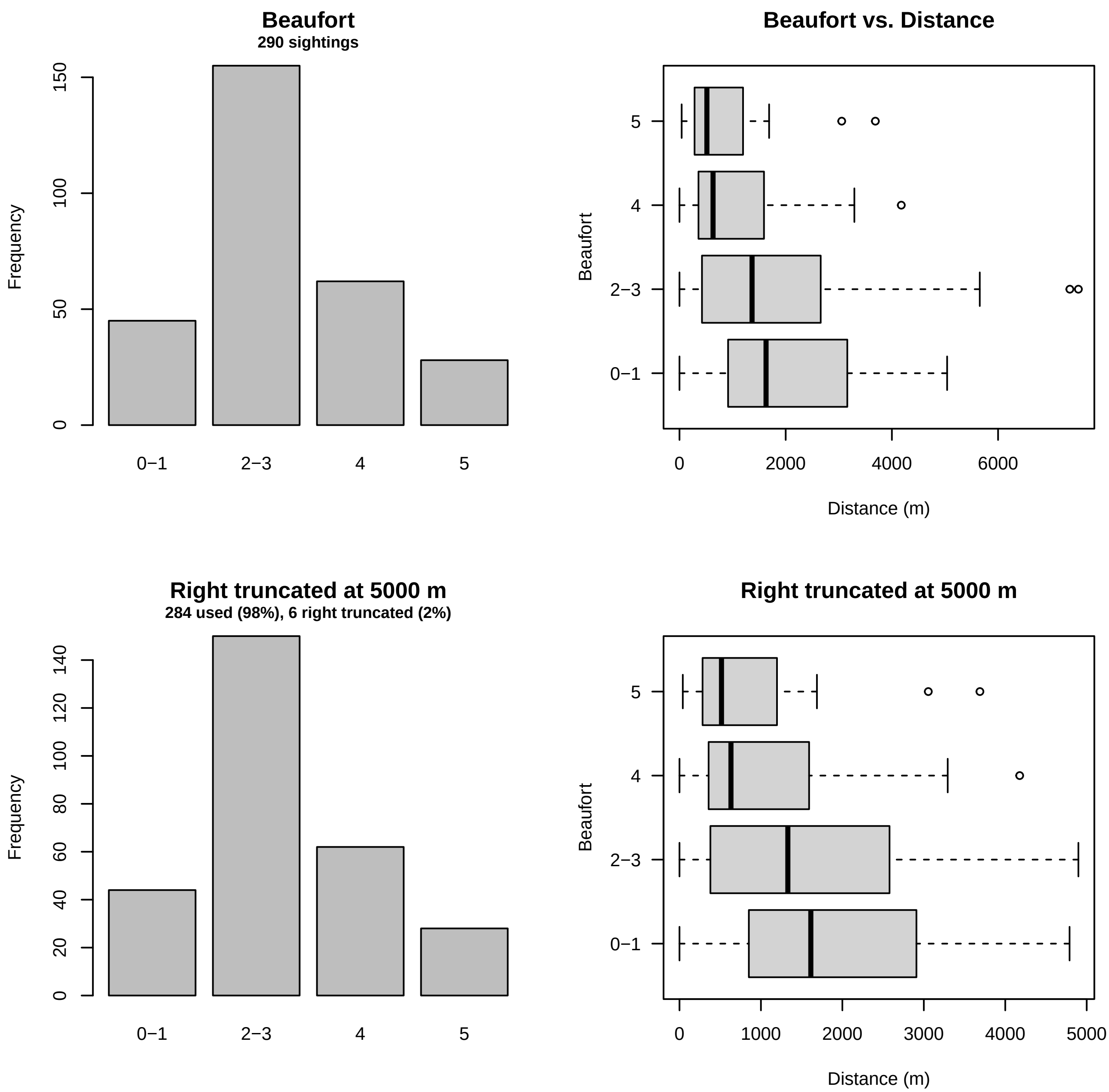

Figure 53: Distribution of the Beaufort covariate before (top row) and after (bottom row) observations were truncated to fit the SEFSC AMAPPS detection function.

2.2.2.3 NJ-DEP

After right-truncating observations greater than 3200 m, we fitted the detection function to the 175 observations that remained (Table 20). The selected detection function (Figure 54) used a hazard rate key function with no covariates.

Table 20: Observations used to fit the NJ-DEP detection function.

ScientificName	n
Delphinus delphis	19
Tursiops truncatus	156
Total	**175**

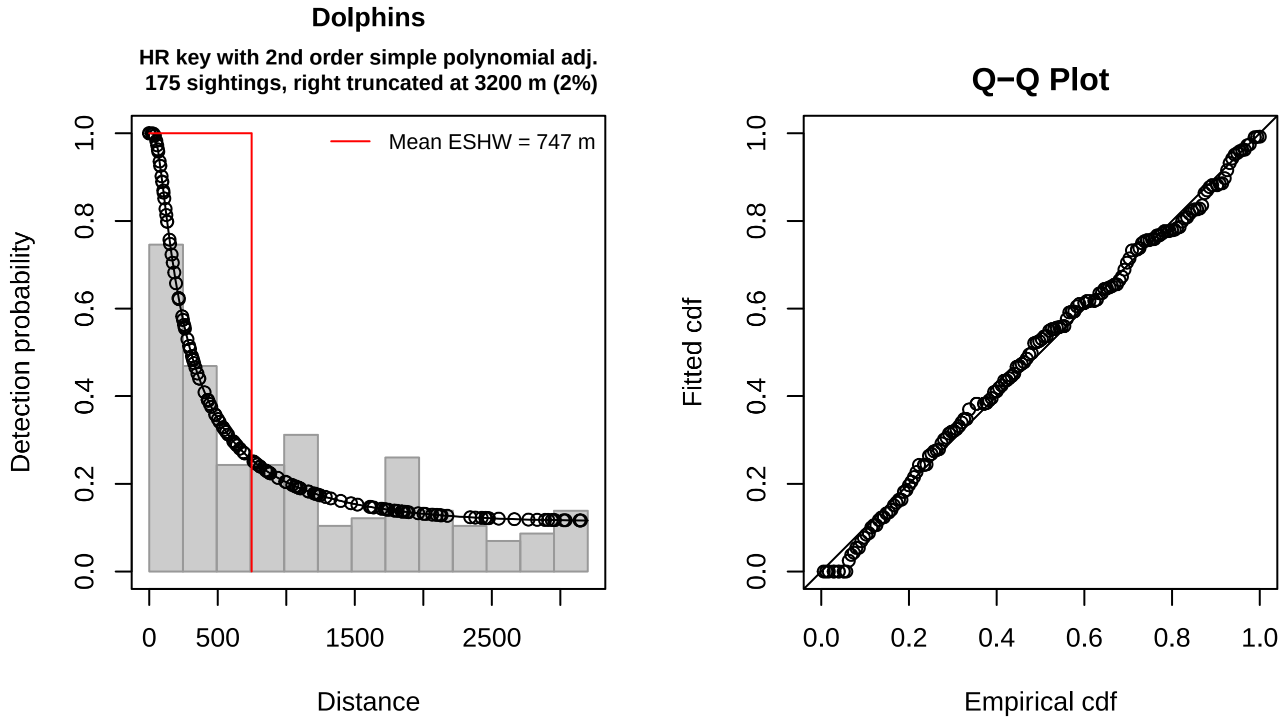

Figure 54: NJ-DEP detection function and Q-Q plot showing its goodness of fit.

Statistical output for this detection function:

```
Summary for ds object
Number of observations :  175
Distance range         :  0  -  3200
AIC                    :  2750.547

Detection function:
 Hazard-rate key function with simple polynomial adjustment term of order 2

Detection function parameters
Scale coefficient(s):
            estimate       se
(Intercept) 5.340225 0.502875

Shape coefficient(s):
                estimate        se
(Intercept) 2.663565e-07 0.3025183
```

```
Adjustment term coefficient(s):
               estimate       se
poly, order 2 0.8448098 1.306568


Monotonicity constraints were enforced.
                       Estimate          SE        CV
Average p             0.2335197   0.05159473 0.2209438
N in covered region 749.4013460 172.84391894 0.2306427

Monotonicity constraints were enforced.

Distance sampling Cramer-von Mises test (unweighted)
Test statistic = 0.069450  p = 0.754942
```

2.2.2.4 Large Vessels

After right-truncating observations greater than 1100 m, we fitted the detection function to the 36 observations that remained (Table 21). The selected detection function (Figure 55) used a half normal key function with no covariates.

Table 21: Observations used to fit the Large Vessels detection function.

ScientificName	n
Lagenorhynchus acutus	36
Total	**36**

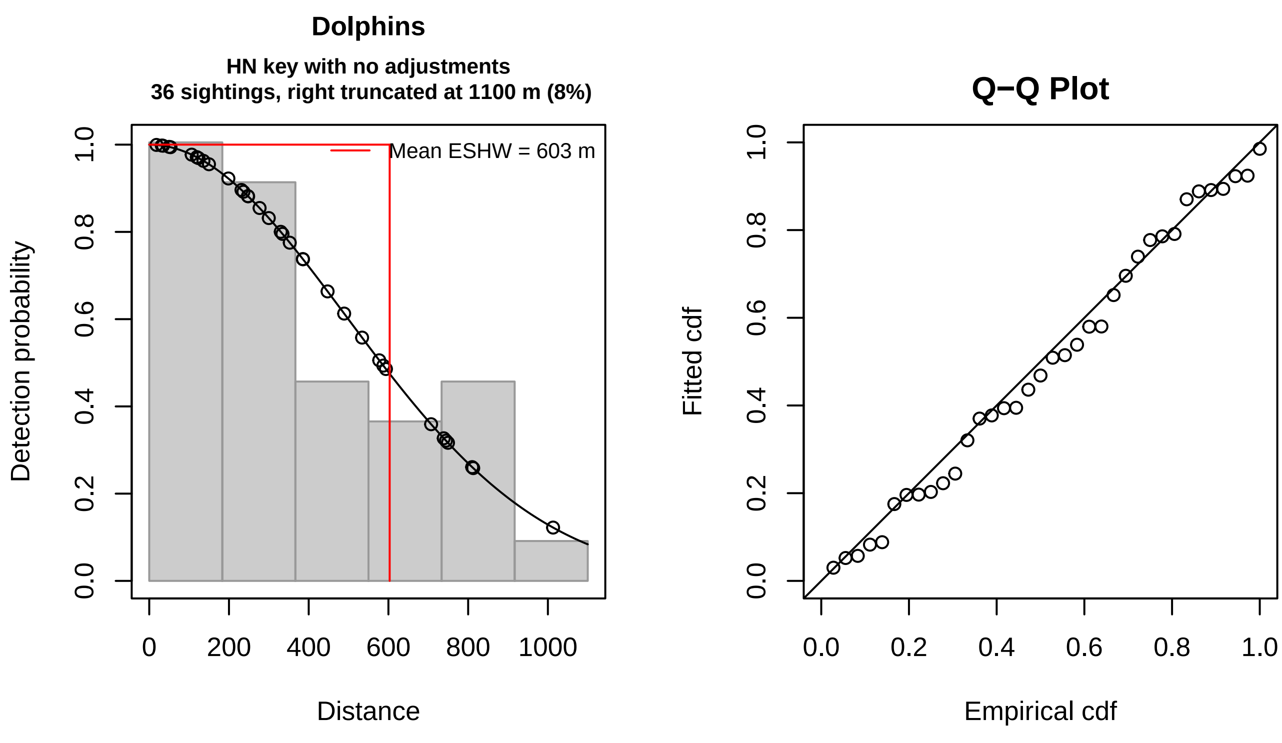

Figure 55: Large Vessels detection function and Q-Q plot showing its goodness of fit.

Statistical output for this detection function:

```
Summary for ds object
Number of observations :  36
Distance range         :  0  -  1100
```

```
AIC                    :  493.4472

Detection function:
 Half-normal key function

Detection function parameters
Scale coefficient(s):
            estimate        se
(Intercept) 6.202683 0.1646341

                      Estimate          SE        CV
Average p            0.5483057  0.07646146 0.1394504
N in covered region 65.6568085 11.74385160 0.1788672

Distance sampling Cramer-von Mises test (unweighted)
Test statistic = 0.026241  p = 0.986825
```

3 Bias Corrections

Density surface modeling methodology uses *distance sampling* (Buckland et al. 2001) to model the probability that an observer on a line transect survey will detect an animal given the perpendicular distance to it from the transect line. Distance sampling assumes that detection probability is 1 when perpendicular distance is 0. When this assumption is not met, detection probability is biased high, leading to an underestimation of density and abundance. This is known as the $g_0 < 1$ problem, where g_0 refers to the detection probability at distance 0. Modelers often try to address this problem by estimating g_0 empirically and dividing it into estimated density or abundance, thereby correcting those estimates to account for the animals that were presumed missed.

Two important sources of bias for visual surveys are known as *availability bias*, in which an animal was present on the transect line but impossible to detect, e.g. because it was under water, and *perception bias*, in which an animal was present and available but not noticed, e.g. because of its small size or cryptic coloration or behavior (Marsh and Sinclair 1989). Modelers often estimate the influence of these two sources of bias on detection probability independently, yielding two estimates of g_0, hereafter referred to as g_{0A} and g_{0P}, and multiply them together to obtain a final, combined estimate: $g_0 = g_{0A} \cdot g_{0P}$.

Our overall approach was to perform this correction on a per-observation basis, to have the flexibility to account for many factors such as platform type, surveyor institution, group size, group composition (e.g. singleton, mother-calf pair, or surface active group), and geographic location (e.g. feeding grounds vs. calving grounds). The level of complexity of the corrections varied by species according to the amount of information available, with North Atlantic right whale having the most elaborate corrections, derived from a substantial set of publications documenting its behavior, and various lesser known odontocetes having corrections based only on platform type (aerial or shipboard), derived from comparatively sparse information. Here we document the corrections used for rough-toothed dolphin.

3.1 Aerial Surveys

Rough-toothed dolphin sightings were reported by aerial surveys conducted by SEFSC and UNCW (Table 1). We applied the perception bias correction for a guild of large dolphins, including rough-toothed dolphin, developed by Palka et al. (2021) using two team, mark recapture distance sampling (MRDS) methodology (Burt et al. 2014) for aerial surveys conducted in 2010-2017 by NOAA SEFSC during the AMAPPS program. To account for the influence of large group sizes on perception bias, we followed Carretta et al. (2000) and set the perception bias correction factor for sightings of more than 25 animals to $g_{0P} = 0.994$.

We caution that it is possible that perception bias was different for the UNCW aerial programs than for the SEFSC AMAPPS program, as UNCW's programs used different aircraft, flew at different altitudes, and were staffed by different personnel. Of particular concern is that UNCW flew Cessna 337 Skymasters, which had flat windows, while NOAA flew de Havilland Twin Otters, which had bubble windows, which likely afforded a better view of the transect line and therefore might have required less of a correction than the Skymasters. Correcting UNCW's program using NOAA's estimate as we have done is likely to yield less bias than leaving it uncorrected, but we urge all programs to undertake their own efforts to estimate perception bias, as resources allow.

We estimated availability bias corrections using the Laake et al. (1997) estimator and dive intervals reported by Palka et al. (2017) for common bottlenose dolphin (Table 23), as we could find no suitable intervals for rough-toothed dolphin in the literature. To estimate time in view, needed by the Laake estimator, we used results reported by Robertson et al. (2015), rescaled linearly for each survey program according to its target altitude and speed. We caution that Robertson's analysis was done for a de Havilland Twin Otter, which may have a different field of view than that of the UNCW aircraft used here, which were Cessna 337 Skymasters with flat windows. However, we note that McLellan et al. (2018) conducted a sensitivity analysis on the influence of the length of the "window of opportunity" to view beaked whales from a Cessna Skymaster on their final density estimates and found that they varied by only a few thousandths of an animal per kilometer when the window of opportunity more than doubled. Still, we urge additional program-specific research into estimation of availability bias.

To address the influence of group size on availability bias, we applied the group availability estimator of McLellan et al. (2018) on a per-observation basis. Following Palka et al. (2021), who also used that method, we assumed that individuals in the group dived asynchronously. The resulting g_{0A} corrections were all very close to 1 (Figure 56), owing to large group sizes. We caution that the assumption of asynchronous diving can lead to an underestimation of density and abundance if diving is actually synchronous; see McLellan et al. (2018) for an exploration of this effect. However, if future research finds that this species conducts synchronous dives and characterizes the degree of synchronicity, the model can be updated to account for this knowledge.

Table 22: Perception bias corrections for rough-toothed dolphin applied to aerial surveys.

Surveys	Group Size	g_{0P}	g_{0P} Source
All	≤ 25	0.740	Palka et al. (2021): SEFSC
All	> 25	0.994	Carretta et al. (2000)

Table 23: Surface and dive intervals for rough-toothed dolphin used to estimate availability bias corrections.

Surface Interval (s)	Dive Interval (s)	Source
3	26.6	Palka et al. (2017): common bottlenose dolphin

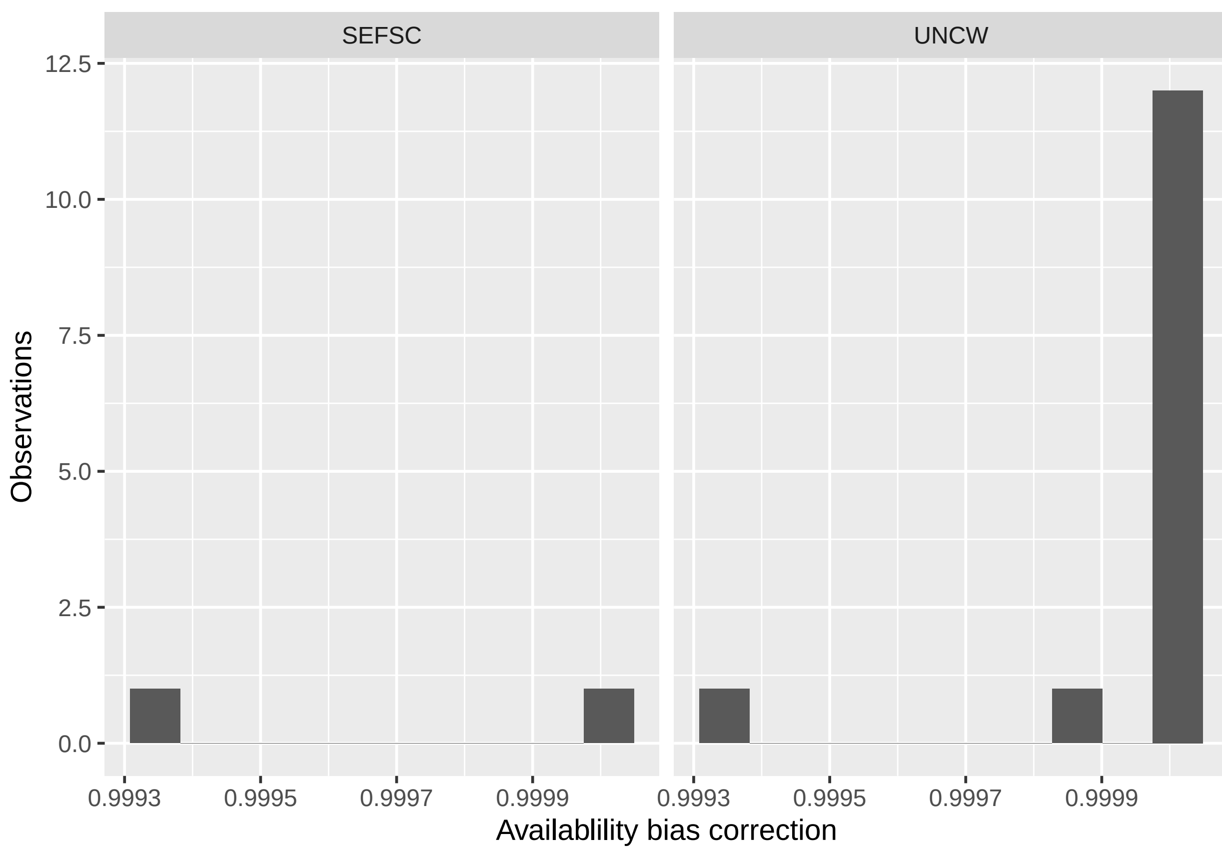

Figure 56: Availability bias corrections for rough-toothed dolphin for aerial surveys, by institution.

3.2 Shipboard Surveys

Most of the shipboard surveys in our analysis used high-power (25x150), pedestal-mounted binoculars. Similar to aerial surveys, Palka et al. (2021) developed perception bias corrections using two team, MRDS methodology (Burt et al. 2014) for high-power binocular surveys conducted in 2010-2017 by NOAA NEFSC and SEFSC during the AMAPPS program. These were the only extant perception bias estimates developed from high-power binocular surveys used in our analysis, aside from estimates developed earlier by Palka and colleagues (Palka 2006; Palka et al. 2017). Those earlier efforts utilized older methods and less data than their 2021 analysis, so we applied the Palka et al. (2021) estimates to all shipboard surveys that searched with high-power binoculars (Table 24).

A few surveys used naked eyes rather than high-power binoculars, but none of these programs reported any sightings of rough-toothed dolphin, so no correction was needed.

For all surveys, to account for the influence of large group sizes on perception bias, we followed Barlow and Forney (2007) and set the perception bias correction factor for sightings of more than 20 animals to $g_{0P} = 0.97$. Given that the dive interval of this species (Table 23) was short relative to the amount of time a given patch of water remained in view to shipboard observers, we assumed that no availability bias correction was needed ($g_{0A} = 1$), following Palka et al. (2021).

Table 24: Perception and availability bias corrections for rough-toothed dolphin applied to shipboard surveys.

Surveys	Searching Method	Group Size	g_{0P}	g_{0P} Source	g_{0A}	g_{0A} Source
NEFSC	Binoculars	≤ 20	0.50	Palka et al. (2021): NEFSC	1	Assumed
SEFSC	Binoculars	≤ 20	0.71	Palka et al. (2021): SEFSC	1	Assumed
All	Binoculars	> 20	0.97	Barlow and Forney (2007)	1	Assumed

4 Density Model

The rough-toothed dolphin is distributed worldwide and generally occurs in warm temperate, subtropical, or tropical waters at a wide range of depths (West et al. 2011; Hayes et al. 2022). Sightings on NOAA surveys have been much more common in the Gulf of Mexico than along the east coast of the U.S (Hayes et al. 2022). Surveys of the Atlantic assembled by our collaboration reported only 26 sightings during the period 1998-2020 (Table 1, Figure 1), and none prior. Given that, we restricted the model to this period.

South of Cape Hatteras, most sightings of rough-toothed dolphin occurred close to the continental shelf break, on both the shallow and deep sides, while one sighting occurred far offshore, east of the Gulf Stream (Figure 57). North of Cape Hatteras, all sightings occurred beyond the shelf break, scattered from the high continental slope out over the abyssal plain. Most sightings occurred in warm water, however on 22 February 2013, an aerial survey of the continental shelf and upper slope by SEFSC reported a sighting near Hudson Canyon with 13.8 °C surface temperature. (At our request, SEFSC reviewed this sighting and reconfirmed the species identification.)

Following the method established in our prior modeling cycle (Roberts et al. 2016), our usual practice for models with only 20-40 sightings was to fit a model with only one covariate. Accordingly, we fitted a series of independent univariate models (one for each covariate available), discarded those that exhibited implausible ecological relationships, and selected from the retained models the one with the best goodness of fit statistics. The best-fitting model used contemporaneous sea surface salinity, which exhibited a positive relationship with density (Figure 60), reflecting the species' preference for the relatively warm, saline waters (Figure 58). Although delphinid distributions often correlate well with SST, salinity performed better in this case because it better distinguished the on-shelf and off-shelf waters north of Cape Hatteras during summer, when higher insolation and increased stratification reduced the temperature difference between surface waters on and off the shelf.

4.1 Final Model

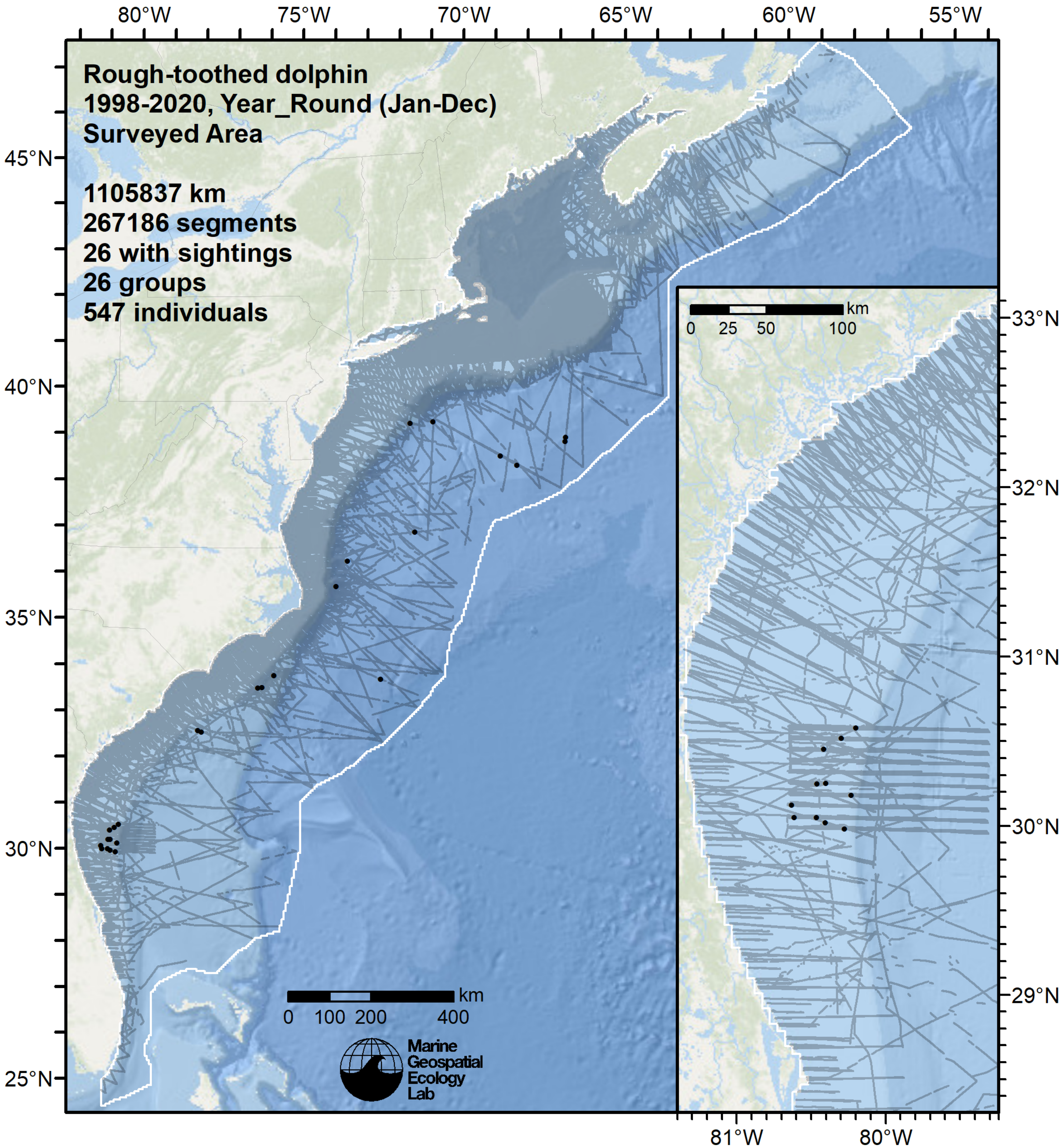

Figure 57: Survey segments used to fit the model. Black points indicate segments with observations.

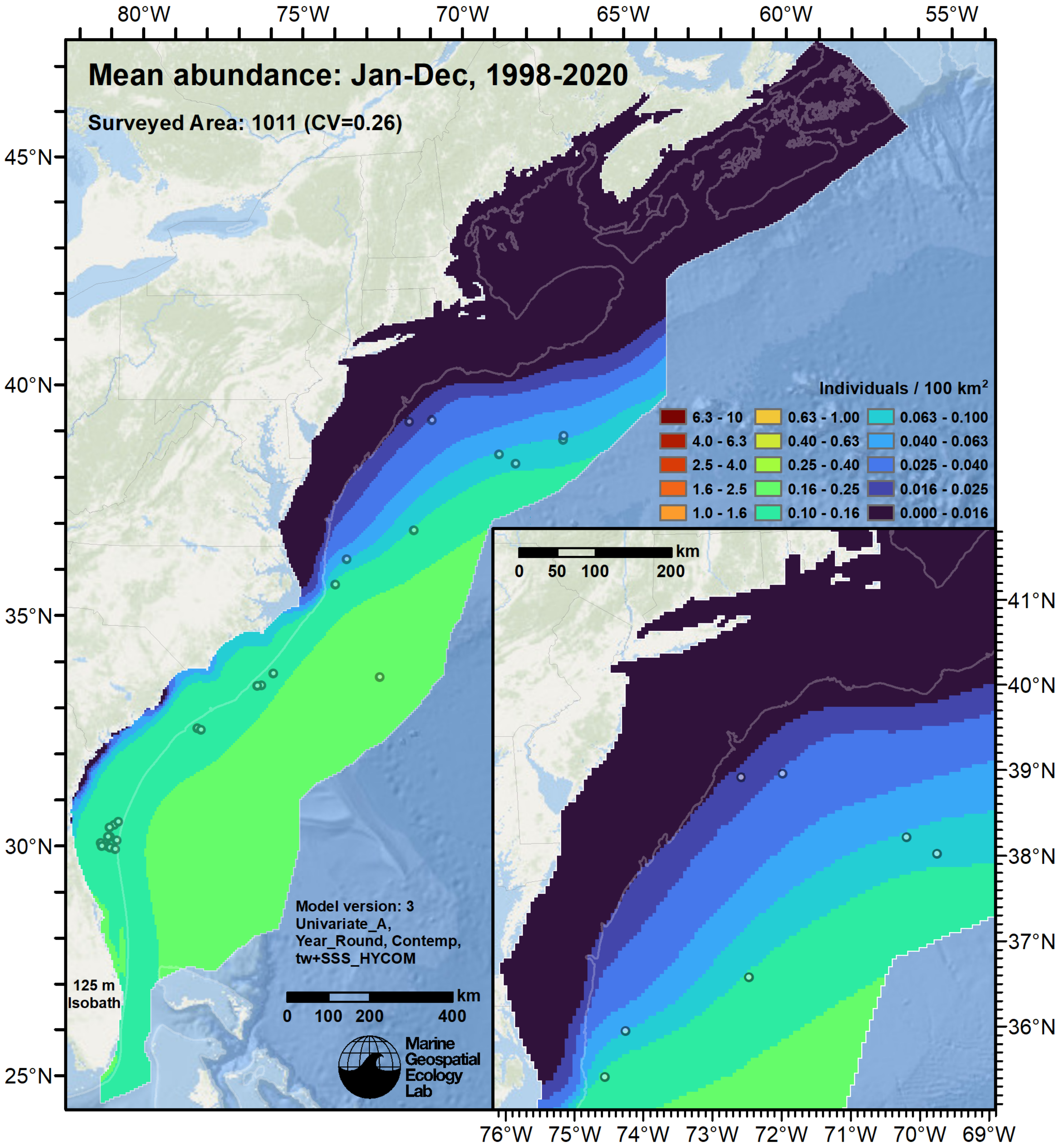

Figure 58: Rough-toothed dolphin mean density for the indicated period, as predicted by the model. Open circles indicate segments with observations. Mean total abundance and its coefficient of variation (CV) are given in the subtitle. Variance was estimated with the analytic approach given by Miller et al. (2022), Appendix S1, and accounts both for uncertainty in model parameter estimates and for seasonal and interannual variability in dynamic covariates.

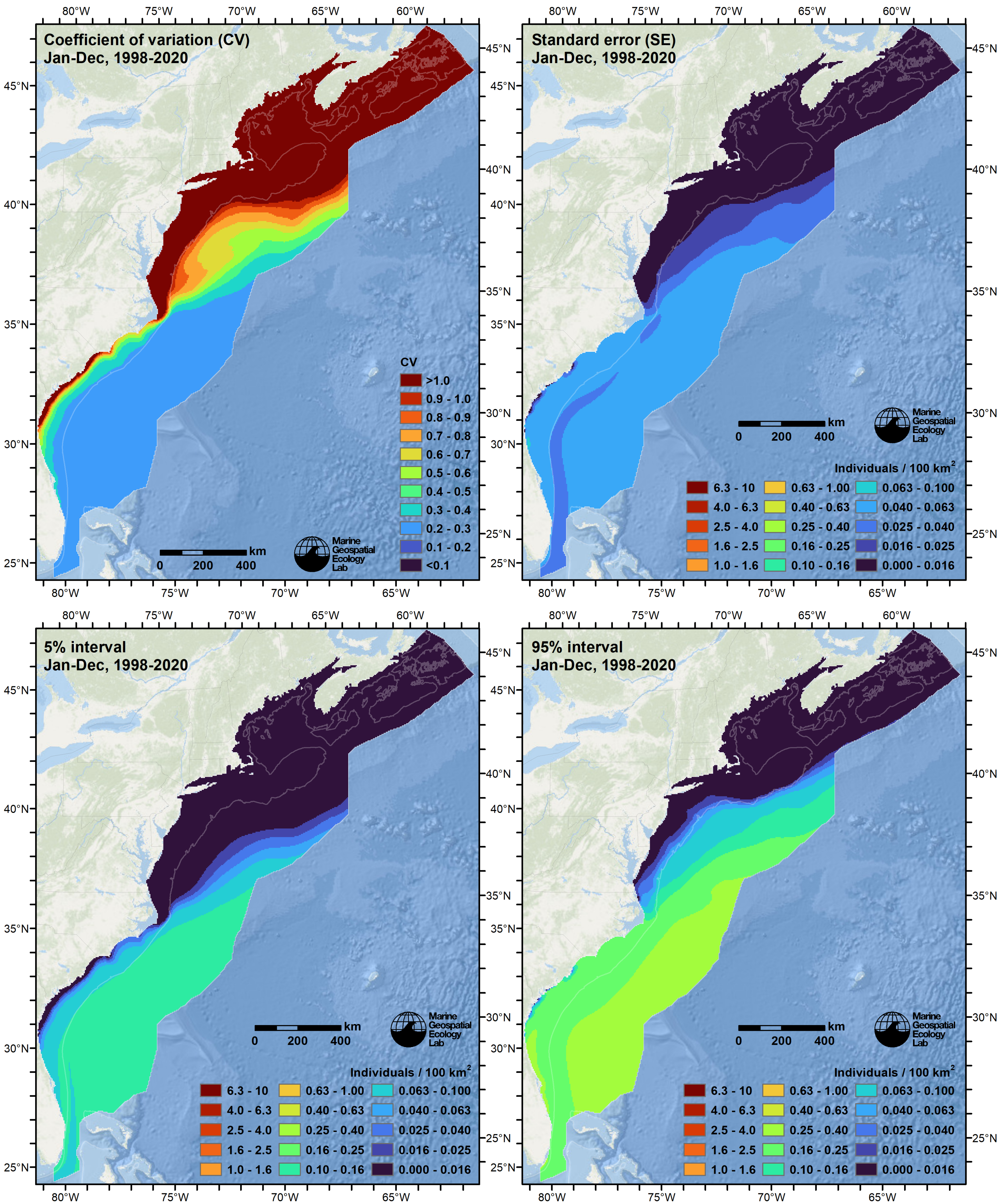

Figure 59: Uncertainty statistics for the rough-toothed dolphin mean density surface (Figure 58) predicted by the model. Variance was estimated with the analytic approach given by Miller et al. (2022), Appendix S1, and accounts both for uncertainty in model parameter estimates and for seasonal and interannual variability in dynamic covariates.

Statistical output for this model:

```
Family: Tweedie(p=1.242)
Link function: log

Formula:
IndividualsCorrected ~ offset(log(SegmentArea)) + s(pmax(31,
    pmin(SSS_HYCOM, 36.5)), bs = "ts")

Parametric coefficients:
            Estimate Std. Error t value Pr(>|t|)
(Intercept) -23.0287     0.5721  -40.25   <2e-16 ***
---
Signif. codes:  0 '***' 0.001 '**' 0.01 '*' 0.05 '.' 0.1 ' ' 1

Approximate significance of smooth terms:
                                     edf Ref.df    F  p-value
s(pmax(31, pmin(SSS_HYCOM, 36.5))) 1.029      9 2.27 4.55e-06 ***
---
Signif. codes:  0 '***' 0.001 '**' 0.01 '*' 0.05 '.' 0.1 ' ' 1

R-sq.(adj) =  6.85e-05   Deviance explained = 18.6%
-REML = 349.92  Scale est. = 115.11    n = 267186

Method: REML   Optimizer: outer newton
full convergence after 13 iterations.
Gradient range [-2.679075e-05,1.87005e-05]
(score 349.9197 & scale 115.1126).
Hessian positive definite, eigenvalue range [0.2720856,261.7655].
Model rank =  10 / 10

Basis dimension (k) checking results. Low p-value (k-index<1) may
indicate that k is too low, especially if edf is close to k'.

                                     k'  edf k-index p-value
s(pmax(31, pmin(SSS_HYCOM, 36.5))) 9.00 1.03    0.04  <2e-16 ***
---
Signif. codes:  0 '***' 0.001 '**' 0.01 '*' 0.05 '.' 0.1 ' ' 1
```

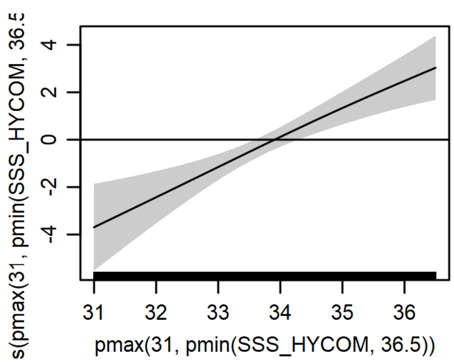

Figure 60: Functional plots for the final model. Transforms and other treatments are indicated in axis labels. *log10* indicates the covariate was $\log_{10}$ transformed. *pmax* and *pmin* indicate the covariate's minimum and maximum values, respectively, were Winsorized to the values shown. Winsorization was used to prevent runaway extrapolations during prediction when covariates exceeded sampled ranges, or for ecological reasons, depending on the covariate. */1000* indicates meters were transformed to kilometers for interpretation convenience.

Table 25: Covariates used in the final model.

Covariate	Description
SSS_HYCOM	Monthly mean sea surface salinity (PSU) from the HYCOM GOFS 3.1 1/12° ocean model (Chassignet et al. (2009))

4.2 Diagnostic Plots

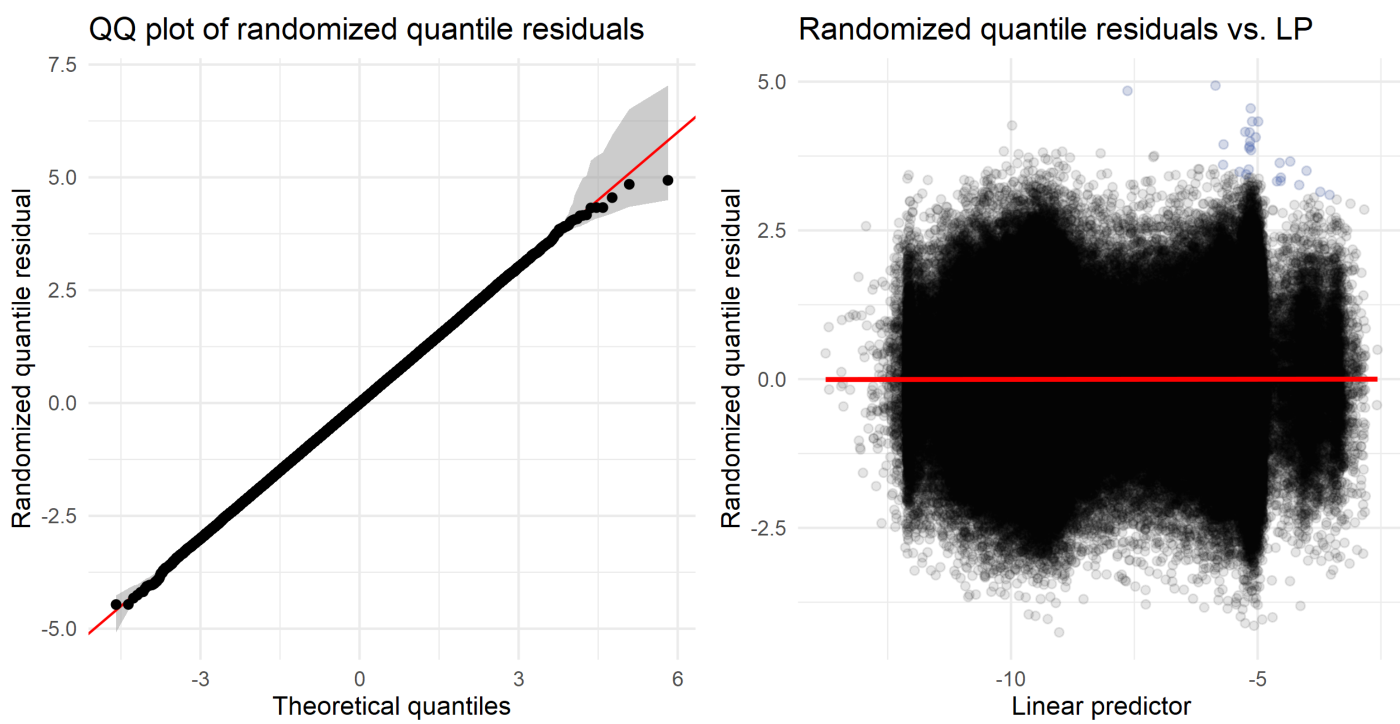

Figure 61: Residual plots for the final model.

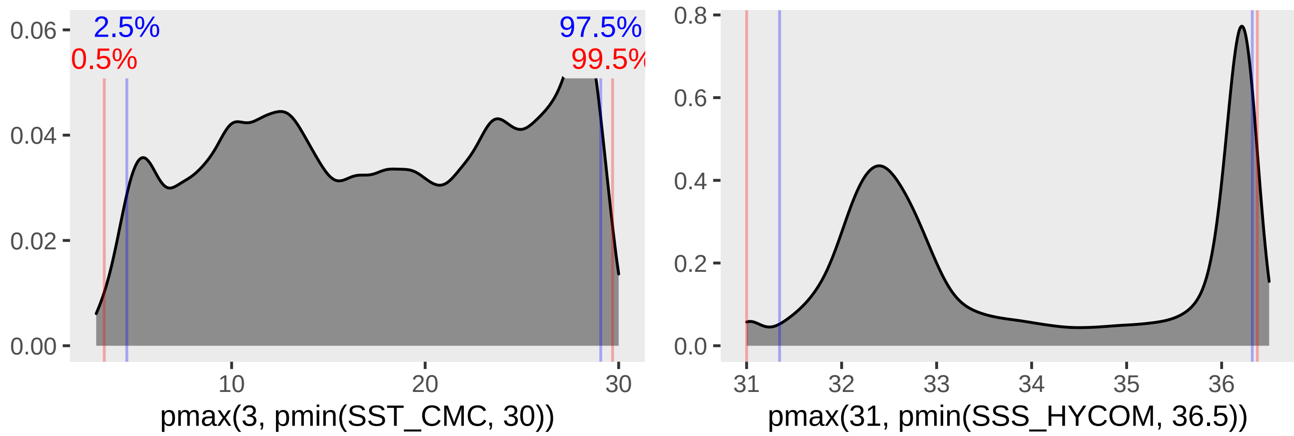

Figure 62: Density histograms showing the distributions of the covariates considered during the final model selection step. The final model may have included only a subset of the covariates shown here (see Figure 60), and additional covariates may have been considered in preceding selection steps. Red and blue lines enclose 99% and 95% of the distributions, respectively. Transforms and other treatments are indicated in axis labels. *log10* indicates the covariate was $\log_{10}$ transformed. *pmax* and *pmin* indicate the covariate's minimum and maximum values, respectively, were Winsorized to the values shown. Winsorization was used to prevent runaway extrapolations during prediction when covariates exceeded sampled ranges, or for ecological reasons, depending on the covariate. */1000* indicates meters were transformed to kilometers for interpretation convenience.

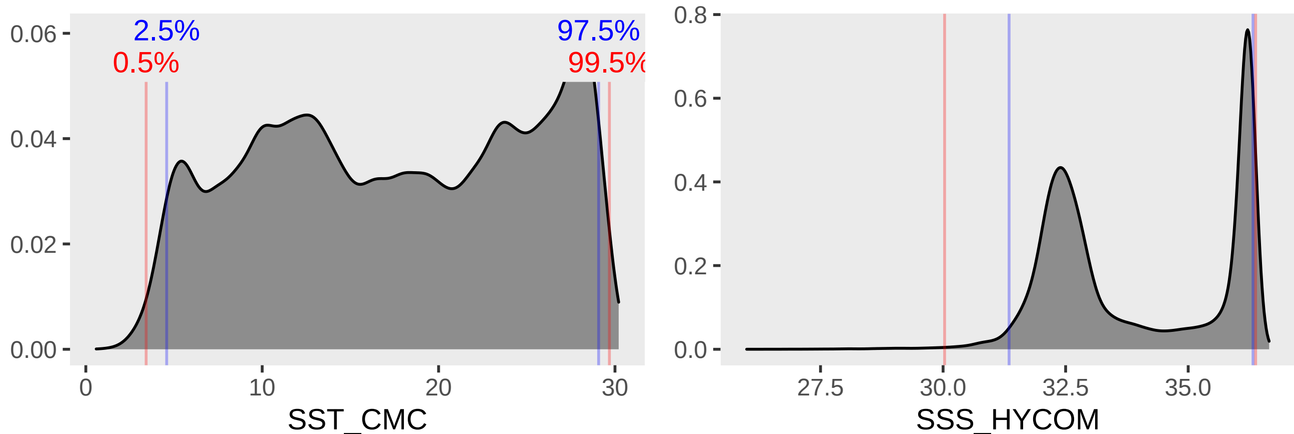

Figure 63: Density histograms shown in Figure 62 replotted without Winsorization, to show the full range of sampling represented by survey segments.

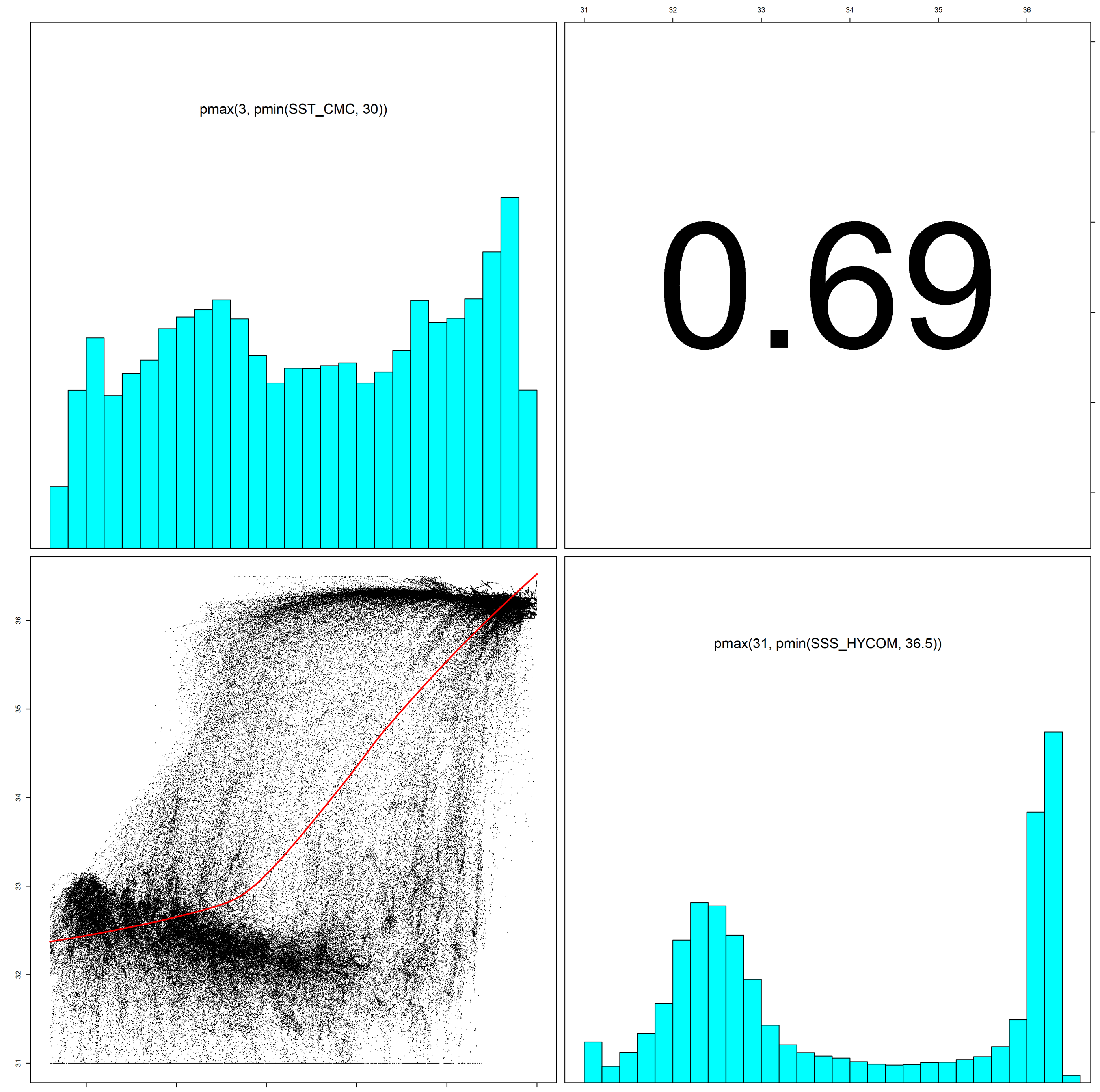

Figure 64: Scatterplot matrix of the covariates considered during the final model selection step. The final model may have included only a subset of the covariates shown here (see Figure 60), and additional covariates may have been considered in preceding selection steps. Covariates are transformed and Winsorized as shown in Figure 62. This plot is used to check simple correlations between covariates (via pairwise Pearson coefficients above the diagonal) and visually inspect for concurvity (via scatterplots and red lowess curves below the diagonal).

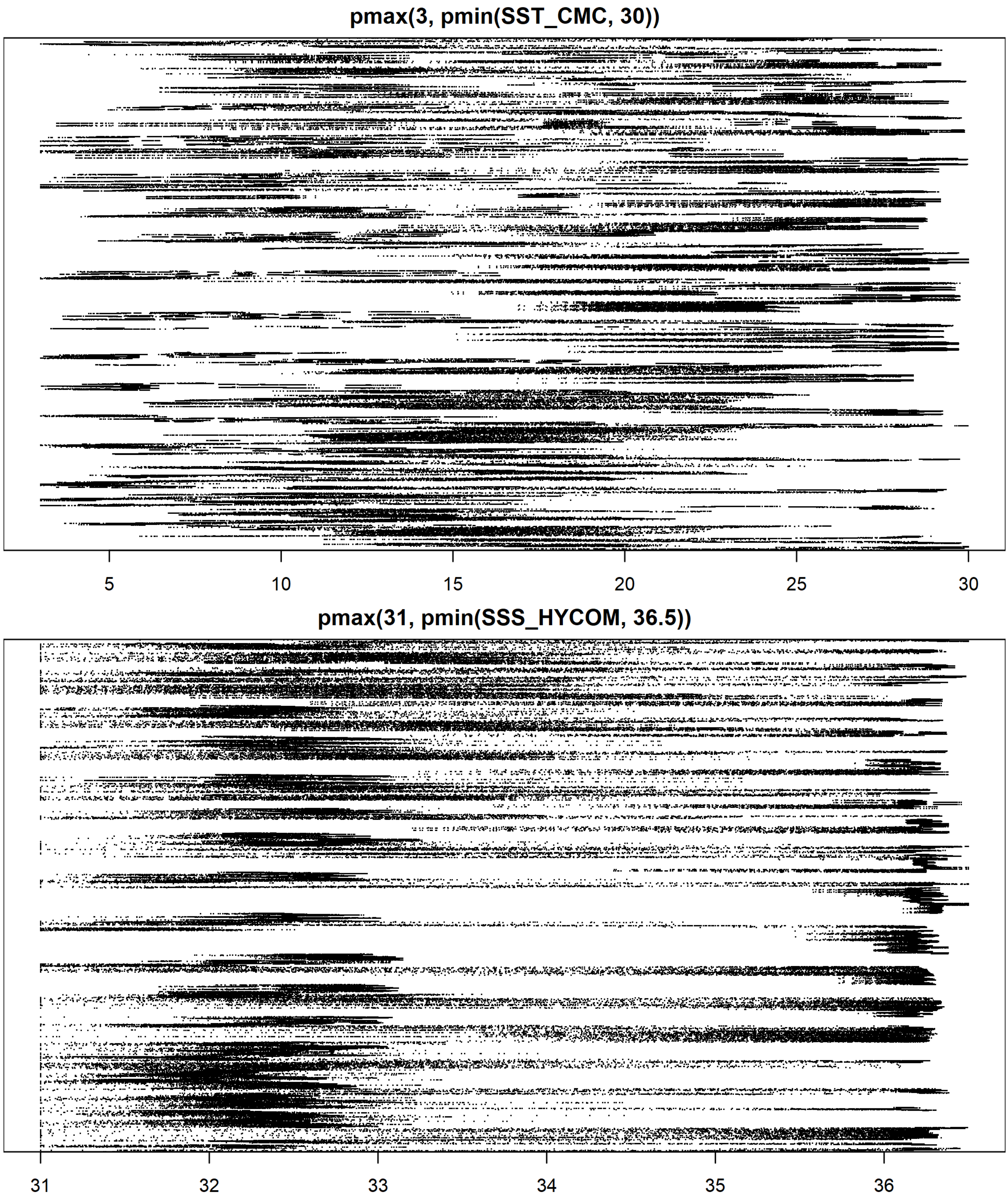

Figure 65: Dotplot of the covariates considered during the final model selection step. The final model may have included only a subset of the covariates shown here (see Figure 60), and additional covariates may have been considered in preceding selection steps. Covariates are transformed and Winsorized as shown in Figure 62. This plot is used to check for suspicious patterns and outliers in the data. Points are ordered vertically by segment ID, sequentially in time.

4.3 Extrapolation Diagnostics

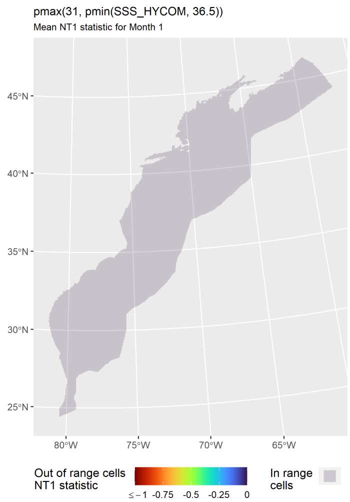

(a) January

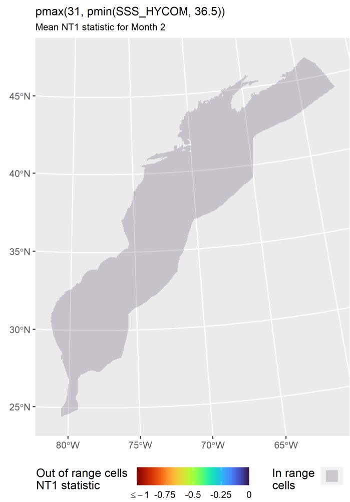

(b) February

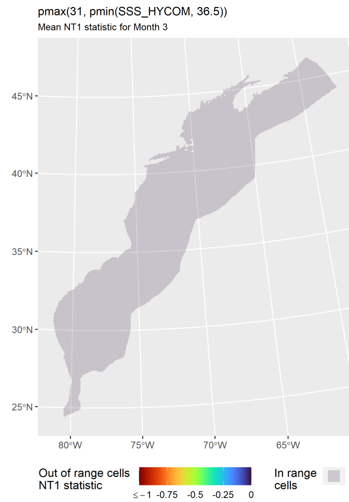

(c) March

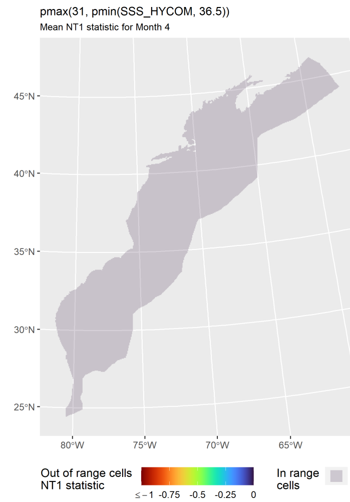

(d) April

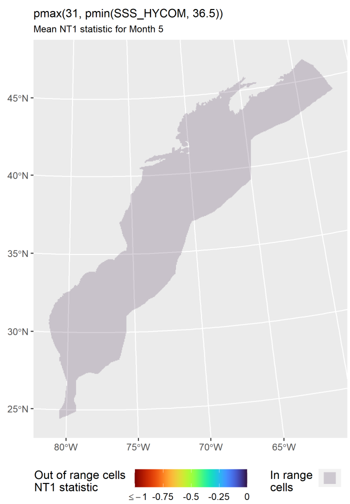

(e) May

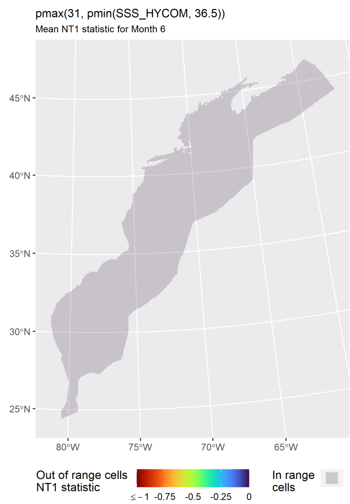

(f) June

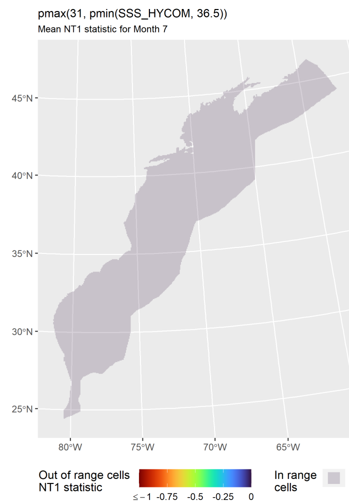

(g) July

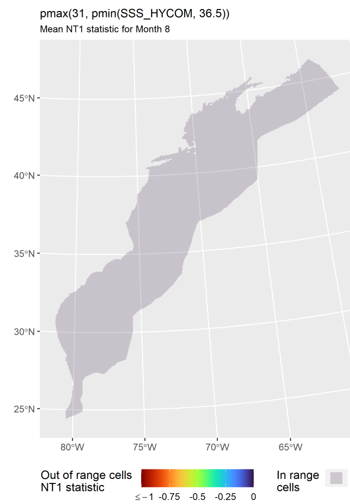

(h) August

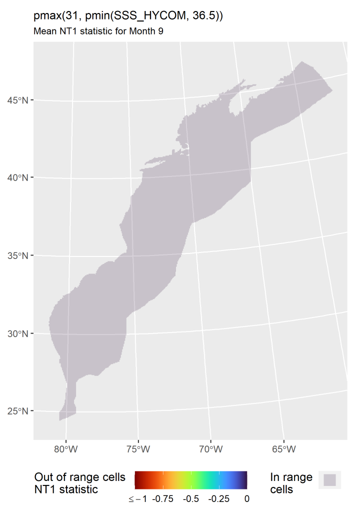

(i) September

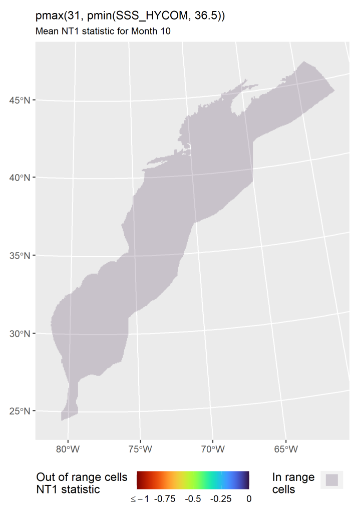

(j) October

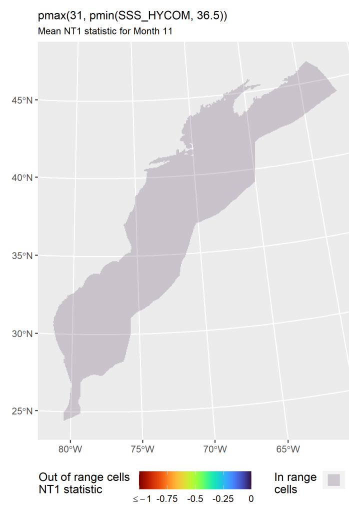

(k) November

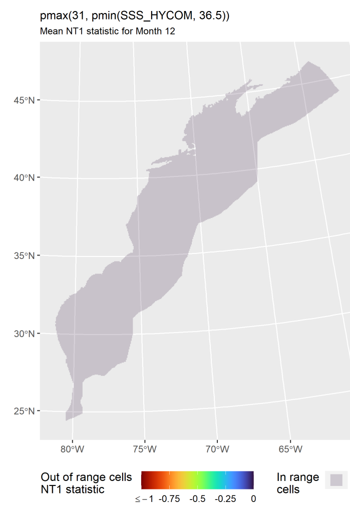

(l) December

Figure 66: NT1 statistic ((ref:Mod1EXmesgaran2014)) for the SSS_HYCOM covariate in the model. Areas outside the sampled range of a covariate appear in color, indicating univariate extrapolation of that covariate occurred there during the month. Areas within the sampled range appear in gray, indicating it did not occur.

5 Predictions

Based on our evaluation of this model in the context of what is known of this species (see Section 6), we summarized its predictions into single, year-round climatological density and uncertainty surfaces (Figure 68). To illustrate the seasonal dynamics that result when predictions are summarized monthly instead, we included monthly mean abundances (Figure 67, Table 26), but to avoid confusion we did not include monthly maps in this report. They are available from us on request, but we recommend the year-round map be used for decision-making purposes, as discussed in Section 6.

5.1 Summarized Predictions

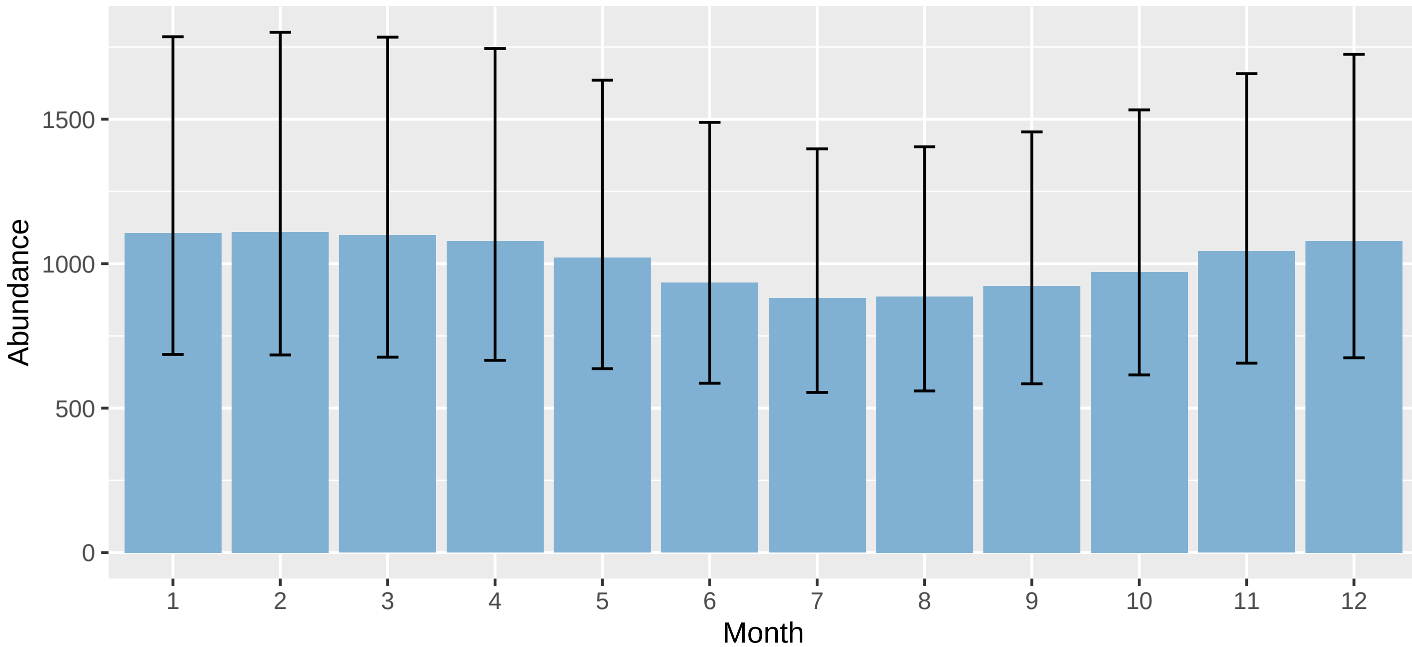

Figure 67: Mean monthly abundance for the prediction area for 1998-2020. Error bars are a 95% interval, made with a log-normal approximation using the prediction's CV. The CV was estimated with the analytic approach given by Miller et al. (2022), Appendix S1, and accounts both for uncertainty in model parameter estimates and for temporal variability in dynamic covariates.

Table 26: Mean monthly abundance and density for the prediction area for 1998-2020. CV and intervals estimated as described for the previous figure.

Month	Abundance	CV	95% Interval	Area (km^2)	Density (individuals / 100 km^2)
1	1,107	0.248	686 - 1,785	1,272,925	0.0869
2	1,110	0.251	684 - 1,801	1,272,925	0.0872
3	1,098	0.251	676 - 1,784	1,272,925	0.0863
4	1,077	0.250	665 - 1,745	1,272,925	0.0846
5	1,020	0.244	637 - 1,635	1,272,925	0.0802
6	934	0.241	586 - 1,489	1,272,925	0.0734
7	880	0.239	554 - 1,398	1,272,925	0.0691
8	887	0.238	560 - 1,405	1,272,925	0.0696
9	922	0.236	584 - 1,456	1,272,925	0.0725
10	971	0.236	615 - 1,532	1,272,925	0.0763
11	1,043	0.240	656 - 1,658	1,272,925	0.0819
12	1,078	0.243	674 - 1,724	1,272,925	0.0847

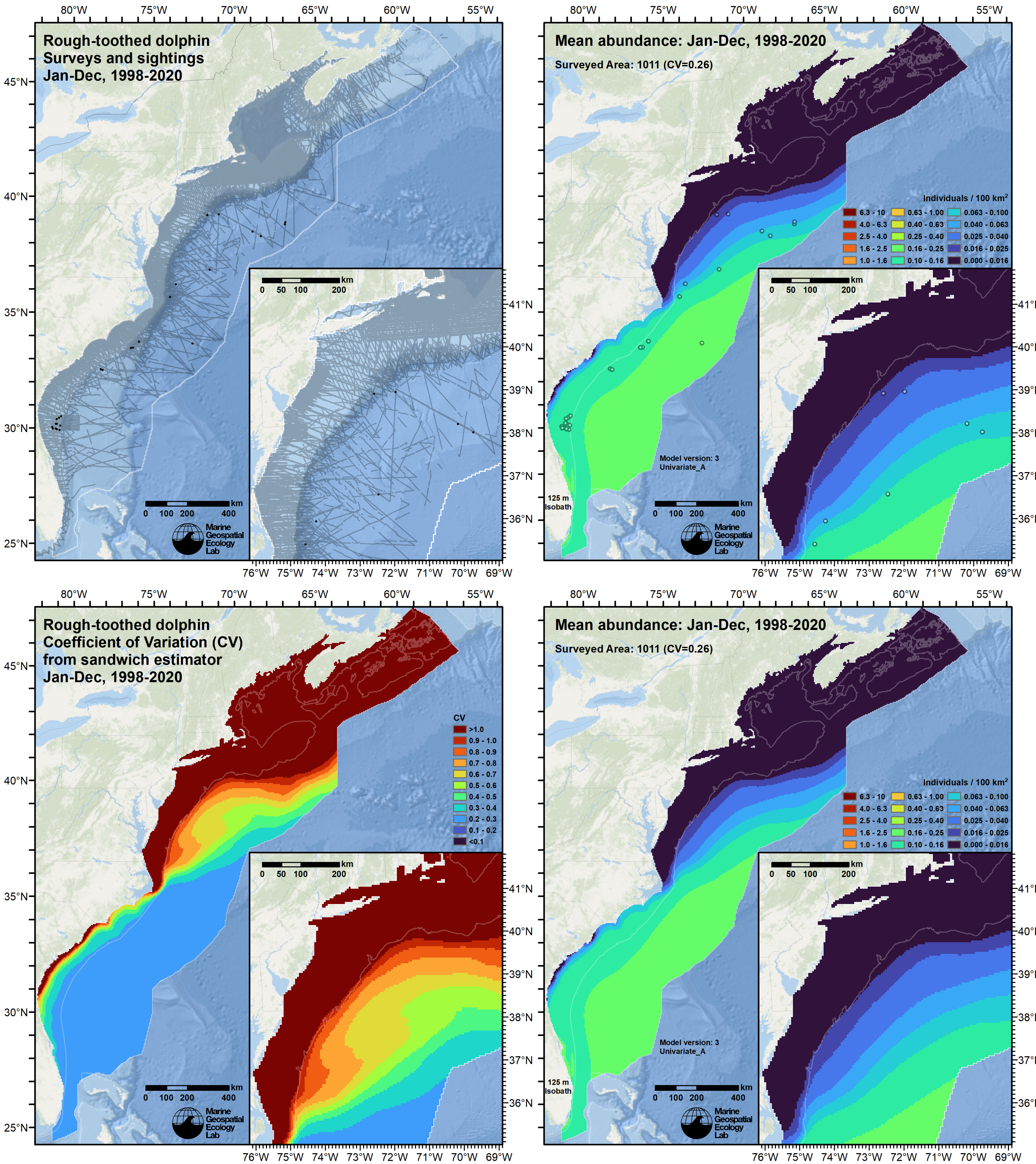

Figure 68: Survey effort and observations (top left), predicted density with observations (top right), predicted density without observations (bottom right), and coefficient of variation of predicted density (bottom left), for the given era. Variance was estimated with the analytic approach given by Miller et al. (2022), Appendix S1, and accounts both for uncertainty in model parameter estimates and for temporal variability in dynamic covariates.

5.2 Abundance Comparisons

5.2.1 NOAA Stock Assessment Report

Table 27: Comparison of regional abundance estimates from the 2018 NOAA Stock Assessment Report (SAR) (Hayes et al. (2019)) to estimates from this density model extracted from roughly comparable zones (Figure 69 below). The SAR estimates were based on a single year of surveying, while the model estimates were taken from the year-round, multi-year mean density surface we provide to model users (Section 5.1).

2019 Stock Assessment Report			Density Model		
Month/Year	Area	N_{est}	Period	Zone	Abundance
Jun-Aug 2011, 2016	Virginia to lower Bay of Fundy[a]	0	Jan-Dec 1998-2020[b]	NEFSC	125
Jun-Aug 2011, 2016	Central Florida to Virginia[c]	136	Jan-Dec 1998-2020	SEFSC	880
Jun-Aug 2011, 2016	Bay of Fundy/Scotian Shelf[d]		Jan-Dec 1998-2020	Canada	2
Jun-Aug 2011, 2016	Total	136	Jan-Dec 1998-2020	Total[e]	1,009

[a] Mean of NEFSC AMAPPS 2011 survey (Palka (2012)) and 2016 survey (which reported no sightings).
[b] We summarized our predictions into a single density surface that applies to all months (see Section 6).
[c] Mean of SEFSC AMAPPS 2011 survey (Garrison (2016)) and 2016 survey (which reported no sightings).
[d] The SAR did not provide an estimate for this area. DFO's 2016 survey of the area did not report any sightings (Lawson and Gosselin (2018)).
[e] This total is slightly less than that shown in Figure 68 because the NEFSC Zone does not quite reach the outer limit of our study area.

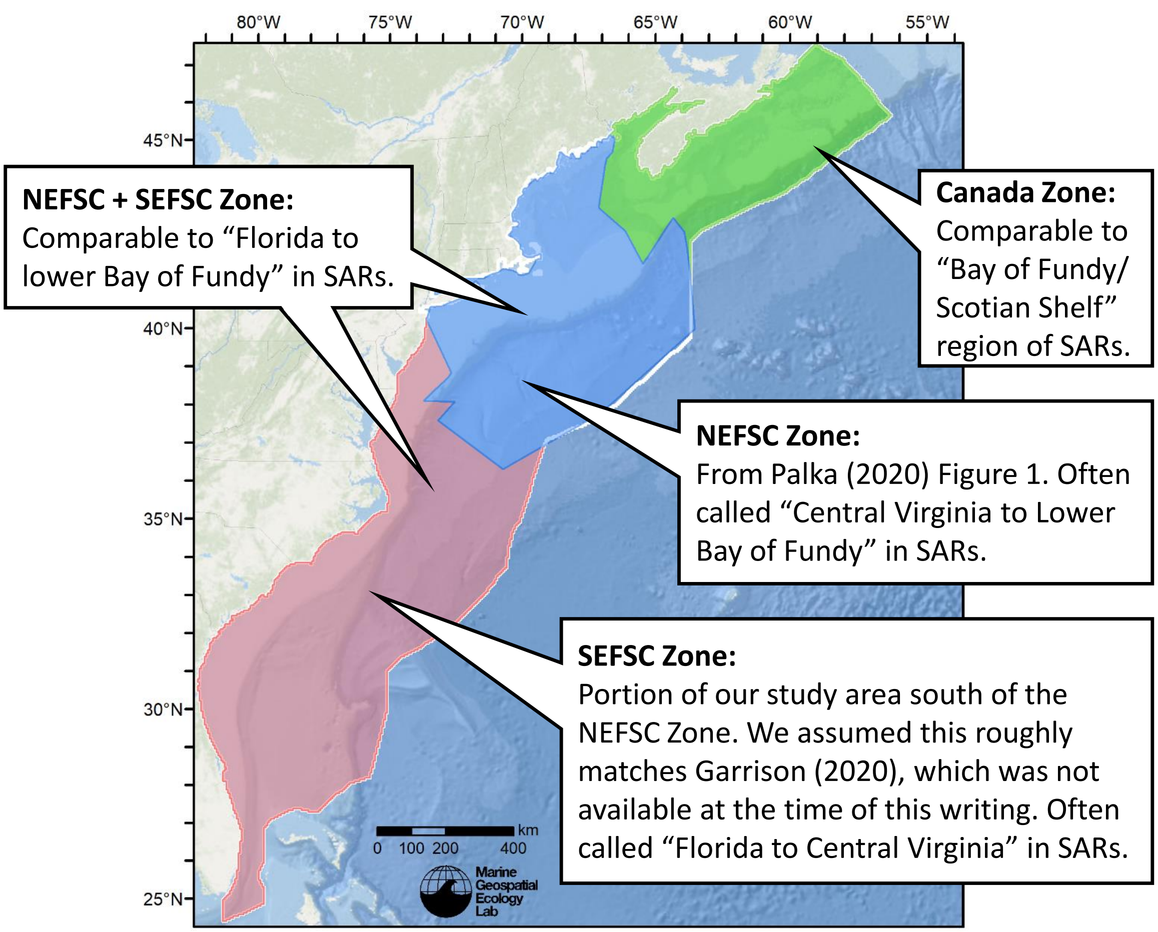

Figure 69: Zones for which we extracted abundance estimates from the density model for comparison to estimates from the NOAA Stock Assessment Report.

5.2.2 Previous Density Model

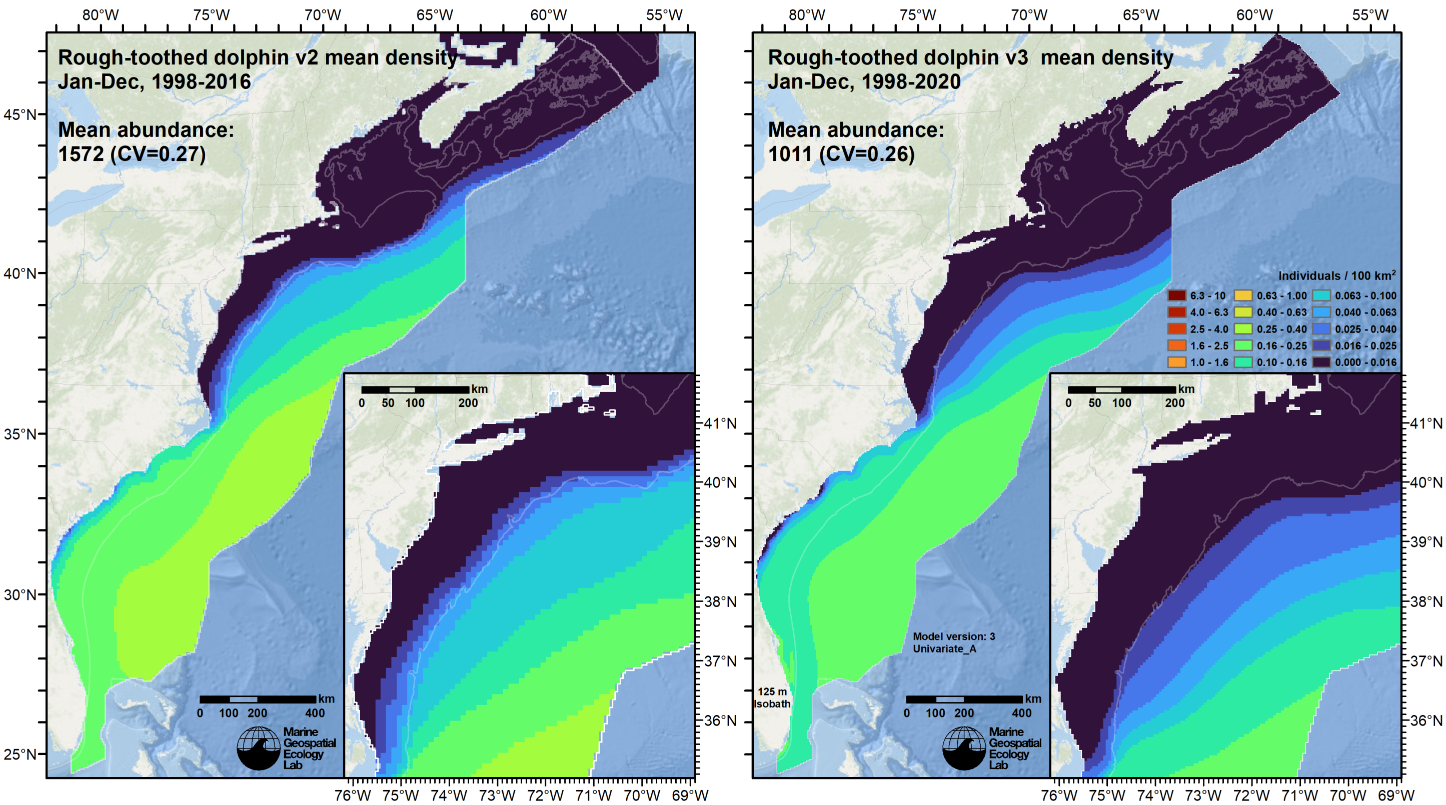

Figure 70: Comparison of the mean density predictions from the previous model (left) released by Roberts et al. (2018) to those from this model (right).

6 Discussion

The small number of sightings available to fit this model were too few to elucidate the seasonal dynamics of this rare species' distribution in our study area. Accordingly, we elected to summarize the model into a single, year-round mean density map (Figure 68). We recommend this be used for species management purposes rather than monthly maps derived from this model.

When summarized across the modeled period (1998-2020), the mean density map (Figure 68) broadly agreed with the literature's description of the rough-toothed dolphin occurring in temperate to tropical waters at a wide range of depths (West et al. 2011; Hayes et al. 2019). Predictions were highest and relatively uniform south of the Gulf Stream, reflecting the higher salinities there, with a decreasing gradient in density between the upper wall of the Gulf Stream and the shelf break, and virtually zero density on the shelf north of Cape Hatteras.

It may be that this species occurs relatively homogeneously in low densities throughout its range. However, ongoing analysis has revealed the presence of multiple insular and genetically-distinct populations around islands throughout the Pacific (Baird et al. 2008; Oremus et al. 2012; Albertson et al. 2017) and an apparently relict population in the eastern Mediterranean that is geographically detached from, and showed some genetic divergence from, populations in the Atlantic, and strong genetic separation from populations in the Indian and Pacific Oceans (Kerem et al. 2016).

According to the current NOAA Stock Assessment Report (SAR) for rough-toothed dolphin (Hayes et al. 2019), there has been no examination of its stock structure in the western North Atlantic. The sightings available for our model, though sparse, showed a pattern potentially indicating distinct metapopulations with differing habitat preferences. All of the sightings near 30 °N, totaling 11 of the 26 available for our model, occurred in the U.S. Navy's Jacksonville study area. This area was heavily surveyed by UNCW in all months for multiple years, with transects laid perpendicular to the shelf break (defined here as the 125 m isobath), each extending 30-50 km on either side of it. All of the sightings occurred on the shallow side of the break, suggesting a distinct preference for shallower water, or some related habitat feature. This contrasted with the remaining 15 sightings, which all occurred at least 2° farther north and on the deep side of the 125 m isobath. Given this pattern, and the finding of isolated metapopulations elsewhere that qualify as separate stocks under the U.S. Marine

Mammal Protection Act, we urge caution in treating all rough-toothed dolphins in U.S. Atlantic waters as a single stock. NOAA notes that additional morphological, genetic, or behavioral data are needed to provide further information on stock delineation (Hayes et al. 2019).

Mean abundance predicted by the model was more than 7 times higher than the abundance estimated by the NOAA 2018 SAR (Table 27), which was the simple average of two estimates. The first, from the 2011 AMAPPS survey of the U.S. Atlantic EEZ, was 271 dolphins, estimated by Garrison (2016) from the single sighting reported on the SEFSC shipboard component of the campaign. The second, from the 2016 AMAPPS survey that essentially replicated the 2011 campaign, was zero; no sightings were reported. (Both of these surveys were included in our model.)

We attribute the large difference between our predicted abundance and NOAA's estimate mainly to the larger amount of data utilized in our model, both sightings and effort. Given that the surveys assembled for our collaboration reported clusters of sightings along the 125m isobath off South Carolina and Florida, where NOAA has never recorded a sighting on broad-scale surveys dating back to 1998 (see Figure 1 of Hayes et al. (2019)), it seems likely that NOAA's surveys have missed part of the population. Also, NOAA's abundance estimate only incorporated sightings made by SEFSC, and did not account for the 6 sightings reported by NEFSC's shipboard surveys (Table 1), of which 4 occurred in the 2011 AMAPPS campaign (Palka 2012). If these were included, it is likely that NOAA's 2011 estimate would have been higher. On the other hand, if the east coast is actually is occupied by several small, spatially-restricted metapopulations, rather than a single broad, homogeneously-distributed population as our model might suggest, then our model could be overestimating the total population size. Until sufficient data are gathered to resolve these questions, we advise caution, particularly where any sightings have been recorded.

Our new model predicted an overall density pattern similar to that of the prior model (Figure 70), with an increasing density gradient in the southeast direction, except that total abundance of the new model was only about 65% of prior model. We believe the main reason for the decrease in abundance is likely to be the adjustments we made to perception and availability bias for aerial surveys, in particular the assumption of $g_{0P} = 0.994$ for aerial sightings of more than 25 individuals and the use of the group availability estimator of McLellan et al. (2018) and Palka et al. (2021), which together resulted in a lower overall correction and therefore lower density. This change particularly affected the southernmost cluster of sightings (in the U.S. Navy's Jacksonville study area) where mean group size (33.8) was substantially higher than the mean (11.7) elsewhere. The larger group sizes in that area warrant additional investigation. In any case, in our study area, for any of the abundance estimates discussed here, the rough-toothed dolphin remains an uncommon delphinid relative to others such as the common bottlenose dolphin or short-beaked common dolphin, which have abundances at least an order of magnitude higher.

References

Albertson GR, Baird RW, Oremus M, Poole MM, Martien KK, Baker CS (2017) Staying close to home? Genetic differentiation of rough-toothed dolphins near oceanic islands in the central Pacific Ocean. Conservation Genetics 18:33–51. doi: 10.1007/s10592-016-0880-z

Baird RW, Webster DL, Mahaffy SD, McSweeney DJ, Schorr GS, Ligon AD (2008) Site fidelity and association patterns in a deep-water dolphin: Rough-toothed dolphins (*Steno Bredanensis*) in the Hawaiian Archipelago. Marine Mammal Science 24:535–553. doi: 10.1111/j.1748-7692.2008.00201.x

Barco SG, Burt L, DePerte A, Digiovanni R Jr. (2015) Marine Mammal and Sea Turtle Sightings in the Vicinity of the Maryland Wind Energy Area July 2013-June 2015, VAQF Scientific Report #2015-06. Virginia Aquarium & Marine Science Center Foundation, Virginia Beach, VA

Barlow J, Forney KA (2007) Abundance and population density of cetaceans in the California Current ecosystem. Fishery Bulletin 105:509–526.

Buckland ST, Anderson DR, Burnham KP, Laake JL, Borchers DL, Thomas L (2001) Introduction to Distance Sampling: Estimating Abundance of Biological Populations. Oxford University Press, Oxford, UK

Burt ML, Borchers DL, Jenkins KJ, Marques TA (2014) Using mark-recapture distance sampling methods on line transect surveys. Methods in Ecology and Evolution 5:1180–1191. doi: 10.1111/2041-210X.12294

Carretta JV, Lowry MS, Stinchcomb CE, Lynn MS, E. CR (2000) Distribution and abundance of marine mammals at San Clemente Island and surrounding offshore waters: Results from aerial and ground surveys in 1998 and 1999. NOAA Administrative Report LJ-00-02. NOAA National Marine Fisheries Service, Southwest Fisheries Center, La Jolla, CA

Chassignet E, Hurlburt H, Metzger EJ, Smedstad O, Cummings J, Halliwell G, Bleck R, Baraille R, Wallcraft A, Lozano C, Tolman H, Srinivasan A, Hankin S, Cornillon P, Weisberg R, Barth A, He R, Werner F, Wilkin J (2009) US GODAE: Global Ocean Prediction with the HYbrid Coordinate Ocean Model (HYCOM). Oceanog 22:64–75. doi: 10.5670/oceanog.2009.39

Cole T, Gerrior P, Merrick RL (2007) Methodologies of the NOAA National Marine Fisheries Service Aerial Survey Program for Right Whales (Eubalaena glacialis) in the Northeast U.S., 1998-2006. U.S. Department of Commerce, Woods Hole, MA

Cotter MP (2019) Aerial Surveys for Protected Marine Species in the Norfolk Canyon Region: 2018–2019 Final Report. HDR, Inc., Virginia Beach, VA

Foley HJ, Paxton CGM, McAlarney RJ, Pabst DA, Read AJ (2019) Occurrence, Distribution, and Density of Protected Species in the Jacksonville, Florida, Atlantic Fleet Training and Testing (AFTT) Study Area. Duke University Marine Lab, Beaufort, NC

Garrison LP (2016) Abundance of marine mammals in waters of the U.S. East coast during the summer 2011. NOAA National Marine Fisheries Service, Southeast Fisheries Science Center, Miami, FL

Garrison LP, Martinez A, Maze-Foley K (2010) Habitat and abundance of cetaceans in Atlantic Ocean continental slope waters off the eastern USA. Journal of Cetacean Research and Management 11:267–277.

Geo-Marine, Inc. (2010) New Jersey Department of Environmental Protection Baseline Studies Final Report Volume III: Marine Mammal and Sea Turtle Studies. Geo-Marine, Inc., Plano, TX

Hayes SA, Josephson E, Maze-Foley K, Rosel PE, Byrd B, Chavez-Rosales S, Cole TVN, Garrison LP, Hatch JM, Henry A, Horstman SC, Litz J, Lyssikatos MC, Mullin KD, Orphanides C, Pace RM, Palka DL, Powell J, Wenzel FW (2019) US Atlantic and Gulf of Mexico Marine Mammal Stock Assessments - 2018. NOAA National Marine Fisheries Service, Northeast Fisheries Science Center, Woods Hole, MA

Hayes SA, Josephson E, Maze-Foley K, Rosel PE, Wallace J, Brossard A, Chavez-Rosales S, Cole TVN, Garrison LP, Hatch J, Henry A, Horstman SC, Litz J, Lyssikatos MC, Mullin KD, Murray K, Orphanides C, Ortega-Ortiz J, Pace RM, Palka DL, Powell J, Rappucci G, Soldevilla M, Wenzel FW (2022) US Atlantic and Gulf of Mexico Marine Mammal Stock Assessments 2021. NOAA National Marine Fisheries Service, Northeast Fisheries Science Center, Woods Hole, MA

Kerem D, Goffman O, Elasar M, Hadar N, Scheinin A, Lewis T (2016) The Rough-Toothed Dolphin, Steno bredanensis, in the Eastern Mediterranean Sea. In: Advances in Marine Biology, Vol. 75. Elsevier, pp 233–258

Laake JL, Calambokidis J, Osmek SD, Rugh DJ (1997) Probability of Detecting Harbor Porpoise From Aerial Surveys: Estimating g(0). Journal of Wildlife Management 61:63–75. doi: 10.2307/3802415

Lawson JW, Gosselin J-F (2018) Estimates of cetacean abundance from the 2016 NAISS aerial surveys of eastern Canadian waters, with a comparison to estimates from the 2007 TNASS. NAMMCO SC/25/AE/09. In: Proceedings of the NAMMCO 25th Scientific Committee (SC). North Atlantic Marine Mammal Commission, Bergen-Tromsø, Norway,

Mallette SD, Lockhart GG, McAlarney RJ, Cummings EW, McLellan WA, Pabst DA, Barco SG (2014) Documenting Whale Migration off Virginia's Coast for Use in Marine Spatial Planning: Aerial and Vessel Surveys in the Proximity of the Virginia Wind Energy Area (VA WEA), VAQF Scientific Report 2014-08. Virginia Aquarium & Marine Science Center Foundation, Virginia Beach, VA

Mallette SD, Lockhart GG, McAlarney RJ, Cummings EW, McLellan WA, Pabst DA, Barco SG (2015) Documenting Whale Migration off Virginia's Coast for Use in Marine Spatial Planning: Aerial Surveys in the Proximity of the Virginia Wind Energy Area (VA WEA) Survey/Reporting Period: May 2014 - December 2014, VAQF Scientific Report 2015-02. Virginia Aquarium & Marine Science Center Foundation, Virginia Beach, VA

Mallette SD, McAlarney RJ, Lockhart GG, Cummings EW, Pabst DA, McLellan WA, Barco SG (2017) Aerial Survey Baseline Monitoring in the Continental Shelf Region of the VACAPES OPAREA: 2016 Annual Progress Report. Virginia Aquarium & Marine Science Center Foundation, Virginia Beach, VA

Marsh H, Sinclair DF (1989) Correcting for Visibility Bias in Strip Transect Aerial Surveys of Aquatic Fauna. The Journal of Wildlife Management 53:1017. doi: 10.2307/3809604

McAlarney R, Cummings E, McLellan W, Pabst A (2018) Aerial Surveys for Protected Marine Species in the Norfolk Canyon Region: 2017 Annual Progress Report. University of North Carolina Wilmington, Wilmington, NC

McLellan WA, McAlarney RJ, Cummings EW, Read AJ, Paxton CGM, Bell JT, Pabst DA (2018) Distribution and abundance of beaked whales (Family Ziphiidae) Off Cape Hatteras, North Carolina, U.S.A. Marine Mammal Science. doi: 10.1111/mms.12500

Miller DL, Becker EA, Forney KA, Roberts JJ, Cañadas A, Schick RS (2022) Estimating uncertainty in density surface models. PeerJ 10:e13950. doi: 10.7717/peerj.13950

Mullin KD, Fulling GL (2003) Abundance of cetaceans in the southern U.S. North Atlantic Ocean during summer 1998. Fishery Bulletin 101:603–613.

Oremus M, Poole MM, Albertson GR, Baker CS (2012) Pelagic or insular? Genetic differentiation of rough-toothed dolphins in the Society Islands, French Polynesia. Journal of Experimental Marine Biology and Ecology 432–433:37–46. doi: 10.1016/j.jembe.2012.06.027

Palka D, Aichinger Dias L, Broughton E, Chavez-Rosales S, Cholewiak D, Davis G, DeAngelis A, Garrison L, Haas H, Hatch J, Hyde K, Jech M, Josephson E, Mueller-Brennan L, Orphanides C, Pegg N, Sasso C, Sigourney D, Soldevilla M, Walsh H (2021) Atlantic Marine Assessment Program for Protected Species: FY15 – FY19 (OCS Study BOEM 2021-051). U.S. Deptartment of the Interior, Bureau of Ocean Energy Management, Washington, DC

Palka DL (2006) Summer abundance estimates of cetaceans in US North Atlantic navy operating areas (NEFSC Reference Document 06-03). U.S. Department of Commerce, Northeast Fisheries Science Center, Woods Hole, MA

Palka DL (2012) Cetacean abundance estimates in US northwestern Atlantic Ocean waters from summer 2011 line transect survey. NOAA National Marine Fisheries Service, Northeast Fisheries Science Center, Woods Hole, MA

Palka DL, Chavez-Rosales S, Josephson E, Cholewiak D, Haas HL, Garrison L, Jones M, Sigourney D, Waring G, Jech M, Broughton E, Soldevilla M, Davis G, DeAngelis A, Sasso CR, Winton MV, Smolowitz RJ, Fay G, LaBrecque E, Leiness JB, Dettloff K, Warden M, Murray K, Orphanides C (2017) Atlantic Marine Assessment Program for Protected Species: 2010-2014 (OCS Study BOEM 2017-071). U.S. Deptartment of the Interior, Bureau of Ocean Energy Management, Washington, DC

Read AJ, Barco S, Bell J, Borchers DL, Burt ML, Cummings EW, Dunn J, Fougeres EM, Hazen L, Hodge LEW, Laura A-M, McAlarney RJ, Peter N, Pabst DA, Paxton CGM, Schneider SZ, Urian KW, Waples DM, McLellan WA (2014) Occurrence, distribution and abundance of cetaceans in Onslow Bay, North Carolina, USA. Journal of Cetacean Research and Management 14:23–35.

Roberts JJ, Best BD, Mannocci L, Fujioka E, Halpin PN, Palka DL, Garrison LP, Mullin KD, Cole TVN, Khan CB, McLellan WA, Pabst DA, Lockhart GG (2016) Habitat-based cetacean density models for the U.S. Atlantic and Gulf of Mexico. Scientific Reports 6:22615. doi: 10.1038/srep22615

Roberts JJ, Mannocci L, Schick RS, Halpin PN (2018) Final Project Report: Marine Species Density Data Gap Assessments and Update for the AFTT Study Area, 2017-2018 (Opt. Year 2), Document Version 1.2. Duke University Marine Geospatial Ecology Lab, Durham, NC

Roberts JJ, Yack TM, Halpin PN (2023) Marine mammal density models for the U.S. Navy Atlantic Fleet Training and Testing (AFTT) study area for the Phase IV Navy Marine Species Density Database (NMSDD), Document Version 1.3. Duke University Marine Geospatial Ecology Lab, Durham, NC

Robertson FC, Koski WR, Brandon JR, Thomas TA, Trites AW (2015) Correction factors account for the availability of bowhead whales exposed to seismic operations in the Beaufort Sea. Journal of Cetacean Research and Management 15:35–44.

Ryan C, Boisseau O, Cucknell A, Romagosa M, Moscrop A, McLanaghan R (2013) Final report for trans-Atlantic research passages between the UK and USA via the Azores and Iceland, conducted from R/V Song of the Whale 26 March to 28 September 2012. Marine Conservation Research International, Essex, UK

Torres LG, Mclellan WA, Meagher E, Pabst DA (2005) Seasonal distribution and relative abundance of bottlenose dolphins, Tursiops truncatus, along the US mid-Atlantic coast. Journal of Cetacean Research and Management 7:153.

West KL, Mead JG, White W (2011) Steno bredanensis (Cetacea: Delphinidae). Mammalian Species 43:177–189.

Whitt AD, Powell JA, Richardson AG, Bosyk JR (2015) Abundance and distribution of marine mammals in nearshore waters off New Jersey, USA. Journal of Cetacean Research and Management 15:45–59.